Computational and experimental studies on the formation of polymer-drug nanoparticles



Ioanna Danai Styliari

School of Pharmacy

University of Nottingham

This dissertation is submitted for the degree of

Doctor of Philosophy

January 2017

The only limits are the ones you put to yourself

keep (re)searching...

Acknowledgements

It has been a journey like no other.

1400 days, 17 conferences/workshops, 3 countries, 13 cities, 21 presentations, and here we are.

It goes without saying that I am thankful to my husband Panagiotis Koutsouras (PhD Candidate at Horizon) and to my lovely family, for their constant moral support and understanding. But let me focus on my "academic family" that kept me busy over the past four years...

First of all I would like to thank all my supervisors, Charlie, Martin and Cameron. I had the pleasure and an amazing opportunity to understand how such academics think and move forward. Your constant support, especially during the last year and months helped me enormously and I would like to thank you each one individually;
Charlie, for always being rational and critical, making me double-check myself and thus making me a better scientist, and for never saying no to me travelling and exposing myself to new environments.
Martin, for all your support and for never losing faith in the project and me. You have been the closest to my "academic father".
Cameron, for giving me this opportunity to be part of the CDT that truly expanded my horizons and for being there during my "darkest" phases.

From GSK, I would like to thank Andrew Theophilus, my industrial supervisor till November 2015, for his enthusiasm, and for all the help he provided during my visits to Stevenage, as well as Izabella Philips and Dr. Andrea D. Goncalves for their help in GSK's labs.

Dr. Claudia Matz, thanks for all your support, especially those early years, for your understanding and for all the care.

Many thanks to Ghaidaa Hameed for providing the valuable cryomilled indomethacin for my experiments. To my fellow colleagues, (some soon-to-be-Drs!) in Cameron's and Charlie's groups; Dr. Joao Vilhena Fernandes Madeira do O, Paola Sanjuán Alberte, Alejandro Nieto Orellana, Alshaimaa Almehmady, Mary Kyobula, Gudrun Frigdeisdottir, Rosa Catania, Dr. Vanessa Loczenski-Rose, Dr. Robbie Mackenzie, Dr. Twana Salih, Dr. Aneesa Ahmed, Mohammed Tumbi to name a few... We made it! Thanks for all the fun moments, all the incredible support, all the laughs that made this PhD a bit easier.

At this point I would like to thank and acknowledge some of the extra-helpful Post Docs that also facilitated my journey; Dr. Francesca Mastrotto, Dr. Eleanor Turpin, Dr. Gareth Shannon thanks a lot; I was coming with questions and I was leaving with answers, suggestions and exciting ideas. I really hope we will collaborate again in the future.

Above all, I would like to express my gratitude to Dr. Vincenzo Taresco, aka the "polymer-master". You have formed me like no other and I wouldn't be able to reach here without your constant support, help, advice and occasional scolding. You were always there in my times of need, my personal touchstone, and I am extremely fortunate to have spent so much good time with you and learn from you. Thank you.

Abstract

Polymer based nanoparticle formulations attract attention as potentially highly tunable drug delivery systems. Interfacial deposition is a well-established technique, based on solvent displacement that is being used to form both polymer nanoparticles, as well as drug loaded polymer nanoparticles.

However currently, there is limited understanding of the underlying polymer - nanoparticle assembly mechanisms and this limits our ability to rationally design and optimise them. At the same time, conventional methods for the preparation of polymer-drug nanoparticles suffer from low encapsulation efficiencies and drug loadings, making them undesirable to the pharmaceutical industry.

In this thesis, a method used to polymer-coat the surface of iron oxide nanoparticles was translated to produce polymer-coated drug nanoparticles. In order to provide an holistic overview of the system and the underlying phenomena, both computational and experimental methods were used.

More particularly, all atom molecular dynamics simulations were employed to study the behaviour of the drug nanoparticles and the polymers during the interfacial deposition method. The system was built as a biphasic model, containing an aqueous-drug loaded-phase

and an organic-polymer rich-phase. The model was a miniature in the atomistic level of the expected experimental set-up, keeping the ratios and concentrations as close as possible to pre-existing iron oxide nanoparticle work.

On a parallel path, experimental studies were performed. The polymers were synthesised and fully characterised. Then, the formation of drug-free polymer nanoparticles via the method was studied and the properties of these nanoparticles were analysed. Interestingly, when the drug was introduced into the method in the form of drug microparticles suspended in the aqueous region, polymer-coated drug nanoparticles were produced. These nanoparticles were stable, significantly different to the drug-free polymer nanoparticles and were characterised for their size and morphology. Further analysis of the polymer-coated drug nanoparticle suspensions revealed high encapsulation efficiencies and impressive drug loadings.

We conclude with some proposed future work on modelling polymer-based drug delivery systems, moving towards a structure based formulation design to complement the process of structure based drug design which is already very well established in the pharmaceutical industry.

Contents

List of figures **xv**

List of tables **xxxiii**

Nomenclature **xxxv**

1 Introduction **1**

1.1 Motivation 2

1.1.1 Nanoparticles as drug delivery systems 2

1.1.2 Interactions between nanoparticles 5

1.1.3 Nanoparticles in pulmonary delivery 7

1.1.3.1 The exciting challenge of drug delivery to the lungs. 7

1.1.4 Initial motivation 11

1.2 Polymers in Drug Delivery Systems 14

1.2.1 mPEG-*b*-PCL polymers in DDS 16

1.3 Nanoparticle preparation techniques 17

1.3.1 Polymer-drug nanoparticles 17

1.3.2 Pure Drug nanoparticles 19

1.3.2.1 Top-down techniques 19

1.3.2.2 Bottom-Up techniques 23

1.4 Reducing trial and error in the lab: the use of computational approaches to provide answers 26

1.4.1 MD simulations of pharmaceutical relevance. . . . 29

1.5 Aims and Objectives 39

2 Methodology **41**

2.1 Computational Work 41

2.1.1 Molecular Dynamics 42

2.1.1.1 The GROMOS 53a6 and 54a7 force fields . 44

2.1.2 Simulation Setup 47

2.1.2.1 Partial charges - Topology files 47

2.1.2.2 Computational Polymer "Synthesis" 48

2.1.2.3 Construction of the Interfacial Deposition Model 49

2.1.2.4 Running Parameters 50

2.1.2.5 Tools used for the analysis of the simulations 51

2.2 Experimental work 53

2.2.1 Polymer Synthesis and Characterisation 53

2.2.1.1 Synthesis and purification of mPEG$-b-$PCL diblock copolymers 53

2.2.1.2 Polymer Characterisation 55

2.2.1.2.1 Proton Nuclear Magnetic Resonance (^{1}H−NMR) 55
2.2.1.2.2 Gel Permeation Chromatography (GPC) 55
2.2.1.2.3 Water Contact Angle (WCA) measurements 55
2.2.1.2.4 Attenuated Total ReflectanceInfrared spectroscopy (ATR-IR) . . 56
2.2.1.2.5 Differential Scanning Calorimetry (DSC) 56
2.2.2 Nanoparticle preparation via the modified interfacial deposition method 57
2.2.2.1 Preparation of polymer nanoparticles . . . 57
2.2.2.2 Preparation of drug nanosuspensions . . . 58
2.2.2.3 Preparation of polymer-coated indomethacin nanoparticles 60
2.2.3 Nanoparticle Characterisation 60
2.2.3.1 Dynamic Light Scattering 60
2.2.3.2 Critical Aggregation Concentration 61
2.2.3.3 Salt Stability 62
2.2.3.4 Zeta-potential 62
2.2.3.5 Transmission Electron Microscopy 63
2.2.3.6 Polarised Optical Microscopy 64
2.2.3.7 Quantification of drug loading via UV-Vis 64

3 Computational Studies **67**

3.1 Diffusion of acetone in water. 68

3.1.1 Testing acetone models in GROMOS53a6 72

3.2 Control simulations in pure solvents 74

3.2.1 $mPEG_{350}$-*b*-PCL_{2000} in pure solvents 75

3.2.1.1 mPEG-*b*-PCL in the presence of acetone . 75

3.2.1.2 mPEG-*b*-PCL in the presence of pure water 77

3.2.2 Indomethacin NP in the presence of pure solvents . 80

3.2.2.1 Indomethacin NP in acetone 80

3.2.2.2 Indomethacin NP in the presence of water 80

3.3 Modelling the interfacial deposition method 83

3.4 Simulations for the formation of mPEG-*b*-PCL polymer nanoparticles 86

3.5 Simulation of indomethacin in the absence of polymer . . . 94

3.6 Simulation for the formation of polymer-drug nanoparticles 96

3.7 Discussion 106

4 Experimental Studies **113**

4.1 Polymer Synthesis and Characterisation 115

4.2 The coating process 123

4.2.1 Derivation of the coating process 123

4.2.2 Formation of polymer nanoparticles 124

4.2.3 Production of drug particles for the aqueous phase 131

4.2.3.1 Wet ball milling 131

4.2.3.2 Cryomilling 132
4.2.3.3 Aqueous indomethacin suspension 132
4.2.4 Formation of drug nanoparticles via the interfacial deposition method 135
4.2.5 Formation of polymer-coated drug nanoparticles . 136
4.3 Discussion 146

5 Conclusions and Future Work **151**
5.1 Overview and Final Discussion 151
5.2 Future Work 154

References **157**

Appendix A Parameter files **173**
A.1 Acetone Topology - UAC.itp 173
A.2 mPEG-PCL topology - polymers.rtp 176
A.3 Acetone models 183
A.4 Packmol Example Building code 185
A.5 Example of topol.top file 186
A.6 grompp.mdp file 187

Appendix B Experimental Appendix **189**
B.1 GPC traces 189
B.2 DSC and equation for the calculation of PCL % crystallinity. 194
B.3 Wet ball milled indomethacin 197
B.4 Cryomilled indomethacin characteristics 198

B.5 DLS intensity distributions 201

B.5.1 Reproducibility of the method 201

B.5.2 Polymer Concentration effect 201

B.5.3 Temperature stability 203

B.5.4 Physical Stability 204

B.5.5 Miscellaneous 204

B.6 UV-Vis calibration 205

List of figures

1.1 NPs can be modified according to their physical properties, their composition, surface chemistry and target ligands for specificity. This flexibility allows the design of multifunctional NPs that can be used as DDS and contrast agents. Taken from [3]. 3

1.2 FDA approved nanoparticles per year (a) and per catergory (b). Data from clinicaltrials.gov stating the different phases of nanoparticles under clinical trials (c) and per category (d). Taken from [10]. 5

1.3 Fate of insoluble particles when dispersed in liquids. Adapted from [11]. 6

1.4 The respiratory system. Particles are inhaled through the mouth and can impact on the pharynx and the bifurcations in the respiratory system. As the particle passes deeper into the lung the processes of sedimentation and diffusion become more important. Taken from [20]. 7

1.5 Factors influencing the deposition of a particle in the lungs. Taken from [22]. 9

1.6 The main questions and motivations that lead this work involve polymer-coated drug NPs. The hydrophilic (light blue) chain of the polymers plays a critical role in the steric effects between other similar NPs while the hydrophobic (dark blue) chain interacts with the drug NP (grey/green) through hydrophobic interactions. The main questions derived from the motivation of the present work are; (a) Can we form polymer-coated drug NPs in which the core is a pure drug NP? Can these polymer-coated NPs form agglomerates of 1-3μm to achieve deep lung deposition? (b) What are the properties of the polymers needed to coat the drug NPs and how will the length of the hydrophilic polymer block affect the agglomerates? (c) The surface chemistry of the polymer-coated drug NPs will be the key parameter affecting their agglomeration and thus their aerodynamic behaviour. Can we coat different drug NPs that will then exhibit the same delivery behaviour? 13

1.7 Manufacturing techniques used to produce drug NPs. Top-down methods include techniques like milling and homogenization. Bottom-up techniques are usually based on nanoprecipitation, where NPs will be formed after the removal or evaporation of the solvent. Taken from [68]. . . 20

1.8 TEM images of indomethacin suspensions milled with F127 (A) and F68 (B). Scale bar of 0.5 μm. Taken from [75]. 22

1.9 Schematic of Flash Nanoprecipitation technique. Taken from [78]. 24

1.10 Simulation methods and their time and spatial resolutions. The most detailed description of a system is achieved by Quantum Mechanics (QM) calculations. All-atom (AA) simulations are used to describe interactions between individual atoms that have been assigned single point charges. Simulations can be accelerating via Coarse Graining (CG), where sets of atoms are grouped into one bead/interaction point. Finally, at larger CG level, Dissipative Particle Dynamics (DPD) are used to study macroscopic effects. Taken from [85]. 27

1.11 Snapshots of multiscale simulation of nanoprecipitation: PGA (grey) collapses and encapsulates dexamethasone phosphate molecules as acetone (blue) disperses in the water region. Water not shown for clarity. Taken from [93]. 29

1.12 Snapshots of a star copolymer formed by 6 mPEG38 (blue)-b-PCL_9 (yellow), at 1 ns and 200 ns. Taken from [107]. . . . 31

1.13 Snapshot after 100ns of MD run of 8 Pluronics P85 chains interacting with a single curcumin molecule, in water (not shown). Taken from [102]. 33

1.14 Interactions of P85 poloxamer with a lipid membrane (DLPC) as reported from Goliaei et al. [115]. A and B are the two simulations were different starting configuration were used, but both resulted in the penetration of the hydrophobic PPO (blue), in the lipid layer. C illustrates a tool used to measure the distance between the centre of masses of the PPO chain and the lipid membrane. 34

1.15 Work performed by Kasimova et al. [101] for the study of hydrophobic drugs incorporation in the lipophilic core of mPEG-hexPLA micelles. (a) mPEG (blue) - hexPLA (red) micelle structure. (b) Snapshot taken from the MD run of mPEG-hexPLA with 21 cyclosporin (grey van der Waals surfaces) molecules. 35

1.16 A PCL chain of 30 monomers, in an acetone(purple)-water(blue) mixture (50:50). The acetone molecules in a distance of 6 A surrounding the PCL chain prevent its aggregation, even in the presence of water in the mixture. Taken from reference [106]. 37

2.1 The evolution of the MD algorithm and the calculations taking place during one time step. 43

2.2 Lennard Jones interaction potential. 45

2.3 Periodic Boundary Conditions as applied to a molecule full of atoms (blue in the centre) and the importance of the cut-off radius. [123] 46

2.4 Bonded interactions between a set of four neighbouring atoms. 47

2.5 Structure of the mPEG-*b*-PCL units for the topology files. . 48

2.6 Biphasic system for the simulation of the interfacial deposition. 50

2.7 Steps in order to calculate the amount of molecules for each of the simulations. 50

2.8 The end-to-end distance (R_{e-e}) and radius of gyration (R_{gyr}) in a polymer chain. 52

2.9 Synthesis of mPEG$-b-$PCL polymers via Ring Opening Polymerisation. In light blue is the hydrophilic mPEG block, while in dark blue is the hydrophobic PCL. 54

2.10 Water contact angle measurements for the determination of the hydrophilicity or hydrophobicity of a surface. 56

2.11 Formation of polymer nanoparticles by the interfacial deposition method. 57

2.12 Structure of indomethacin. 58

2.13 Dynamic Light Scattering (DLS) Schematic. Taken from [141]. 61

2.14 Potentials at different distances from the surface of a negatively charged particle. Taken from [143]. 63

2.15 UV-Vis schematic taken from [144]. 65

3.1 Five $mPEG_{350}$ (in light blue)-*b*-PCL_{2000} (in dark blue) chains simulated in pure acetone (not shown for clarity). The polymer chains remain untangled during the 80 ns simulation. PBC conditions apply, where the molecules can move across the end of the box. 75

3.2 End-to-End distances (a) and Radius of gyration (b) for the control simulation of 5 $mPEG_{350}$-*b*-PCL_{2000} polymers in pure acetone. Graph (c) gives the average values for each of the blocks and error bars correspond to the standard deviation of the measurements. Acetone is a good solvent for the above polymers so the radius of gyration and the end-to-end distances fluctuate over the course of the simulation. 76

3.3 Five $mPEG_{350}$ (in light blue)-*b*-PCL_{2000} (in dark blue) chains simulated in pure water (SPC model, not shown for clarity). PBC conditions apply, where the molecules can move across the end of the box. The formation of single polymer chain aggregates takes place during the first 4 ns of the simulation which later start interacting one with another, leading into the formation of one larger polymer aggregate (32ns). 78

3.4 End-to-End distances (a) and Radius of gyration (b) for the control simulation of 5 $mPEG_{350}$-*b*-PCL_{2000} polymers in pure water. Graph (c) gives the average values for each of the blocks and error bars correspond to the standard deviation of the measurements. Water is a good solvent for the $mPEG_{350}$ block of the polymers but a bad solvent for the PCL_{2000}. The radius of gyration and end-to-end distance are decreased immediately at the start of the simulation, when the single polymer chains are formed and then they plateau for the rest of the simulation. 79

3.5 A 5nm diameter indomethacin NP simulated in the presence of pure acetone. PBC conditions apply, where the molecules can move across the end of the box. The indomethacin NP is almost fully dissolved after 60 ns, displaying the high solubility indomethacin has in acetone. . 81

3.6 A 5nm diameter indomethacin NP simulated in the presence of pure water. PBC conditions apply, where the molecules can move across the end of the box. The indomethacin NP stays intact for the whole of the simulation, displaying a very poor aqueous solubility. 82

3.7 Starting configuration for the simulations set for the formation of the polymer NPs (Systems A, B, C and D of table 3.2). 86

3.8 System A: Simulation for the formation of $mPEG_{350}$-*b*-PCL_{2000} polymer NP: The spatial distribution of the acetone and water molecules across the x-axis of the simulated box in 10 ns reveal a solvent separation, i.e. the system is not fully equilibrated. 87

3.9 Radius of gyration and end-to-end distances for the hydrophilic blocks of the polymers over the course of a 10ns simulation in the biphasic systems (Systems A, B, C and D, table 3.2). The larger the molecular weight of the polymer, the higher the radius of gyration and end-to-end distances. 88

3.10 System A: $mPEG_{350}$ (light blue)-*b*-PCL_{2000} (dark blue) polymer chains in the interfacial deposition simulation, for the formation of a polymer NP. The polymers are placed in the acetone (pink) region, while water is not shown for clarity. 89

3.11 System A: mPEG$_{350}$ (light blue)-*b*-PCL$_{2000}$ (dark blue) polymer chains in the interfacial deposition simulation, for the formation of a polymer NP. Snapshots taken at every 20 ns, solvents not shown for clarity. The polymer chains start to aggregate, as the presence of water in their surrounding environment increases. However their full aggregation is not facilitated due to the presence of the acetone. 90

3.12 System A: mPEG$_{350}$ (light blue)-*b*-PCL$_{2000}$ (dark blue) polymer chains in the interfacial deposition simulation, for the formation of a polymer NP. Snapshots taken at the end of every 10 ns MD run where acetone molecules (pink) are replaced by water molecules, mimicking acetone's evaporation. A polymer NP is formed as the polymers aggregate in the increasing aqueous environment. Water is not shown for clarity. 91

3.13 System A analysis: mPEG$_{350}$-*b*-PCL$_{2000}$ polymer chains in the interfacial deposition simulation for the formation of a polymer NP. End-to-end distances ((a), (c)) and Radius of gyration ((b), (d)) for the different blocks of mPEG$_{350}$-*b*-PCL$_{2000}$ polymer chains for the complete simulation of 140 ns (top row) and the acetone evaporation steps during the last 40 ns (bottom row). The hydrophobic PCL$_{2000}$ block starts to aggregate during the replacement of the acetone molecules, thus reducing its spatial conformation. 93

3.14 Control simulation of the indomethacin NP (grey) to evaluate the NP's stability in the biphasic system. The drug NP stays intact till 70 ns, however as the acetone's (pink) presence increases in the NP's surrounding environment, the NP starts to swell up and to slowly dissolve. Water is not shown for clarity. 95

3.15 System A* for the formation of polymer-drug NP. The starting point of the simulation of $mPEG_{350}$ (light blue)-*b*-PCL_{2000} (dark blue) in the acetone region, in the presence of the amorphous indomethacin NP (grey) in the aqueous phase. 96

3.16 System A*: Interfacial deposition simulation of $mPEG_{350}$ (light blue)-*b*-PCL_{2000} (dark blue) polymer chains in the presence of a 5 nm indomethacin NP (grey). Solvents are not shown for clarity. PBC conditions apply, where the molecules can move across the end of the box. Snapshots taken at various time points of the simulation. The polymer chains start to aggregate slowly as the acetone diffuses towards the water region. The indomethacin NP stays intact in the aqueous region till it reaches close proximity with the polymer chains and gets dissolved at 108 ns. . . . 97

3.17 System A*: Interfacial deposition simulation of $mPEG_{350}$ (light blue)-*b*-PCL_{2000} (dark blue) polymer chains in the presence of a 5 nm indomethacin NP (grey). Solvents are not shown for clarity. PBC conditions apply, where the molecules can move across the end of the box. Later snapshots over the course of the 280 ns simulation; the polymer chains strongly interact with the indomethacin molecules but the presence of the acetone inhibits the formation of a dense polymer-drug NP. 98

3.18 System A*: (a) Number of contacts between the indomethacin molecules and the blocks of the $mPEG_{350}$ (light blue)-*b*-PCL_{2000} (dark blue) polymer chains. The increase after the contact occurs at 108 ns, demonstrates the dynamic interaction between the indomethacin molecules and the polymer chains. (b) Distance between the centre of mass of the indomethacin NP and the PCL chains, which becomes zero when indomethacin interacts with the polymers. 99

3.19 System A*: Interfacial deposition simulation for the formation of a polymer-drug NP. The spatial distribution of the acetone and water molecules across the x-axis of the simulated box at the start and at 28- ns of the simulation. A satisfactory distribution of the solvent molecules across the box is achieved, and the system is considered fully equilibrated. 101

3.20 System A*: Acetone (pink) replacement during the interfacial deposition simulation of $mPEG_{350}$ (light blue)-*b*-PCL_{2000} (dark blue) polymer chains in the presence of indomethacin (grey). Water is not shown for clarity. PBC conditions apply, where the molecules can move across the end of the box. Snapshots after each 10 ns MD run simulating acetone's "evaporation". The polymer chains and the indomethacin molecules aggregate and form a dense polymer-drug NP of 7 nm diameter. 102

3.21 System A*: End-to-end distances ((a), (c)) and Radius of gyration ((b), (d)) for the different blocks of $mPEG_{350}$-*b*-PCL_{2000} polymer chains for the complete simulation (top row) and the acetone evaporation steps (bottom row). The hydrophobic PCL starts to aggregate thus reducing its spatial conformation. 104

4.1 ^{1}H NMR spectra of PEG350PCL at the end of the reaction (30 minutes). 117

4.2 ATR-IR spectra of mPEG-b-PCL polymers. 118

4.3 Analysis of ΔH measurements from DSC revealed a decrease in the percentage of crystallinity of the PCL block of the copolymers with an increase of the length of the hydrophilic block. 121

4.4 Water contact angle measurements for the assessment of the wettability properties of the polymers. Error bars correspond to the standard deviation calculated from four measurements. The θ values decrease with the increase of the hydrophilic block reflecting the increased hydrophilicity of the polymers. 122

4.5 Hydrodynamic diameter (DLS, Number distribution) of the PEG2000PCL polymer NPs in a range of different polymer in acetone concentrations (mg/ml). Error bars correspond to the SD as measured by the instrument. Hydrodynamic diameter of PEG2000PCL polymer NPs varies according to the concentration from 25 to 50nm. 124

4.6 Hydrodynamic diameter (DLS, Number distribution) of the PEG2000PCL polymer NP prepared from a starting 10 mg/ml polymer in acetone concentration. 125

4.7 Hydrodynamic diameter (DLS) of polymer NPs in a range of high polymer in acetone concentrations (mg/ml). Error bars correspond to the SD as measured by the instrument. NPs formed with PEG550PCL and PEG750PCL were unstable, aggregated and finally sedimented within 24 hours. 126

4.8 Hydrodynamic diameter (DLS) of polymer NPs of all the four diblock copolymers in different polymer in acetone concentrations (mg/ml). Error bars correspond to the SD of 3 measurements. Black filled symbols (dots, squares and triangles) correspond to the polydispersity index values (right graph bar) as reported from the measurements. . . . 127

4.9 Zeta potential of the polymer NPs, in water. Error bars correspond to the SD of 3 measurements. The NP populations exhibit a values larger than -20 mV with the exception of PEG750PCL (-16 mV). 128

4.10 TEM image of the PEG350PCL NPs formed at 0.05 mg/ml starting concentration in acetone. (Size range 143.5±47.4 nm, Scale bar 500 nm). 130

4.11 DLS distribution of indomethacin particles as used in the aqueous phase (1mg/ml). The peak is the average intensity distribution of three measurements. The sonnicated indomethacin particles demonstrate a population of submicron particles of 712(±357) nm diameter (PDI 0.377). . . 133

4.12 POM image of indomethacin particles as used in the aqueous phase; (a) without and (b) with the polariser. Indomethacin is clearly crystalline. (Magnification 10x). . . . 134

4.13 TEM image of indomethacin particles as used in the aqueous phase; the indomethacin demonstrates well defined crystal planes. (Scale bar 2 μm). 134

4.14 Hydrodynamic diameter (via DLS) of indomethacin particles as used in the aqueous phase (grey) and after their exposure to pure acetone during the interfacial deposition (blue). The peak and error bars correspond to the average intensity distribution and SD of three measurements. A clear size reduction has been achieved in the absence of the polymer resulting in pure-drug NP suspensions. 135

4.15 Overlay of 3 DLS samples to show 3 different NP populations: PEG350PCL polymer NPs (green, 0.05 mg/ml), indomethacin sonicated as used in the aqueous suspension (red, 1mg/ml) and the result, polymer-coated indomethacin NP (blue). Each peak corresponds to the average intensity distribution of three measurements. 137

4.16 Hydrodynamic diameter and PDIs (DLS) of polymer-coated indomethacin NPs; indomethacin 1 mg/ml in water, polymers 0.05 mg/ml in acetone. The polymer coated NPs demonstrate sizes significantly smaller than the starting indomethacin population suggesting a new population. Circular dots correspond to the PDI value of the sample. . 137

4.17 DLS measurement of the PEG350PCL-coated indomethacin NP population, before (red line) and after (green line) the centrifugation/purification process. Peak corresponds to the average of 3 measurements. 139

4.18 POM images of the PEG350PCL-coated indomethacin NPs. (a1) and (a2) prior to centrifugation/purification, where uncoated drug particles form aggregates, and (b1), (b2) after the purification where no crystals are observed. (Magnification 10x) 139

4.19 TEM image of the polymer-coated indomethacin NPs in the lowest PEG350PCL concentration used (0.05mg/ml). Scale bar corresponds to 200 nm. The core consists of crystalline indomethacin, while a very thin polymer coating has smoothed the surface of the drug. (Scale bar 200nm). . 140

4.20 TEM image of the polymer-coated indomethacin NPs in the highest PEG350PCL concentration used (1 mg/ml). Scale bar corresponds to 200 nm. The core consists of crystalline indomethacin while the polymer coating is evidently thicker than in figure 4.19. (Scale bar 200nm). 141

4.21 Unpaired t-tests to demonstrate the statistical difference ($p<0.0001$) between the drug-free polymer NPs versus the polymer-coated drug NPs, ($p<0.0001$) and the polymer-free drug NPs versus the polymer-coated drug NPs ($p=0.0006$). Indomethacin (1 mg/ml) was mixed with PEG350PCL (0.05 mg/ml). Error bars correspond to the SD of 9 measurements. 142

4.22 Hydrodynamic diameter and PDIs (DLS) of polymer-coated indomethacin NPs using different indomethacin concentrations and PEG350PCL, PEG550PCL (0.05 mg/ml in acetone) for the coating. In grey, the sonicated indomethacin population, prior to the interfacial deposition, in blue, the control polymer-free indomethacin NPs, while yellow and orange the polymer-coated drug NPs of PEG350PCL and PEG550PCL respectively. The error bars correspond to the SD of 3 measurements. 143

5.1 Thesis map and flowchart, demonstrating the parallel work undertaken during this PhD showing how the timelines of the two tracks coincided. Some key points with reference to the relevant chapter are described in the yellow boxes. . 152

5.2 Interpretation of the phenomena that take place during the modified interfacial deposition. A population of micron-sized indomethacin particles in an aqueous environment is exposed to a flow of polymer and acetone. The drug particles are either broken down, or dissolved due to the synergistic effect of the acetone and the polymers. The polymers are able to coat the surface of the drug NPs, making a population that can be stable due to steric interactions, while the rest of the uncoated drug particles aggregate and finally precipitate during centrifugation. 154

B.1 GPC chromatograph of PEG350PCL. 190

B.2 GPC chromatograph of PEG350PCL. 191

B.3 GPC chromatograph of PEG750PCL. 192

B.4 GPC chromatograph of PEG2000PCL. 193

B.5 DSC of PEG350PCL. 194

B.6 DSC of PEG550PCL. 194

B.7 DSC of PEG750PCL. 195

B.8 DSC of PEG2000PCL. 195

B.9 Indomethacin after the wet-bead milling in the absence of a surfactant. A white foam has been created in the pot resulting in great drug losses. 197

B.10 Indomethacin suspension created by wet-bead milling in the absence of a surfactant. The suspension was very unstable and was sedimenting quickly. 197

B.11 DSC of indomethacin as received. 198

B.12 DSC of freshly cryomilled indomethacin. 198

B.13 DSC of indomethacin as used for the interfacial deposition method, 3 weeks after it was cryomilled. 199

B.14 ATR-IR spectra of freshly cryomilled indomethacin (black line) and as received (red line). The absence of the sharps peaks in the cryomilled sample indicate a lack of crystallinity in comparison with the original state of the drug. . 199

B.15 X-Ray Powder Diffraction spectra of indomethacin as received, after the cryomilling and after 24h. The drug is no longer amorphous during the interfacial deposition. Data from Ghaidaa Hameed. 200

B.16 Reproducibility of interfacial deposition method; Overlay of size measurements (DLS) of 4 batches of polymer NPs formed with PEG350PCL at a 0.05 mg/ml polymer concentration. 201

B.17 Reproducibility of interfacial deposition method; Overlay of size measurements (DLS) of 5 batches of the PEG350PCL-coated indomethacin NPs, (0.05 mg/ml polymer concentration in acetone, 1 mg/ml indomethacin concentration in water.) 201

B.18 Overlay of 3 DLS samples to show 3 different NP populations: PEG350PCL polymer NPs (green 0.5 mg/ml), indomethacin sonnicated as used in the aqueous suspension (red 1mg/ml) and polymer-coated indomethacin NP (blue). Each peak corresponds to the average intensity distribution of three measurements. 202

B.19 Overlay of 3 DLS samples to show 3 different NP populations: PEG350PCL polymer NPs (green 0.1 mg/ml), indomethacin sonnicated as used in the aqueous suspension (red 1mg/ml) and polymer-coated indomethacin NP (blue). Each peak corresponds to the average intensity distribution of three measurements. 202

B.20 Stability of the PEG550PCL polymer NPs in 4 different temperatures, (25, 37, 45 60 ^{o}C) 203

B.21 Stability of the PEG750PCL polymer NPs in 4 different temperatures, (25, 37, 45 60 ^{o}C) 203

B.22 Stability of the PEG350PCL polymer NPs (final polymer concentration in water 0.2 mg/ml): The original measurement in red, the same sample after 1 month in green and the latter after 5 minutes of sonnication. The size distribution is the same in all 3 cases. 204

B.23 Critical Aggregation concentration (CAC) as measured by DLS. 204

List of tables

3.1 United atom acetone models: Diffusion in SPC water . . . 73

3.2 Systems for the formation of polymer NPs 85

3.3 Systems for the Interfacial Deposition in the presence of an indomethacin NP 85

3.4 Radius of gyration (nm) of PCL_{2000} block compared with the existing literature and models. 110

4.1 Polymer and monomer characterisation by ^{1}H NMR ^{a}, GPC ^{b} and DSC 120

4.2 UV-Vis measurements for the determination of drug loading and the entrapment efficiency of the method when using indomethacin in the aqueous phase (1 and 0.5 mg/ml). 144

Nomenclature

Acronyms / Abbreviations

ϵ-CL	epsilon-Caprolactone
API	Active Pharmaceutical Ingredient
ATR-IR	Attenuated Total Reflectance-Infrared Spectroscopy
CAC	Critical Aggregation Concentration
$CHCL_3$	Chloroform
DCM	Dichloromethane
DDS	Drug Delivery System
DLS	Dynamic Light Scattering
DLVO	Derjaguin-Landau-Verwey-Overbeek
DP	Degree of Polymerisation
DPI	Dry powder inhaler
DSC	Differential Scanning Calorimetry
EM	Energy Minimisation
FNP	Flash Nanoprecipitation

GPC	Gel Permeation Chromatography
IONP	Iron Oxide Nanoparticle
LJ	Lennard-Jones
MD	Molecular Dynamics
mPEG	Monomethoxy poly(ethylene glycol)
MSD	Mean Square Displacement
NMR	Nuclear Magnetic Resonance
NP	Nanoparticle
NSAID	Nonsteroidal anti-inflammatory drug
OPLS	Optimised force field for Liquid Simulations
PBC	Periodic Boundary Conditions
PBE	Population balance equation
PCL	Polycaprolactone
PDI	Polydispersity Index
PEO	Poly(ethylene oxide)
PGA	Poly-glycerol adipate
PLA	Poly(lactic acid)
PLGA	poly(DL-lactic-coglycolic acid)
pMDI	Pressurised metered dose inhaler
PME	Particle-Mass Ewald

POM	Polarised Optical Microscopy
PPO	Poly(propylene oxide)
QM	Quantum Mechanics
SPC	Single Point Charge
TEM	Transmission Electron Microscopy
WBM	Wet Ball Milling
WCA	Water Contact Angle

CHAPTER 1

Introduction

This thesis describes research into the formation of polymer-coated drug nanoparticles (NPs) through the combination of both experimental and computational methods. Drug NPs can be coated with polymer via a method called interfacial deposition [1, 2] which is a solvent displacement method. The outcome of this method is an aqueous polymer-coated drug NP suspension which falls under the category of polymer-based drug delivery systems (DDS).

In this chapter the motivation that spurred this work will be discussed. The concepts of "polymers as Drug Delivery Systems (DDS)" and "polymer-drug NPs" will be introduced and the main experimental methods used for their preparation will be discussed. In addition to the experimental part, the theoretical approaches via computational methods will be introduced, followed by a discussion over the current state and successes of the field.

1.1 Motivation

1.1.1 Nanoparticles as drug delivery systems

An ideal drug delivery system (DDS) is non-toxic, biodegradable and biocompatible, able to encapsulate sufficient amount of drug to provide a therapeutic action, which then will be successfully released in a specific target. From a practical perspective, it has to be cheap, easy to manufacture, and stable prior its administration.

One of the main DDS that have attracted a lot of interest in the pharmaceutical field are nanoparticles (NPs). NPs are usually particles in the range of 10-500 nm (diameter). Categories include polymer and inorganic NPs, liposomes and carbon nanotubes among others. NPs can be sophisticated, cost-friendly, easy to make and can combine properties to meet the needs of each delivery system; they can have targeting ligands, modified surface chemistries, different shapes and thus physical properties. An illustrative summary of all the above can be seen in figure 1.1.

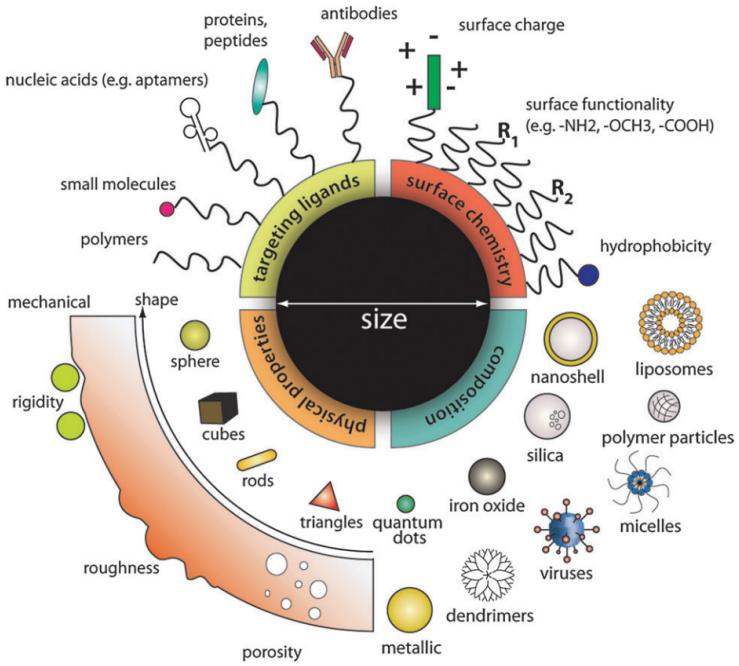


Fig. 1.1 NPs can be modified according to their physical properties, their composition, surface chemistry and target ligands for specificity. This flexibility allows the design of multifunctional NPs that can be used as DDS and contrast agents. Taken from [3].

More importantly NPs attract interest not just due to their fine-tuning but their small sizes. Particles with sizes in the nanoscale have an enormous surface area which increases their saturation solubility. The dependence of the saturation solubility of the particles with their radius is described by the Ostwald-Freundlich equation (eq. 1.1.1, [4]):

$$ln\frac{S_s}{S_0} = \frac{2M\gamma}{RT\rho r} \tag{1.1.1}$$

where S_s is the saturation solubility, S_0 the solubility of a flat solid sheet (when r$\rightarrow \infty$), γ is the interfacial tension on solubility, M is the molar weight of the solid, R is the gas constant, T is the absolute temperature, ρ is the density of the solid substance and r is the radius of the particles. Reducing the size of the particles cause an increase in the drug's solubility.

At the same time their dissolution kinetics is accelerated; this is described in the Noyes-Whitney equation [5]:

$$\frac{dc_x}{dt} = \frac{DA}{h}(S_s - c_x) \tag{1.1.2}$$

where $\frac{dc_x}{dt}$ is the dissolution rate, A is the surface of the particle, D is the diffusion coefficient, h is the thickness of the diffusional layer, S_s is the saturation solubility of the drug and c_x is the concentration in the surrounding liquid at time x. Reducing the particles' size leads to an increase in the surface area (A) and thus, from equation 1.1.2, to an accelerated dissolution rate.

These effects are very important especially when considering formulations of drugs that exhibit low aqueous solubility. It is estimated that 40% of the existing substances and 70-90% of the new candidate APIs are poorly soluble in water [6, 7, 8]. Lipophilic or hydrophobic APIs can penetrate a cell membrane to be absorbed, however they demonstrate poor bioavailability and can precipitate uncontrollably after dosing [8]. Particle size reduction in order to improve the formulations' performance has been established in the pharmaceutical industry as a common strategy and can be achieved via various techniques like high pressure homogenization (HPH), wet ball milling (WBM), and flash nanoprecipitation (FNP). The latter two are of specific interest to this thesis and will be discussed in more detail later in this Introduction.

Nanoparticles demonstrate enhanced biodistribution and efficacy; there are 51 FDA-approved nanoparticle formulations that either act as therapeutics or as imaging agents with 77 more currently being in clinical trials (figure 1.2) [9, 10]. Two successful polymer-based nanoparticles are Copaxone® and Neulasta®. Copaxone® is a large amino-acid based poly-

mer used for multiple sclerosis while Neulasta® is a PEGylated protein used in chemotherapy.

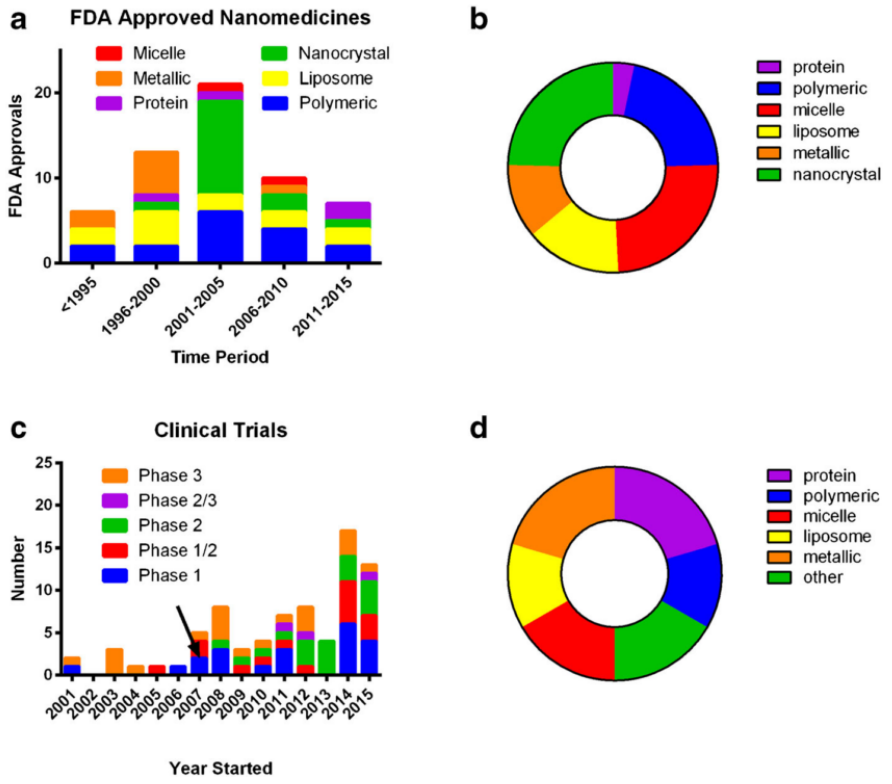


Fig. 1.2 FDA approved nanoparticles per year (a) and per catergory (b). Data from clinicaltrials.gov stating the different phases of nanoparticles under clinical trials (c) and per category (d). Taken from [10].

1.1.2 Interactions between nanoparticles

Whether the NPs are in a dry-powder like-form or in a liquid suspension, the stability of the formulation depends on the interparticle forces, as these can cause instability issues. In general, once insoluble particles are placed in a liquid, they can follow any of the three following routes; they can remain dispersed, bind loosely together (agglomerate) or bind strongly together (aggregate). All these phenomena are illustrated in figure 1.3.

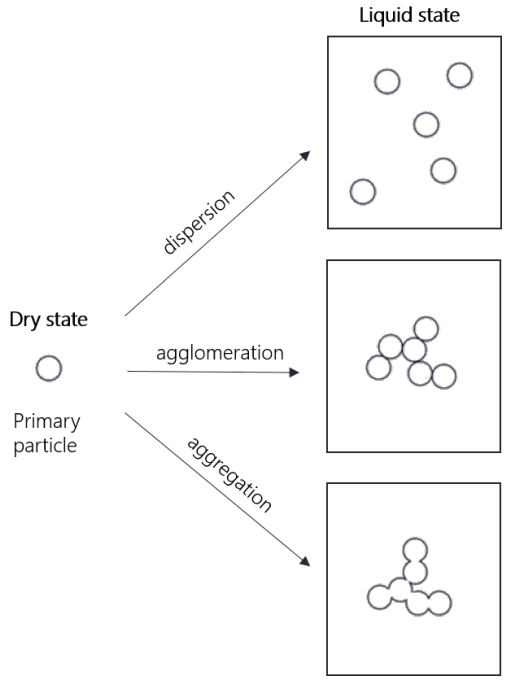


Fig. 1.3 Fate of insoluble particles when dispersed in liquids. Adapted from [11].

According to the Derjaguin-Landau-Verwey-Overbeek theory (DLVO) [12, 13, 14], the main factor that determines the particles' stability is the interparticle forces that are developed. These forces consist of the attractive van der Waals and the repulsive electrostatics [15, 16]. If the particles have a surface coating as well, then steric forces are added to the repulsive sum. Thus, the main factors that affect the aggregation or agglomeration behaviour of NPs are their primary size, the surface charge, and the surface coverage. Each of these parameters has to be carefully evaluated when a NP formulation is under investigation.

1.1.3 Nanoparticles in pulmonary delivery

1.1.3.1 The exciting challenge of drug delivery to the lungs.

The lungs are an ideal organ for the delivery of drugs designed for systemic disorders due to the large surface area (80 - 140 m^2), the good vascularisation, the thin alveolar epithelium (0.5 - 1.0 μm), as well as the ability for solute exchange and the avoidance of first-pass metabolism [17, 18, 19]. In order to achieve systemic delivery through the lungs, the drug has to reach in the deep lung region, called the alveolar region (figure 1.4).

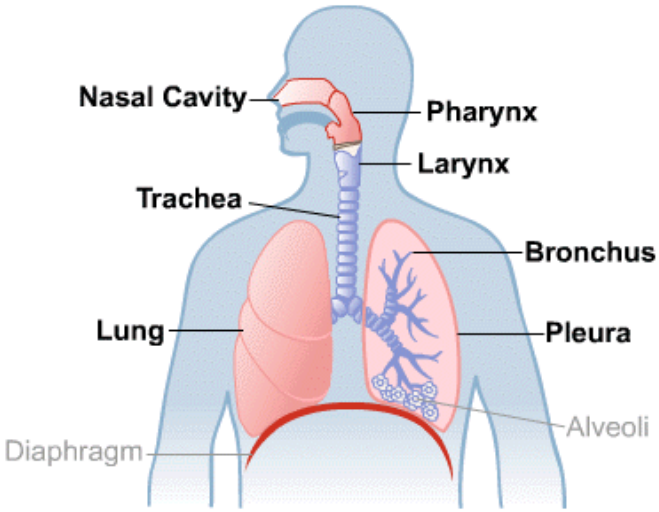


Fig. 1.4 The respiratory system. Particles are inhaled through the mouth and can impact on the pharynx and the bifurcations in the respiratory system. As the particle passes deeper into the lung the processes of sedimentation and diffusion become more important. Taken from [20].

Three main delivery systems have been devised for pulmonary delivery and these are the pressurised metered dose inhaler (pMDI), the nebuliser, and the dry powder inhaler (DPI). In this thesis interest focuses on the latter, the DPI.

DPIs are breath-actuated devices that deliver a dry powder drug through shear-induced aerosolization [21]. Due to this fact, drug deposition in the lungs using DPIs is affected by the patient as well as by the physical properties of the aerosols (figure 1.5). From a drug delivery viewpoint, the airway anatomy and breathing pattern of the individual (flow rate, breath-holding, ventilation volume) and the time of aerosol pulse injection in the breathing cycle play a critical role in determining the particle deposition [18, 22].

The aerosol performance is affected by the dry powder formulation and by the design of the inhaler device. In terms of the formulations, the particle size and the presence of carriers are the two main parameters affecting particle deposition.

The particle size can be best described by the aerodynamic diameter d_{aero} which is given by equation 1.1.3:

$$d_{aero} = d_{geo}\sqrt{\frac{\rho}{\rho_{ref} * \gamma}} \tag{1.1.3}$$

where d_{geo} is the geometric particle diameter, ρ is the particle density, ρ_{ref} is the reference density (typically 1 g/cm^3) and γ is a shape factor (1 for spherical particles)[23].

Particles with aerodynamic diameter larger than than 5 μm are filtered out in the upper airways (mouth and throat) while when in the range of 1-5 μm diameter, particles are considered to result in increased deep lung deposition (alveolar region, figure 1.4) [23, 24].

Powder particles that have been finely milled (aerodynamic diameter less than 1 μm) display high cohesive forces, have a high probability to agglomerate uncontrollably, do not flow freely and can be exhaled [23].

In order to deal with this it is common to use larger carriers like lactose to increase the aerodynamic size of the particle [25]. It is important that these carriers are formulated correctly both to ensure a consistent manufacturing process and to have effective action as a medicine [26]. The use of carriers/excipients affects the biophysical properties of the particles (size, charge, shape, density) thus their deposition and uptake, leading the industry to investigate other particle formulations.

At the same time the formulation strategy has to be revisited for every different compound under investigation. This results in great losses, both from an economical and a manufacturing point, in the pharmaceutical industry. An overview of the formulations' complexity and the factors affecting deposition is presented in figure 1.5. Each one of the steps has to be revisited when the original compound (Active pharmaceutical ingredient - API) differs.

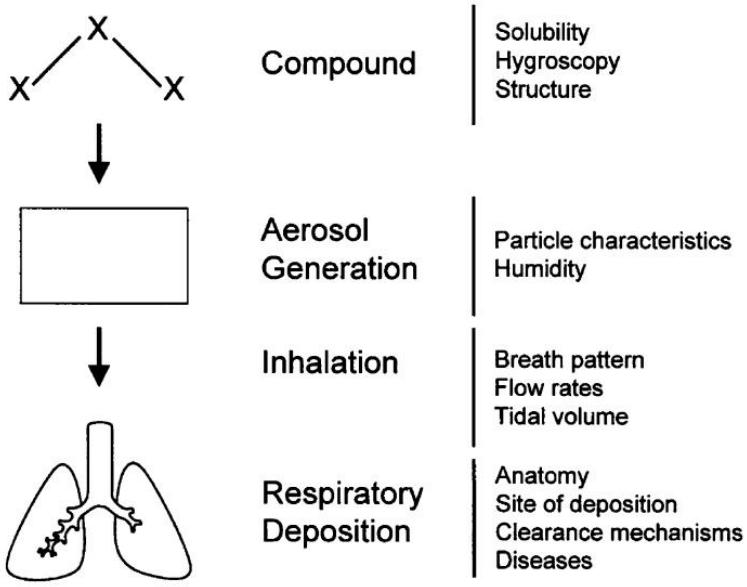


Fig. 1.5 Factors influencing the deposition of a particle in the lungs. Taken from [22].

NP formulations aiming to be deposited in the lower respiratory system face many stability problems. As the particle size decreases, the cohesion between the particles increases and they undergo Ostwald ripening (causing the larger particles to grow on the expense of the smaller ones [27, 28]) or even secondary crystallization. This leads to uncontrolled aggregation and then their deposition would no longer be governed by just diffusion and breath-holding. Also from a industrial manufacturing point, this cohesive behaviour is resulting in great drug loss during the manufacturing process.

It has been reported that particles of 100-200 nm size remain for longer periods in the lungs in comparison to micro-sized particles [29]. At the same time, although they can be deposited throughout the lungs, approximately just a 20% is deposited in the desired alveolar region [30].

Taking into consideration that the optimal particle aerodynamic diameter for alveolar deposition should be in the range of 1-3μm [31], different approaches to use NPs in pulmonary delivery have been studied in an attempt to create a "Nano-in-Micro" DDS; this ideal DDS should combine the benefits of a NP formulation with the aerodynamic behaviour of the microparticles. Two main approaches exist in order to achieve such DDS: the creation of porous micron-sized particles, and the formation of NP agglomerates.

One example of the first approach is the work of Tsapis et al. [32] where NPs were formulated into hollow structures. In that way, according to equation 1.1.3, their density is smaller but their aerodynamic diameter is increased so they can be deposited in the desired alveolar region [18]. In a more recent study, Hu et al. [28] created pure sodium cromoglicate porous NPs for improved aerosol performance.

On the latter approach, NPs that agglomerate in a controlled manner should be formed. NP agglomeration is affected by the primary particle size [33] and it results in changes of the total particle area, the surface properties, the aerodynamic parameters and in the end, the uptake by the targeted cells and eventually the actual delivered dose [34, 16]. As a phenomenon it has been studied in the fields of material manufacturing, air pollution, toxicology and atmospheric sciences [35, 36, 11].

Various groups have reported such NP agglomeration deliveries: Bhavane et al. worked with agglomerates of ciprofloxacin [37, 38], El-Gendy et al. focused more on asthma therapeutics studying fluticasone - albuterol [39]. Salem et al. synthesised agglomerates of theophylline (a poorly water-soluble drug) with the use of surfactants and ionic solutions, that were stable and with sizes in the desired range [40]. Shi et al. have formed biodegradable nanoparticle flocs using poly(DL-lactic-coglycolic acid) (PLGA) NPs that were coated with oppositely charged polyelectrolytes [23]. The electrostatic interactions between the two populations induced the self-assembly of the agglomerates. More recently, Strydom et al. reported a layer-by-layer coating approach with polyelectrolytes using four hydrophobic drugs [41].

1.1.4 Initial motivation

It is clear from the previous discussion that NP agglomerates for lung delivery of APIs with low aqueous solubility are under evaluation since they have the potential to achieve deep lung delivery. It would be ideal to produce soluble NPs that agglomerate in order to have the correct aerodynamic size and behaviour for lung delivery but then de-agglomerate in the lung ready for rapid dissolution. In the present work, this *Nano-in-Micro*

DDS was envisioned to be achieved by the formation of polymer-coated drug NPs.

Since the agglomeration of the NPs would be affected only by the surface chemistry of the coated drug NPs, then polymer-coated drug NPs containing a different API in the core, would agglomerate in the same manner (i.e. have the same delivery behaviour). This would have a huge impact on the trial-and-error approach that currently exists in the pharmaceutical industry as it would mean that the delivery technique would be transferable to other APIs.

In figure 1.6 the three motivations/questions that lead this work are illustrated:

1. Can we form a polymer-coated drug NP? This NP was envisioned to have a pure drug core and a polymer coating. The idea behind this type of NP emerged from previous work by Abushrida et al. [2] that successfully produced polymer-coated iron oxide NPs (IONPS) and will be discussed in more detail in the following section. Assuming the polymer is a diblock copolymer consisting of a hydrophobic and a hydrophilic block, it is expected the hydrophobic block will interact with the drug NP- core while the hydrophilic will provide the steric stabilisation of the NPs.

2. Once this polymer-coated drug NP is formed, will it produce loosely bound agglomerates with the appropriate aerodynamic diameter?

3. What effect does the length of the hydrophilic chain has on the size of the agglomerates? What is the ideal length for the steric stabilisation of the NPs?

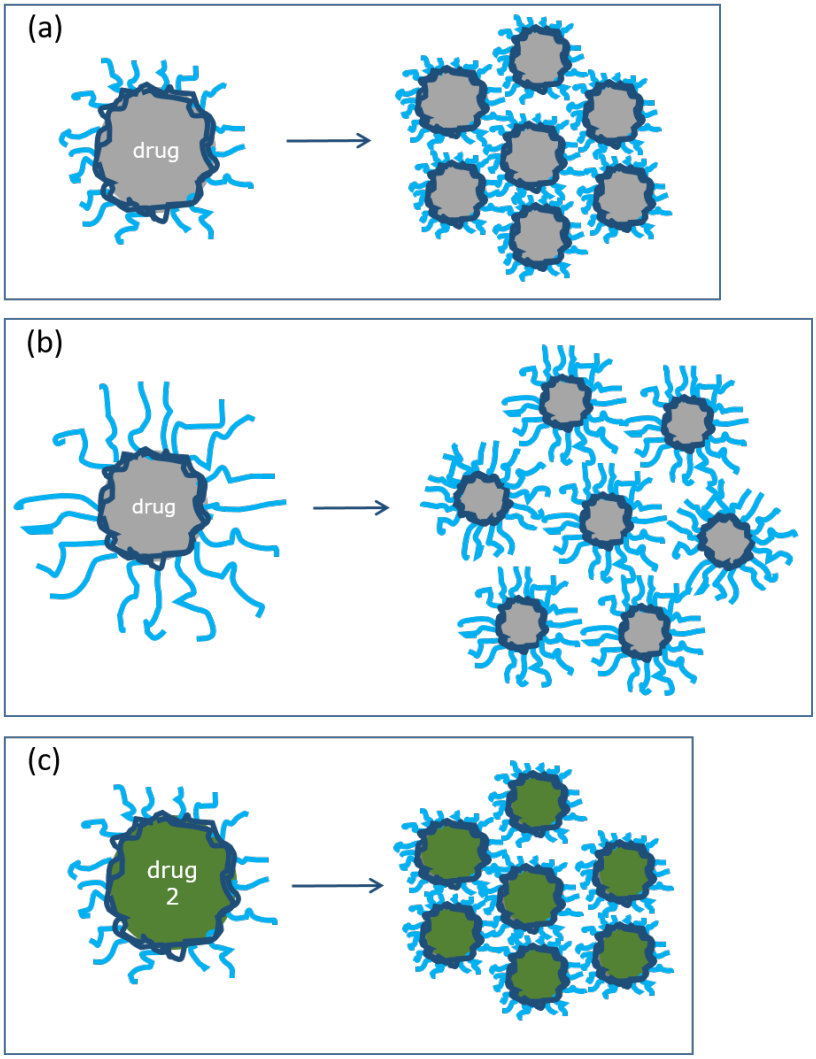


Fig. 1.6 The main questions and motivations that lead this work involve polymer-coated drug NPs. The hydrophilic (light blue) chain of the polymers plays a critical role in the steric effects between other similar NPs while the hydrophobic (dark blue) chain interacts with the drug NP (grey/green) through hydrophobic interactions. The main questions derived from the motivation of the present work are; (a) Can we form polymer-coated drug NPs in which the core is a pure drug NP? Can these polymer-coated NPs form agglomerates of 1-3μm to achieve deep lung deposition? (b) What are the properties of the polymers needed to coat the drug NPs and how will the length of the hydrophilic polymer block affect the agglomerates? (c) The surface chemistry of the polymer-coated drug NPs will be the key parameter affecting their agglomeration and thus their aerodynamic behaviour. Can we coat different drug NPs that will then exhibit the same delivery behaviour?

Although all of the above questions were the starting point of this PhD, the work presented in this thesis focuses on the first part; Can we translate an existing inorganic NP preparation method to form polymer-coated drug NPs? What type of interactions are important in this coating?

To answer these questions, a combined approach was adopted: both experimental and computational methods were used, in order to provide an holistic overview of the coating method and to understand the governing interactions. The information retrieved would allow any future work to be more focused and less trial-and-error based.

In the next sections a more detailed discussion over the current state in NP formulation methods, both from the experimental and the computational field, will be presented. The use of amphiphilic copolymers as DDS will be analysed, and a comparison between the various NP preparation methods currently employed will be analysed. An overview of the computational simulations field and the current state follows, alongside some recent developments. In each of the above sections, the importance or relevance with the present work will be further discussed.

1.2 Polymers in Drug Delivery Systems

Polymer-based DDS have attracted a lot of interest in the past decades. The plethora of biodegradable polymers that can be tailored to meet the needs of the drug delivery system is one of the reasons behind the ever increasing research in the field. In particular some of the most popular systems are based on amphiphilic block copolymers that consist of a hydrophilic block and a hydrophobic block and can self-assemble when in aqueous medium [42].

The self-assembly in an aqueous environment leads to the formation of polymer particles, (micelles) that usually have narrow size distributions in the nano-scale range. The hydrophobic segments are in the inside core of the particle, while the outer shell consists of the hydrophilic part. During the micellisation process, the hydrophobic block could assist a drug loading process, in which drug molecules, usually hydrophobic, can be encapsulated inside the core. This would result into a polymer-drug nanoparticle, that due to its hydrophilic shell and its small size can be easily distributed throughout the body [43]. The importance of the size of the particles in DDS has been previously discussed. The size of the blocks can be easily modified to improve many parameters like the hydrophilic/hydrophobic ratio, the critical micellar concentration (CMC), the size of the final micelle among others.

Poly(lactic acid) (PLA) is one polymer that has attracted interest over the past years due to its biocompatibility. Riley et al. [44] performed studies using PEG_{5000}-PLA, varying the length of the PLA in order to assess the effect this would have in the formation of polymer NPs. It was found that for a range of PEG:PLA molecular weight ratios, the hydrodynamic size of the NPs was scaling linearly following $N_{PLA}^{\frac{1}{3}}$ where N_{PLA} corresponds to the monomer PLA units of the block. Garofalo et al. reported different tree-shaped structures for PEG_{2000}-PLA and their effect on the micelle formation [45].

Other polymers of interest are Pluronics (or Poloxamers). These triblock copolymers consist of hydrophilic poly(ethylene oxide) PEO and hydrophobic poly (propylene oxide) (PPO) in the sequence PEO-PPO-PEO. The hydrophilic to hydrophobic ratio can be easily tuned by the length of the chains, affecting the properties of the polymers such as their CMC and their critical micellisation temperature [46]. This fine tunability

has led Pluronics to be extensively used in the pharmaceutical industry in order to increase the solubility of lipophilic drugs [47].

The fact that the polymers can be tailored to meet the needs of each system has made them an ideal candidate for DDS. However as briefly discussed before, there are a plethora of different polymers in the literature and constantly novel polymers with new and enhanced properties are presented. It is not the purpose of this introduction to provide a full review on the current state of polymers in DDS. Our attention is focused to DDS using monomethoxy poly(ethylene)-*b*-polycaprolactone (mPEG-*b*-PCL) dibock copolymers.

1.2.1 mPEG-*b*-PCL polymers in DDS

mPEG-*b*-PCL diblock copolymers have been used and studied by many groups [48, 49, 50, 51, 52, 53]. Both mPEG and PCL are polymers that are well-tolerated by humans and approved by the Food and Drug Administration (FDA) for DDS.

PEG is hydrophilic, soluble in organic solvents, non-toxic and industrially available at a low cost [54]. It has been reported that when PEG has been used to coat NPs of 100-200nm for pulmonary delivery, the NPs were able to penetrate the human airway mucus [55]. However PEG is not biodegradable, and one alternative to couple it with is a polyester, like PCL. PCL is a biocompatible, hydrophobic polymer of semicrystalline nature. The presence of the ester groups in the polymer backbone makes it biodegradable as they can be cleaved either by passive hydrolysis or by enzymnatic reaction [56]. It's degradation behaviour can also be controlled via the length of the PCL block [57].

mPEG-*b*-PCL polymers are synthesised via Ring Opening polymerisation; the mPEG is the macroinitiator and the catalysts can be metals like Stannous Octoate [48, 58], calcium ammoniate [49] or organic catalysts [59]. Bogdanov et al. [60] synthesised and studied the thermal properties of mPEG-*b*-PCL in three different structural types: diblocks, star copolymers and triblock copolymers. It was reported that the melting behaviour and the crystallisation of the polymer is dependent on the chain lengths. On a similar note He et al. [49] studied mPEG-*b*-PCL using mPEG chains of either 2000 or 5000 Da and PCL chains between 2000- 33000 Da. The group reported the effect PEG had on the crystallisation of the PCL chains; if the PEG chain is longer than the one of PCL it will crystallize faster and will cause an imperfect crystallisation of PCL.

Consequently, mPEG-*b*-PCL polymers have already been investigated for the delivery and controlled release of many drugs, including the anti-cancer drugs paclitaxel [61] and docetaxel [62], the nonsteroidal anti-inflammatory drug (NSAID) indomethacin [63, 53, 64], ibuprofen [64] albumin [48, 50] among others.

In the following sections the techniques used to form such polymer-drug NPs will be presented, and this will be expanded to the general field of NP preparation techniques for the pharmaceutical industry.

1.3 Nanoparticle preparation techniques

1.3.1 Polymer-drug nanoparticles

Polymeric NPs, i.e. polymer-drug bearing NPs, can be produced in various ways. One of the most used methods is nanoprecipitation. Nano-

precipitation, also known as "co-solvent" or interfacial deposition method, involves an organic phase where the polymers and the API are dissolved and an anti-solvent medium where the polymers are insoluble (in most cases this means water). The selection of the organic phase is important as it has to be a solvent miscible with the anti-solvent. The polymers used in nanoprecipitation are amphiphilic.

The organic phase is added in the anti-solvent leading to the formation of the polymeric NPs due to hydrophobic forces: as the polymers' surrounding environment changes from the favourable-organic to the unfavourable-aqueous, the polymers collapse in order to form a NP or a micelle. During this process, drug molecules in vicinity can be encapsulated into the polymer matrix, forming the final polymeric NP. As a final step, the organic solvent is slowly removed.

The amount of literature for polymeric NPs formed via the above method is huge and outside the scope of this Introduction. We focus on some examples of polymeric NPs of interest to this project. Fessi et al. [1] were the first to introduce the interfacial deposition method and used PLA and acetone as the organic phase to prepare indomethacin loaded NPs. Shin et al. [65] and Kim et al. [53, 66] have also prepared mPEG-*b*-PCL indomethacin loaded NPs with average diameters of less than 200 nm.

In order to enlighten the critical parameters that affect the formation of the NP, de Oliveira et al. [67], used PLGA to form unloaded polymer NPs using different polymer concentrations, organic solvents, temperature and ionic strength. It was observed that the size of the NPs can be tuned according to the needs of the system via changes in the nature of the solvent or the polymer concentration.

1.3.2 Pure Drug nanoparticles

A lot of discussion in the recent decades has been around the production of "pure drug NPs" also referred as drug nanocrystals. In comparison to any other nanoparticulate systems like the polymer-drug NPs presented above, drug NPs consist mainly of pure API [68]. Forming drug nanocrystals is considered to be a robust approach, aiming at the creation of formulations for the delivery of poorly water soluble drugs: as discussed above, the high surface area of the NPs enhances their dissolution kinetics as well as their saturation solubility. However, the small size of the drug NPs increases the instability of the system as due to the high free energy, the NPs can undergo Ostwald ripening [27] or agglomerate.

In order to ensure the stability of the drug NPs, surface stabilisers are introduced in the various nanosizing methods. The stabiliser usually is amphiphilic, able to improve the solubility of the poorly soluble API via its hydrophilic part and to stabilise the NPs in the suspension medium via its hydrophobic part. Various polymers have been used in the formulations, like Pluronics, polyvinyl alcohol and polyvinyl pyrrolidone among others [69, 68].

The techniques employed for the formation of the drug NPs are categorised in either top-down or bottom-up methods, both of which are discussed in the following sections and are illustrated in figure 1.7.

1.3.2.1 Top-down techniques

Top-down methods to produce drug NPs are based on comminution; the starting material is usually a solid powder, with particles larger than the wanted NP population. Particle size reduction is achieved via mechanical

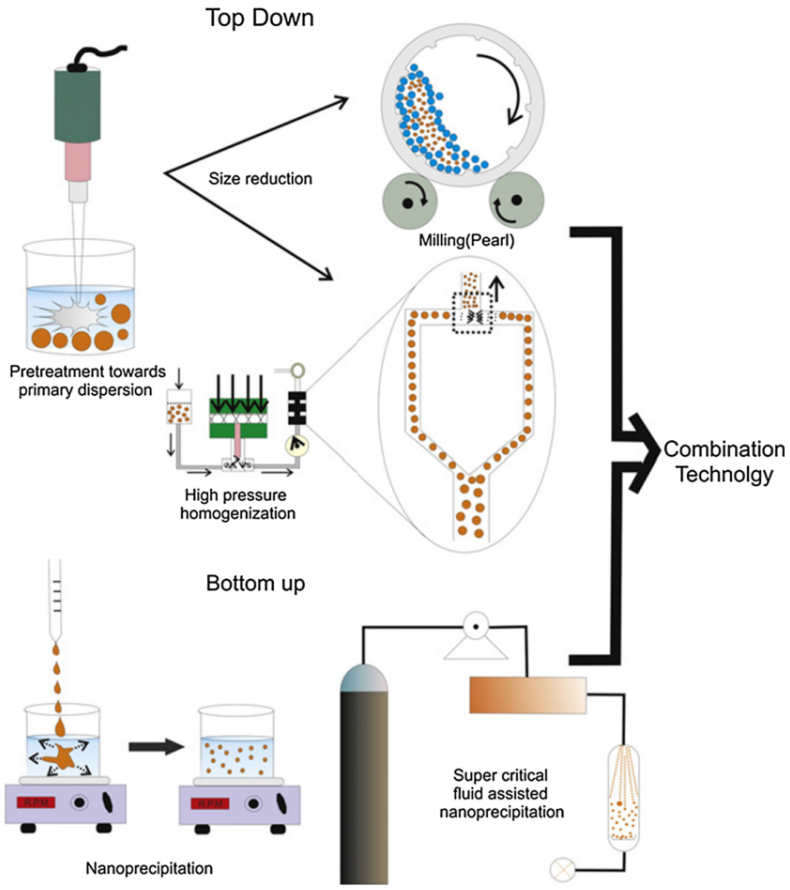


Fig. 1.7 Manufacturing techniques used to produce drug NPs. Top-down methods include techniques like milling and homogenization. Bottom-up techniques are usually based on nanoprecipitation, where NPs will be formed after the removal or evaporation of the solvent. Taken from [68].

methods like milling (wet or jet) or high pressure homogenisation (HPH) [25, 70, 71]. Wet ball milling (WBM) and HPH are scalable and reliable, making them the most mature top-down techniques used to produce drug NPs with narrow size distributions [72]. For the needs of this thesis focus will be on formulations produced by WBM.

WBM is performed in a milling chamber: milling pearls (or beads), the drug powder, stabilisers and an antisolvent medium (usually water) are placed inside a pot. The pot is then rotated at high speed in order to cause the rotation of the grinding beads and the drug powder particles

are crushed into smaller sizes. The grinding media can be made from glass, zircon oxide, or polysterene (PolyMill^{TM}) and their size affects the final drug NP size.

During WBM, many phenomena take place; the drug particles are broken down and can be either dissolved or precipitate, while the polymers can be absorbed on the surface of the drug particles or form micelles. The polymer micellisation is an unwanted phenomenon that depends on the polymer's concentration as it competes with the surface absorption [73]. The final suspension is collected and analysed, or further processed. Usual reported sizes for the NPs produced via WBM are in the range of 100-400 nm [5, 74].

The advantage of WBM is that almost any API can be processed via this technique [6]. It remains then to find a suitable stabiliser to use in the formulation. Unfortunately, this is the Achilles heel of the technique as the selection of the optimum polymeric stabiliser is non trivial and there is a lack of understanding of the issue. In an attempt to elucidate this, Lee et al. [73] employed 11 drugs of low aqueous solubility, high melting points and relatively high molecular weights, and 5 polymers among which Pluronics (F68, F127) and PEG. F68 was the most versatile in terms of successfully produced drug nanosuspensions, however no apparent trend in the selection of the polymer was presented.

Liu et al. [75] used 4 stabilisers at 4 different concentrations on indomethacin and itrazonazole. It was reported that F68 when used at a very high concentration (80 wt% to drug amount) produced fine nanosuspensions (figure 1.8, (B)) which was attributed to the low molecular weight of F68 which could have higher kinetics in the surface absorption, and thus produce better nanosuspensions.

In a more recent work, Liu et al. [76] studied again indomethacin with 5 stabilizers and reported that the best binding efficiency was achieved with Pluronics L64, which performed better than F68. The authors discussed that this was due to the protruding PEO chains; F68 has longer PEO chains which provide steric stabilisation but can also prevent other polymer chains to be absorbed close to each other.

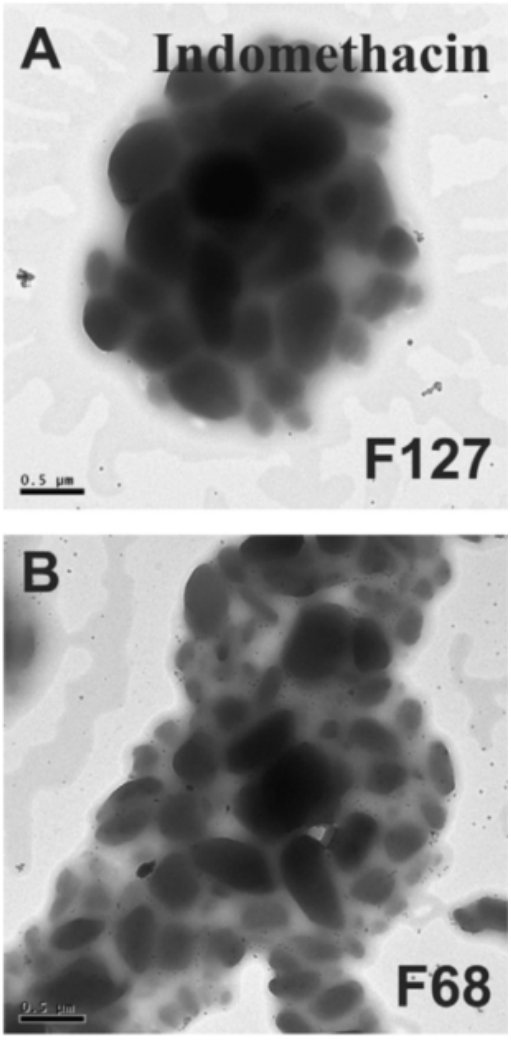


Fig. 1.8 TEM images of indomethacin suspensions milled with F127 (A) and F68 (B). Scale bar of 0.5 μm. Taken from [75].

All of the above add up to the fact that choosing the right stabiliser for WBM is still based on trial-and-error. At the same time, WBM is time consuming, can possibly induce contamination from the milling

materials [5], can induce amorphicity leading to formulation instability, and requires a lot of energy. To our knowledge inhaled drugs produced via WBM have not been yet approved.

For a more detailed description of WBM, the reader is pointed towards the reviews of Van Eerdenbrugh [72] and Moschwitzer [5].

1.3.2.2 Bottom-Up techniques

Bottom-up techniques for the formation of drug NPs are based on the nanoprecipitation method as described above. The NPs are prepared from dissolved drugs via a controlled crystallisation.

One of the methods used is Flash Nanoprecipitation (FNP). FNP is a rapid procedure where the mixing conditions affect the final NP distribution [77]. The drug molecules are completely dissolved in an organic solvent, in the presence of a stabiliser. This stabiliser is an amphiphilic block copolymer that self assembles in an aqueous environment. If a condition of high supersaturation is imposed on the system, nucleation begins and the drug particles start to crystallise and to grow. This condition is created when a stream of anti-solvent (water) is mixed rapidly with the organic phase. The drug molecules and the polymers precipitate simultaneously. The polymer then is adsorbed onto the drug NP's surface due to hydrophobic interactions. Via this surface absorption, the nucleation is inhibited resulting into small particle sizes, and the NPs formed are stabilised.

When the solute is a hydrophobic API, a low ratio of organic solvent to water is preferred, as it results in high supersaturation levels, i.e. the formation of the NPs is favoured [77]. The organic solvent needs to be

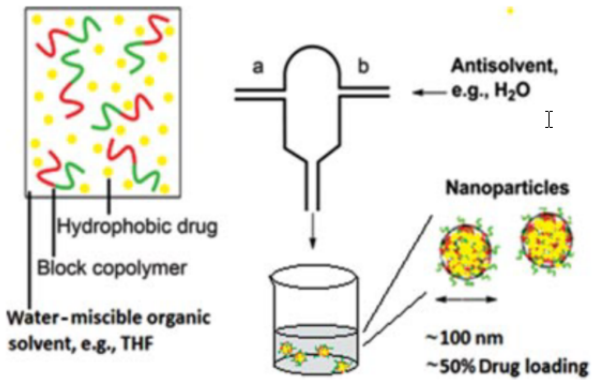


Fig. 1.9 Schematic of Flash Nanoprecipitation technique. Taken from [78].

carefully selected as if it is not removed completely at the end of the process, it can cause instability or toxicity [70].

FNP can take place in various chambers: starting from the simple T-mixer there are also Confided Impingement Jets mixer (CIJ) [78], and multiple inlet vortex mixers (MIVM). Since the only requirement for FNP is the creation of turbulent mixing conditions in a confined space, other mixing geometries can also be considered, but we will focus on research conducted using either T-mixers or CIJs.

Johnson et al. [79] used FNP to produce PS-*b*-PEO β-carotene loaded NPs. Kumar et al. [80] used PS-b-PEO and Pluronics P407 to form NPs with itraconazole and odanacatib in order to evaluate the physical parameters that affect the NP formation. It was discussed that solubility parameters relating to the drug solute and the hydrophobic block of the polymer greatly affects the stability of the formed NPs. Pustulka et al. [81] used PEG-*b*-PCL and PEG-*b*-PLGA with varying hydrophobic lengths to form NPs with β-carotene and curcumin [81]. It was reported that PEG_{5000} is an ideal hydrophilic block however, the molecular weight of the hydrophobic block did not affect the particle size, but the properties of the polymer (glass transition temperature) did play a role.

In comparison with WBM, nanoprecipitation by solvent-anti solvent mixing is appealing as it is scalable, cost-effective, fast and easy. At the same time combinations of drugs can be used and the NP can be more easily tuned. This has also lead into the investigation of the parameters that are important using computational methods and more precisely Computational Fluid Dynamics (CFD). Di Pasquale has used CFD and molecular dynamics simulations [82, 83] to model the solvent−displacement which leads to the formation of NPs, and improved the classical nucleation model to account for the changing solvent composition. Finally, Lince et al. [84], studied the efficiency of the mixers geometry via CFD and reported that CIJs perform better than T-mixers and that the velocity of the mixing is a critical parameter.

Should the reader be more interested in FNP, we suggest the reviews by Saad et al. [77] and D'Addio [29].

1.4 Reducing trial and error in the lab: the use of computational approaches to provide answers

Despite the sophisticated DDS that have been presented above, there is an increasing need to understand the basic principles that lead to a successful DDS. This requires knowledge of the fundamental interactions between the moieties that comprise the systems mainly through their chemical characteristics. A useful tool that sheds light on molecular interactions is computer simulation. With the increase of the computational power year-by-year, simulations provide invaluable information of the interactions that take place at a molecular level and of the physicochemical properties of both the drugs and the carriers.

In general, computer simulations describe the physical representation of a given system. According to the level of detail required for this description, simulations can be used to model systems from the picosecond and Angstrom time and space scales, up to second and meter scales. A visualisation of the different levels of detail are presented in figure 1.10.

The highest level of detail is achieved by Quantum Mechanics calculations, were electronic properties can be calculated. However in such a level it is impossible to investigate dynamic phenomena that evolve through larger time scales like NP formation; the amount of calculations needed would surpass the computational power available.

In order to accelerate the simulations, the degrees of freedom need to be constrained; rather than calculating the electronic properties explicitly, the charges are assigned to atoms as point charges. The atoms then inter-

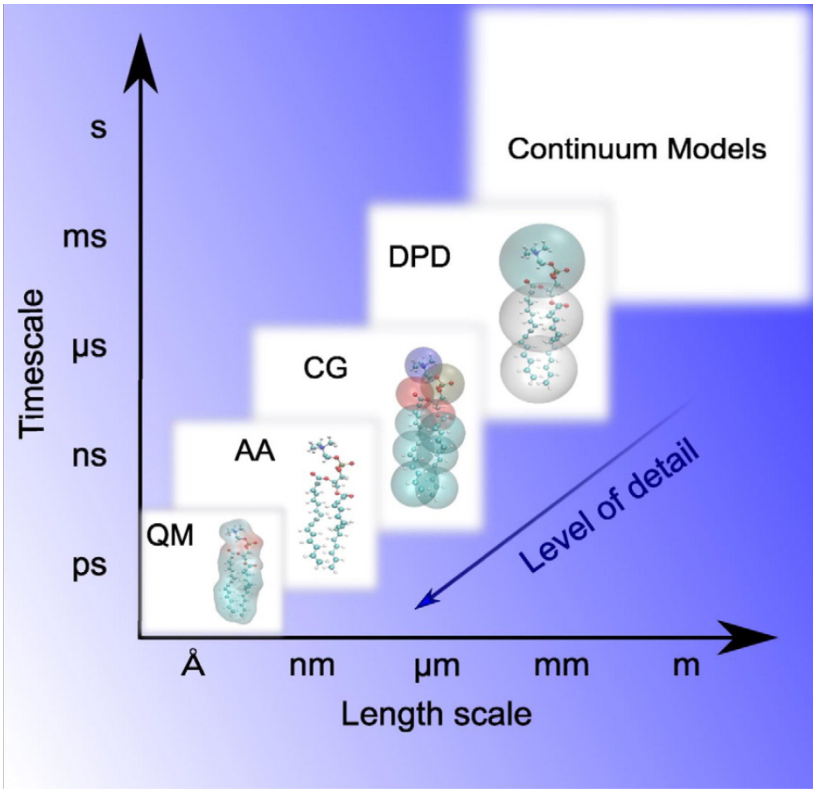


Fig. 1.10 Simulation methods and their time and spatial resolutions. The most detailed description of a system is achieved by Quantum Mechanics (QM) calculations. All-atom (AA) simulations are used to describe interactions between individual atoms that have been assigned single point charges. Simulations can be accelerating via Coarse Graining (CG), where sets of atoms are grouped into one bead/interaction point. Finally, at larger CG level, Dissipative Particle Dynamics (DPD) are used to study macroscopic effects. Taken from [85].

act between themselves through empirical forcefields that describe the non-bonded long range forces (electrostatic (coulomb) and van der Waals) as well as the bonded interactions (bonds, angles, dihedrals between connected atoms). This technique is called Molecular Mechanics (MM). When the simulated system propagates in time, the technique is called Molecular Dynamics (MD). MD allows the simulation of larger systems that can reach up to microseconds [86] and it will be discussed in more detail in Chapter 2. In the field of biochemistry and biophysics, MD was

firstly used to study the dynamics of protein folding [87] in the late 1970 and has since been used in a plethora of systems.

If the atomistic description of a system is not a priority, then coarse-grained (CG) methods can be utilised. In CG, groups of atoms are represented as one bead that corresponds to one interaction site. Using CG methods the simulation of larger scales systems are feasible. In order to calculate the motion of the beads and thus the evolution of the system CG force fields are employed. One of the most used is the MARTINI force field [88], that has been utilised in the field to simulate polymer structures [89, 90, 91, 92], polymer-drug interactions [93, 94] as well as membrane penetration [95, 96].

The above simulation methods can provide information at many different levels of detail; sometimes a combination of methods is used to accelerate the calculations but keep important information under the light; such an approach would then be called a multiscale method. One example from a previous group member is the development of a multiscale force field to simulate the nanoprecipitation method [93]: a drop of acetone containing PGA chains and dexamethasone phosphate molecules was placed in the centre of a box, and was surrounded by water (figure 1.11). As the acetone diffused towards the water, the polymer aggregated and encapsulated the drug molecules. However, although some tools exist to facilitate the process like MagiC [97], these multiscale force fields are very challenging as require parametrisation and constant evaluation of the accuracy of the systems.

In this thesis MD was considered to be the best fit for the time and space scales that would provide information over the coating procedure of a drug NP. A more detailed description of the theory behind MD, the

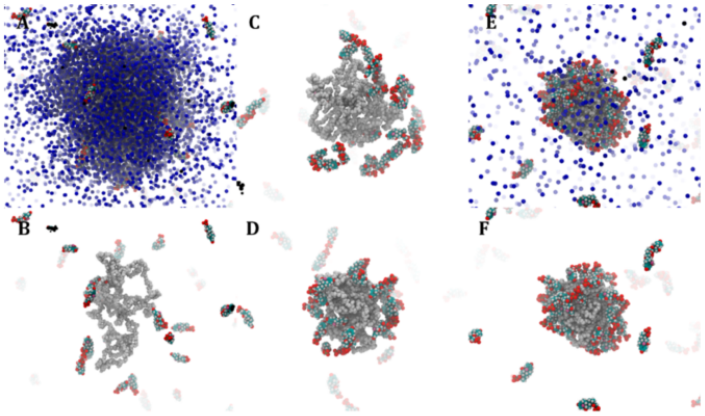


Fig. 1.11 Snapshots of multiscale simulation of nanoprecipitation: PGA (grey) collapses and encapsulates dexamethasone phosphate molecules as acetone (blue) disperses in the water region. Water not shown for clarity. Taken from [93].

force field used and how the system was created are presented in chapter 2.1. For the needs of this introduction, a review over the successes of MD simulations follows.

1.4.1 MD simulations of pharmaceutical relevance.

All-atom simulations have been employed to investigate the encapsulation efficiency of various polymer-drug combinations [98, 99, 100, 101, 102, 103], interactions of drugs and/or polymers with membranes[104, 105] and understanding fundamental parameters for nanoparticle/micellar formation and interactions [106, 107, 108, 109, 93, 110].

The significance of computer simulations as tools for the understanding of fundamental properties and their enormous potential as predictive tools was greatly discussed and exhibited in the works of Huynh et al. [98] and Costace et al. [99]. In the former, MD simulations were used to calculate the solubility and the Flory-Huggins interaction parameters between the hydrophobic anti-cancer drug docetaxel and a number of excipients. In the latter, docking and MD were used to investigate the

interactions between 4 hydrophobic drugs and a triblock copolymer. In both the cases, a successful correlation between experimental values and the predicted ones was presented and as the authors themselves discussed, the simulations are not supposed to substitute the experimental part but to enhance and accelerate the whole procedure.

On a similar mentality, Patel et al. [100] studied the effect the spatial distribution of hydrogen donors and acceptors of hydrophobic drugs had on their encapsulation efficiency by PEO-*b*-PCL polymers. The Flory-Huggins parameters between the drugs that had evenly distributed hydrogen donors/acceptors and the polymers were found to decrease when the PCL chains were increased. A low Flory-Huggins parameter indicates an increase in solubility and thus an increase in the drug loading.

Subashini et al. [111] also used MD to simulate drug encapsulation by polymers. The combinations of 3 drugs with 6 polymers were studied and compared with experimental data from the same group. Although the simulations were performed using small molecular weight polymers (6-10 monomers per polymer chain) in water, the number of hydrogen bonds between the drugs and the polymers were calculated and a good agreement between the MD simulations and the experimental data was uncovered. The value of the MD simulations as predictive tools was appraised and the authors suggested future work to include different solvent mixtures and other polymers. They also concluded by stating the importance of hydrophobic interactions in the uptake of drug molecules by polymers.

Huynh et al. [107] studied star copolymers of mPEG-PCL in order to investigate their unstable micellar behaviour that lead into the formation of multimolecular micelles. The authors studied a plethora of various

mPEG-*b*-PCL molecular weight ratios with the OPLS all-atom forcefield to evaluate the hydration of the two chains. A dense core, consisting of packed PCL chains was reported in all the micelles formed and a correlation between the number of PEG units and the complete coverage of the PCL core was discussed (figure 1.12). It was observed that the instability was due to the partial hydration of the PCL core. The results suggest that when a the PCL block has molecular weight $\leq$2 kDa, and the PEG unit of 14.6 kDa, the core is protected from water molecules and thus stable unimolecular micelles will be formed. This work was of great significance as it used the diblock copolymers that are of interest to the present work and as it evaluated the effect the different lengths of PEG and PCL had on the formation of the micelles.

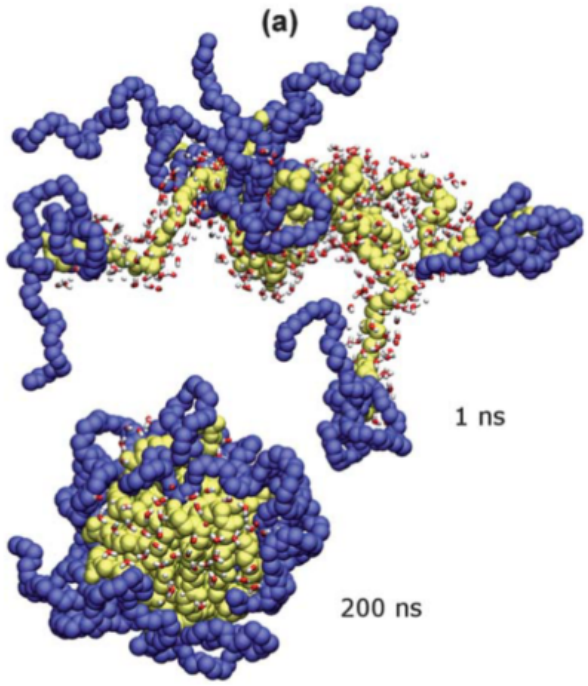


Fig. 1.12 Snapshots of a star copolymer formed by 6 mPEG38 (blue)-b-PCL_9 (yellow), at 1 ns and 200 ns. Taken from [107].

Rigo et al. performed atomistic simulations to understand the effect the presence of a solvent has in the grafting density of silica NPs

[108]. The NPs had either hydrophilic (PEG) or hydrophobic (sulfonic acid) head functionalisations and the formation and hydration energies were calculated using LAMPPS and the CHARMM force-field. It was demonstrated that the presence of water and subsequently of a solvent does affect the grafting density of the NPs and suggest that this should be an interesting prediction for the estimation of the grafting density for experiments.

Although an inorganic core was considered, the effect of the grafting density and the surface coverage is important for the stabilisation of NP formulations. This was also noted in the work of Salerno et al. [109], where PEO-coated silica NPs were formed and studied for the effect the length of the PEO chain and the surface coverage had on the shape of the NP and on the interaction between NPs.

Other studies that focused on the coating of inorganic cores involve research about polymer-coated gold NPs [112, 113, 114], however as this thesis focuses on more organic core materials, we will not expand this section.

Among the many polymers that have a pharmaceutical application and interest are the PEO-PPO-PEO triblock copolymers, also known as Pluronics or Poloxamers. Similarly to the experimental work, Pluronics have been studied in many MD cases; Nawaz et al. [105] performed both MD and experimental studies for the interactions of different Pluronics with lipid membranes. It was observed that the hydrophilic PEO chains interacted strongly with the polar head groups of the lipid chains, indicating a membrane permeation effect.

Samanta et al. [102] also studied interactions of Pluronics with curcumin, a poorly water-soluble drug that has attracted a lot of interest

due to its therapeutic potential as an anticancer drug, naturally occurring. The model used for curcumin was built and parametrised from scratch for the GROMOS96 forcefield. After the control simulations of curcumin in various pure solvents to establish the molecule's behaviour, MD runs were performed in the presence of one, and of 8 Pluronic P85 chains in an aqueous environment. A polymer-curcumin aggregate was formed and it was reported that the hydrophobic interactions between the PPO blocks and curcumin were leading the aggregation. However after 100 ns of simulations, just 3 Pluronic chains have aggregated around the single curcumin molecule, suggesting that either the simulation time was not sufficient, or the amount of Pluronics used was overestimated.

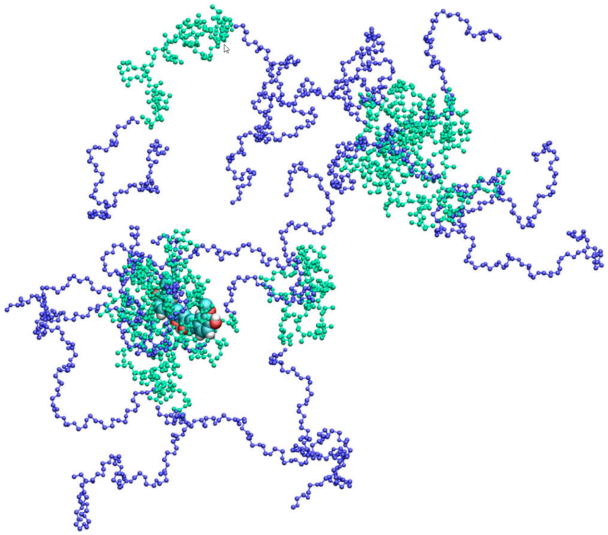


Fig. 1.13 Snapshot after 100ns of MD run of 8 Pluronics P85 chains interacting with a single curcumin molecule, in water (not shown). Taken from [102].

More recently, a united-atom model for Pluronics was reported by Goliaei et al. [115]. The group used two different Pluronics, P85 and P188 that have a different hydrophilic/lipophilic character to study their interaction with lipid bilayers. Once they validated the performance of the polymers built using parameters from the GROMOS53a6 forcefield,

simulations were set to see their interactions with a lipid membrane (figure 1.14).

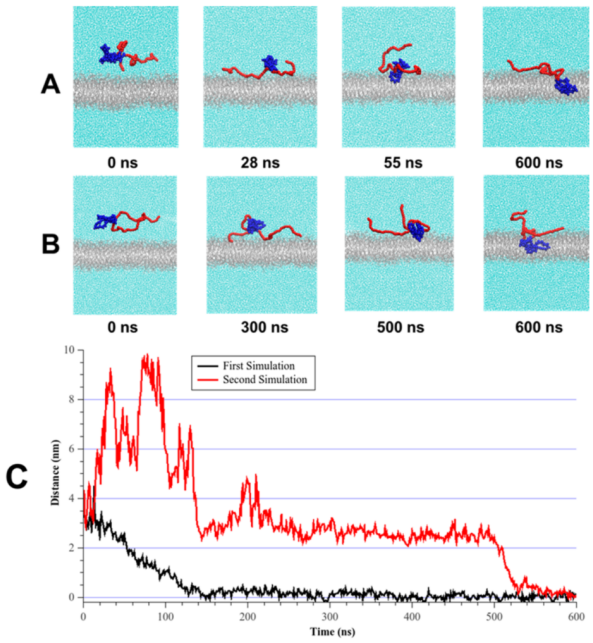
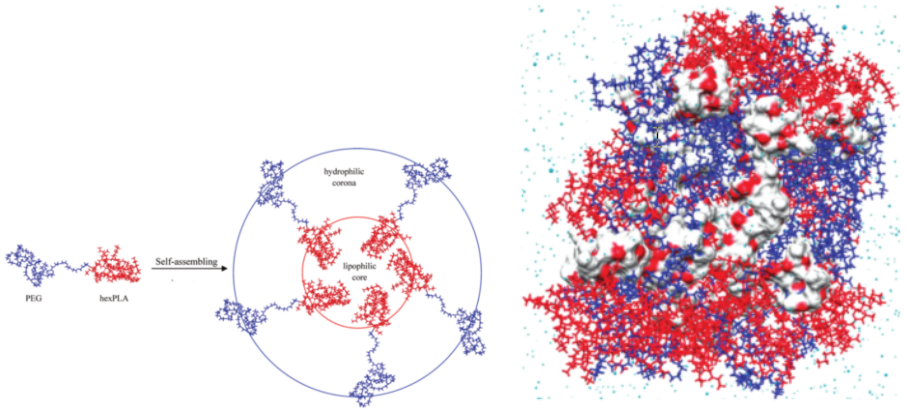


Fig. 1.14 Interactions of P85 poloxamer with a lipid membrane (DLPC) as reported from Goliaei et al. [115]. A and B are the two simulations were different starting configuration were used, but both resulted in the penetration of the hydrophobic PPO (blue), in the lipid layer. C illustrates a tool used to measure the distance between the centre of masses of the PPO chain and the lipid membrane.

The MD simulations reproduced successfully the expected behaviour; over two 600 ns MD runs, the hydrophobic PPO penetrated the lipid bilayer, while the hydrophilic PEO interacted with the polar region. The group used the united atom simulations as a validation of a modified CG forcefield they previously reported and used that to study the "healing" ability Pluronics have on damaged membranes. A gap was formed in the layer and the polymers were able to reach as an aggregate inside the pore, forcing water out of the gap and thus partially mending the lipid membrane disruption. Studies like this indicate the constant need

to perform simulations in the all-atom spectra in order to ensure that any CG representation is valid.

Continuing the research concerning hydrophobic drugs, Kasimova et al. [101] performed both experimental and MD simulations to study the incorporation of four different lipophilic drugs into micelles prepared from a novel PEG-poly(hexyl-substituted PLA) (PEG-hexPLA) excipient. The simulations were not allowed to evolve dynamically over time, but were compacted in vacuum in order to resemble a drug-loaded micelle core (figure 1.15). This facilitated the calculation of the Flory-Huggins interaction parameters that once plotted against the experimentally obtained drug-content per polymer data showed an almost perfect linear fit.



(a) **(b)**

Fig. 1.15 Work performed by Kasimova et al. [101] for the study of hydrophobic drugs incorporation in the lipophilic core of mPEG-hexPLA micelles. (a) mPEG (blue) - hexPLA (red) micelle structure. (b) Snapshot taken from the MD run of mPEG-hexPLA with 21 cyclosporin (grey van der Waals surfaces) molecules.

MD simulations were also carried out to understand the interactions between hydrophobic drugs and lipid membranes. Kang et al. [104], calculated the free energy of a single paclitaxel molecule across a lipid bilayer. Paclitaxel is a hydrophobic drug used to treat solid tumours but its hydrophobicity causes the molecules to aggregate. The group found

that there is a concentration dependence behaviour of the drug in the lipid membrane. Studies like this aim at facilitating the design of better DDS.

Another chemotherapy drug that attracts interest is doxorubicin; Karatasos [103] performed all atom simulations of doxorubicin molecules in a polymer-free and in the presence of PEGylated polyester dendrimers. It was observed that the drug molecules would aggregate but their spatial distribution would differ according to the polymer's presence. The results of the simulation were in accordance with the experimental trend that has been reported, where the more effective clustering resulted in a higher drug loading which corresponds to the more effective therapeutic action.

As presented till now, PEG is considered a "safe" choice for DDS, so MD studies regarding just PEG chains could not be absent. Lee et al. [116] studied the hydrodynamic radius and other static properties of PEG chains in water, under the CHARMM force field. Bunker [117] performed MD simulations to understand the importance of PEGylation, by simulating PEGylated lipid membranes resembling PEGylated liposomes. It was observed that PEG could penetrate the lipid membrane, possibly leading to liposome membrane disruption and thus instability, as well as that the density of PEG in the membrane affected the interaction with the surrounding sodium and chlorine ions, making the surface of the liposome change its surface charge. The surface charge is of importance in DDS as it can influence the opsonisation and thus the therapeutic effect of the particles.

To great interest of this thesis is the work of Di Pasquale et al. [106] where plain PCL chains in different lengths were simulated in the presence of pure water, pure acetone and in mixtures of both. In this study

the effect of the solvent displacement, the fundamental interaction that leads the formation of NPs was under evaluation. The hydrophobic PCL chain remained flexible in the presence of acetone and aggregated while in aqueous environment. However, when an intermediate solvent composition was used, acetone molecules clustered around PCL (figure 1.16) favouring an extended arrangement, resembling the behaviour of PCL in pure acetone.

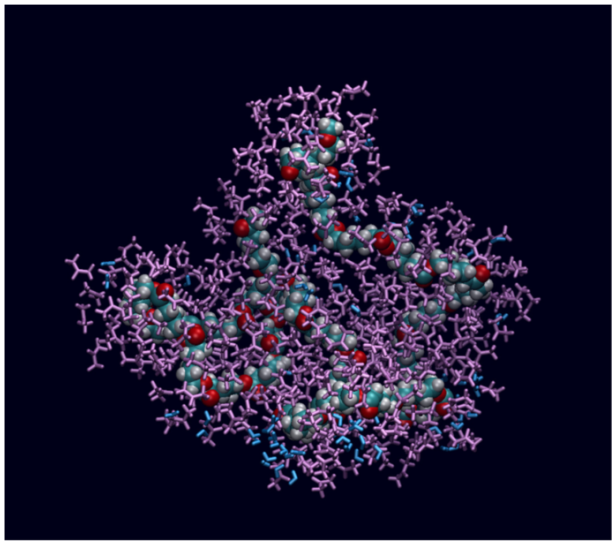


Fig. 1.16 A PCL chain of 30 monomers, in an acetone(purple)-water(blue) mixture (50:50). The acetone molecules in a distance of 6 A surrounding the PCL chain prevent its aggregation, even in the presence of water in the mixture. Taken from reference [106].

From all the aforementioned work, it is clear that MD simulations can both accurately reproduce experimental observations and also have enormous potential to be used as a prediction tool, saving time and money. Combined studies that use both experimental and computational approaches in an attempt to provide an holistic description of the systems increase over the years. One example is the work of Taresco et al. [110] where the group studied the self-assembly and structural properties of

micelles formed by copolymers, reporting a good agreement between the experimental and the all-atom simulations' results.

It would be ideal to use MD simulations in order to provide valuable insight in phenomena that can only macroscopically be described via experimental methods. Such an insight, describing the fundamental interactions has the potential to minimise the costly, laborious, trial-and-error experimental approaches that currently dominate the pharmaceutical field. At the same time, MD simulations have the potential to describe the atomistic behaviour of systems, but with the increase in the computational power every year it yet remains to establish them as a means to a *formulation-by-design* approach in the pharmaceutical industry [117, 118, 119]. This could come as a compliment to the well established drug-by-design approach the pharmaceutical industry follows and would result in the improvement of DDS.

1.5 Aims and Objectives

This thesis is the story of the transferability of a method aiming to produce polymer-coated drug NPs. An existing IONP coating method [2] where PGA was used for the coating, needed to be transferred to coat drug NPs with mPEG-*b*-PCL copolymers.

mPEG-*b*-PCL were selected as are biocompatible and PCL is biodegradable, while indomethacin was selected as a model drug as it demonstrates low aqueous solubility. At the same time, keeping in mind the general objectives of the project that involved around the agglomeration of the aforementioned polymer-coated drug NPs, different mPEG lengths needed to be used to evaluate the interparticle interactions.

This project was dependent on various parameters; the solubility of indomethacin in acetone, the polymer concentration needed for the coating, the production of an aqueous indomethacin NP suspension to name a few.

The aims of the present work are summarised by the two following questions:

- Can we produce polymer-coated drug NPs?
- What type of interactions influence the coating method?

In order to understand the system at a greater detail both computational and experimental studies were performed. Although both the routes were performed in parallel, it was decided to present the work of this thesis in two separate chapters according to the nature of the studies.

In Chapter 2 the description of the methods used is presented. A brief theoretical background of MD is also discussed.

Chapter 3 focuses on the computational part of the project. The solvents' mixing behaviour needs to be optimised and studies of the behaviour of the indomethacin NP and the copolymers in pure solvents have to be carried out. The best way to model the interfacial deposition system needs to be clarified. Then, in order to ensure the full description of the system, simulations split in three categories need to run: (a) in a drug-free environment for the formation of polymer NPs, (b) in a polymer-free environment for the investigation of the fate of the indomethacin aqueous suspension and (c) the method in the presence of both the polymers and the indomethacin NPs. In all the simulations metrics to describe the behaviour of the system quantitatively needed to be investigated.

In Chapter 4 the experimental studies are presented. Firstly the polymer synthesis and characterisation had to take place. Once the polymers would be fully characterised, the existing methods to produce the aqueous nanosuspension of indomethacin needed to be under evaluation. Once an indomethacin aqueous nanosuspension would be created, the interfacial deposition method experiments needed to be split in the same three categories as in the computational chapter: (a) formation of polymer NPs, (b) investigation of the fate of the indomethacin aqueous suspension and (c) polymer-coated indomethacin NPs. In all of these combinations the NPs need to be characterised for their size and their morphology and drug loading.

CHAPTER 2

Methodology

The goal for this thesis is to provide a holistic overview of the desired system and for this both experimental and computational work has been undertaken. In order to replicate the proposed experimental setup in a computational environment simulations using Molecular Dynamics were performed. In parallel, the design, synthesis and characterisation of mPEG$-b-$PCL diblock copolymers with various hydrophilic to hydrophobic ratios was undertaken. The successful production of the polymers with the desired properties allowed us to employ them in the pre-existing nanoparticle formation method. These experiments lead into the production of polymer nanoparticles (i.e. drug$-$free) and in a later stage into polymer-coated drug nanoparticles.

2.1 Computational Work

It is not the purpose of this PhD thesis to provide a complete description of the vast field of Molecular Dynamics. Should the reader be interested in a more details, we suggest the excellent book from A.Leach [120].

However a brief description of the theory behind the method needs to be discussed.

2.1.1 Molecular Dynamics

Molecular Dynamics is a method used in order to follow the time−evolution of a system by solving Newton′s laws of motion (Equation 2.1.1 [120])

$$\mathbf{F} = m_i \frac{d^2 \mathbf{x}_i}{dt^2} \tag{2.1.1}$$

where m_i, x_i are the mass and the co-ordinates of each atom (x,y,z) respectively. Assume a system in which the positions and the velocities of all the atoms present are known. The force applied to each one of the atoms is computed via equation 2.1.2, where V is the potential that describes the bonded and the non-bonded interactions between a pair of atoms. The interaction potentials compose the force field used in each simulation and are discussed in more detail in section 2.1.1.1.

$$\mathbf{F} = -\nabla V \tag{2.1.2}$$

In all-atom simulations, each computational step usually corresponds to a 1-2 fs time step. During this step, the potential and kinetic energies for each of the atoms are calculated and thus the configuration of the system is updated through a numerical solution of Netwton's equations of motion. The whole procedure is repeated for the designated number of steps and the final configuration is provided as an output. This iteration composes the MD algorithm, which is summarised in figure 2.1.

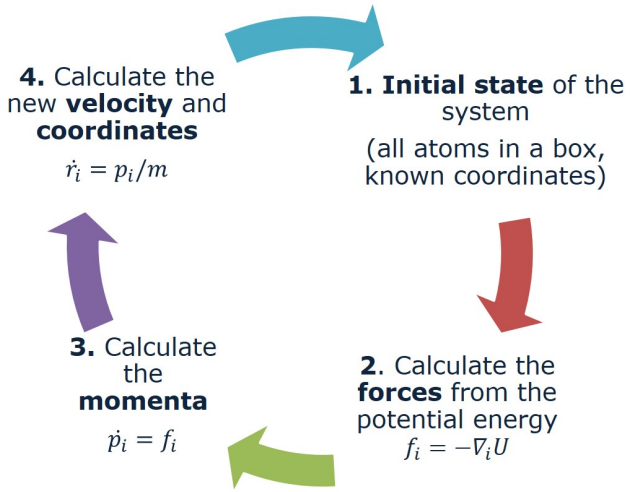


Fig. 2.1 The evolution of the MD algorithm and the calculations taking place during one time step.

The integration of the equations of motion is achieved via the *leap-frog* algorithm, which uses positions $\mathbf{r}$ at time t and velocities $\boldsymbol{v}$ at time t-$\frac{1}{2}\Delta t$; it updates the positions and the velocities using the equations:

$$\boldsymbol{v}(t+\frac{1}{2}\Delta t) = \boldsymbol{v}(t-\frac{1}{2}\Delta t) + \frac{\Delta t}{m}\mathbf{F}(t) \tag{2.1.3}$$

$$\mathbf{r}(t+\Delta t) = \mathbf{r}(t) + \Delta t\boldsymbol{v}(t+\frac{1}{2}\Delta t) \tag{2.1.4}$$

The wall time needed for the completion of one iteration depends on the initial size of the systems. Simulations with millions of atoms in their starting configuration need high-performance computing clusters, able to perform these calculations in a reasonable period of time. Although such systems are becoming more accessible, MD, and particularly all-atom simulations, are limited according to the availability of computational power.

Another critical aspect of MD is their nature; it is a classical approach and is not able to provide answers when the nature of the interactions

fall under Quantum Mechanics (QM) i.e. electronic interactions like formation or breaking of covalent bonds. In MD the movement of the atoms is calculated from interaction potentials $V(\mathbf{r})$ which are described in various empirical force fields. There are many force fields available and each one has been optimised to reproduce characteristic properties of different molecules. This means that selecting the best force field for a molecular system is not a trivial matter. A universal force field, able to describe any physical system accurately, is still a utopia in the field of computational chemistry.

2.1.1.1 The GROMOS 53a6 and 54a7 force fields

As discussed above, the potential energy that defines the interactions of the atoms in space is the key parameter in MD simulations. In classical MD, the potential function is usually a summation of bonded and non-bonded interaction functions between atoms.

Non-Bonded Interactions The non-bonded interactions contain a repulsion term, a dispersion term and an electrostatic term. The first two terms are described via a 6-12 Lennard-Jones (LJ) potential (equation 2.1.5):

$$V_{LJ}(\mathbf{r}_{(ij)}) = 4\epsilon_{(ij)}\left[\left(\frac{\sigma_{(ij)}}{r_{(ij)}}\right)^{12} - \left(\frac{\sigma_{(ij)}}{r_{(ij)}}\right)^{6}\right] \tag{2.1.5}$$

The ϵ and σ parameters are unique for each atom type defined in a force field; σ represents the collision diameter, the distance at which the energy is zero, and ϵ is the well depth. This is illustrated in figure 2.2. The attractive part of LJ potential is described by the r^{-6} term while the

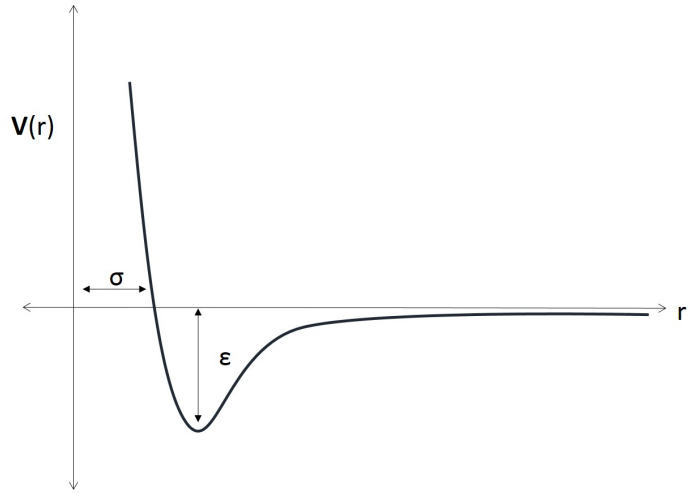


Fig. 2.2 Lennard Jones interaction potential.

repulsive part by the r^{-12}.

The partial charges of the atoms are calculated via quantum mechanical (QM) methods and are assigned to the atoms according to their environment and their position. However, the charges remain fixed during the simulations, as a continuous update would increase the computational cost.

The electrostatic, i.e. Coulomb interaction, between two charged particles, is given by equation:

$$V_C(r_{ij}) = \frac{1}{4\pi\epsilon_0}\frac{q_i q_j}{\epsilon_r r_{ij}} \tag{2.1.6}$$

where q_i, q_j are the charges of the atoms, ϵ_0 is the permittivity of free space and ϵ_r is the relative permittivity of the media.

In order to study bulk systems, periodic boundary conditions (PBC) are used in most MD simulations. As illustrated in figure 2.3, when PBC are used, an atom close to one side of the box-system can move towards the end of the side and it will re-appear on the opposite side of

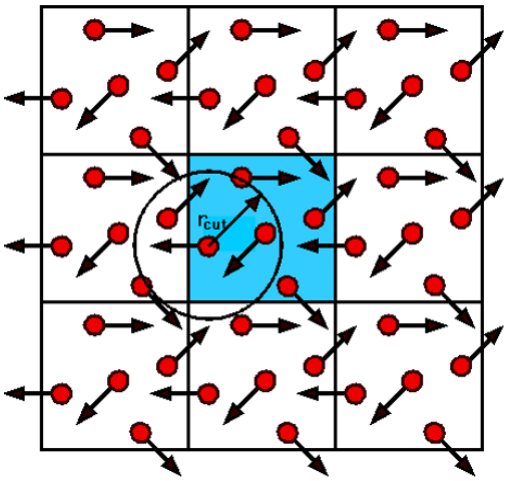


Fig. 2.3 Periodic Boundary Conditions as applied to a molecule full of atoms (blue in the centre) and the importance of the cut-off radius. [123]

the box. In order to avoid the calculation of long distance interactions a distance threshold has been introduced. This is called cut-off distance ($r_{cut-off}$) and minimises the amount of non-bonded interactions that need to be calculated. At the same time, a shift function can be introduced in the non-bonded potentials in order to replace the truncated forces by continuous ones that have continuous derivatives in the $r_{cut-off}$. With the introduction of such shift functions, the long-range electrostatics are calculated either via Ewald summation or, as used in this thesis, by Particle-mesh Ewald (PME) [121, 122].

Bonded interactions The bonded interactions between atoms characterise the type of interaction each atom has with it's neighbouring atoms. These interactions involve the bonds, angles, proper and improper dihedrals that exist between sets of 4 atoms and is illustrated in figure 2.4

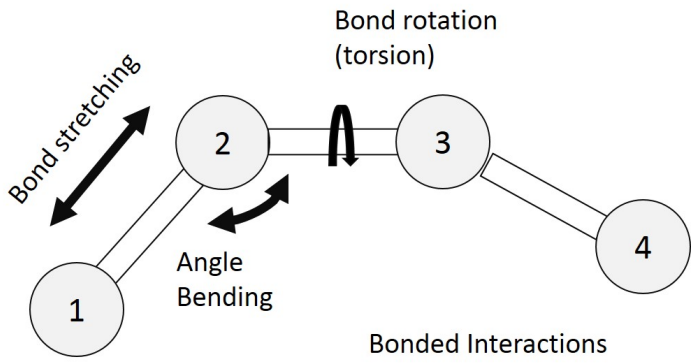


Fig. 2.4 Bonded interactions between a set of four neighbouring atoms.

In the GROMOS force field, these interactions are described by harmonic oscillation potentials (with the exception of the dihedral potential) and follow equation 2.1.7:

$$\begin{aligned} V_{bonded} = & \frac{1}{2}\sum_{ij} k^{b}_{ij}(r_{ij} - b_{ij})^2 \\ & + \frac{1}{2}\sum_{ijk} k^{\theta}_{ijk}(\theta_{ijk} - \theta^{0}_{ijk})^2 \\ & + \frac{1}{2}\sum_{ijk} k_{\phi}[1 + cos(n\phi - \phi_s)] \\ & + \frac{1}{2}\sum_{ijkl} k^{id}_{ijl}(\xi_{ijk} - \xi^{0}_{ijk})^2 \end{aligned} \tag{2.1.7}$$

2.1.2 Simulation Setup

2.1.2.1 Partial charges - Topology files

Partial charges for the polymers and acetone as well as their topology files were obtained from the Automated topology builder (ATB) [124, 125]. The original coordinate (.pdb) files were created in ChemDraw3D and were submitted to the ATB. ATB is a tool created to facilitate the development of force fields (GROMOS 53a6 and currently 54a7) for biomolecular simu-

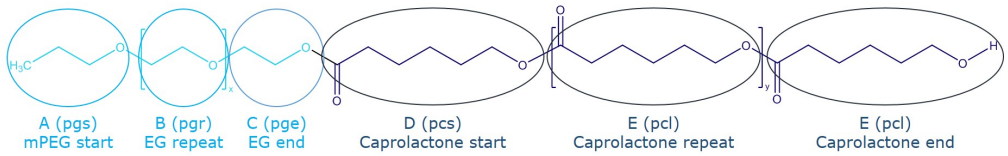


Fig. 2.5 Structure of the mPEG-*b*-PCL units for the topology files.

lations. While under estimation from the ATB, the molecule is initially optimised at the HF/STO-3G and then re-optimised at the B3LYP/6-31G* levels of theory in implicit water. The initial charges are estimated by fitting the electrostatic potential using the Kollmann-Singh scheme and the Hessian matrix is calculated. The topology files are created for either the all-atom or united atom representations; in united atoms the hydrogens of the aliphatic groups are not considered as individual atoms but are part of a larger group of atoms. One example is a methyl group (CH_3); in the all-atom representation it would involve 4 atoms while in the united atom it is considered as 1. The united atom representation saves computational time from the calculation of the hydrogen atoms' movement and for this reason it was selected in this work.

2.1.2.2 Computational Polymer "Synthesis"

It was essential for this project to simulate polymers with the same molecular weight ratios as the polymers that would be synthesised experimentally. The protocol to achieve this for GROMACS was as follows: Trimer structures of the polyethylene(glycol) and the polycaprolactone segments were submitted to the ATB[125]. Then the output parameters were used to build a residue topology file (.rtp) that would define the atoms and the connections between the monomers. This .rtp file included information about the start, the repeat and the connecting monomers of both mPEG (A, B, C) and PCL (D, E, F) as seen in figure 2.5.

All the bonded interactions and their connections were defined with the built-in parameters of the aforementioned GROMOS53a6 or 54a7 [126] force-fields .

After that, the "synthesis" of the polymers was achieved with the tool *tleap* of AMBERtools; a sequence of A B C D E F units was defined and then the output file (.pdb) was used in *gmx pdb2gmx* tool to create the final topology (.top) file. The residue (.rtp) files and the final topology (.top) file for mPEG$_{350}$-*b*-PCL$_{2000}$ can be seen in full detail in the Appendix (A.2).

Prior to using the polymers in the interfacial deposition simulations, the polymers underwent an energy minimisation (EM) of 10.000 steps using the steepest descent algorithm and in vacuo NVT simulation to relax any unphysical structures. Random polymer configurations were extracted from this simulation and were used in the creation of the following models.

2.1.2.3 Construction of the Interfacial Deposition Model

As discussed in more detail on section 2.2.2 and in the Computational Studies at chapter 3.3, the interfacial deposition method was envisioned as a biphasic model, where two regions, the organic and the aqueous, were allowed to mix.

A large cubic box (edge of 26.7 nm) was built using Packmol [127] that contained the aqueous region. For the coating studies a 5nm (diameter) amorphous indomethacin sphere, containing 145 molecules, was placed in the centre of the box. The box was solvated in GROMACS using the *gmx solvate* tool, using the SPC water model [128], resulting in a 4.12 mg/ml indomethacin in water suspension.

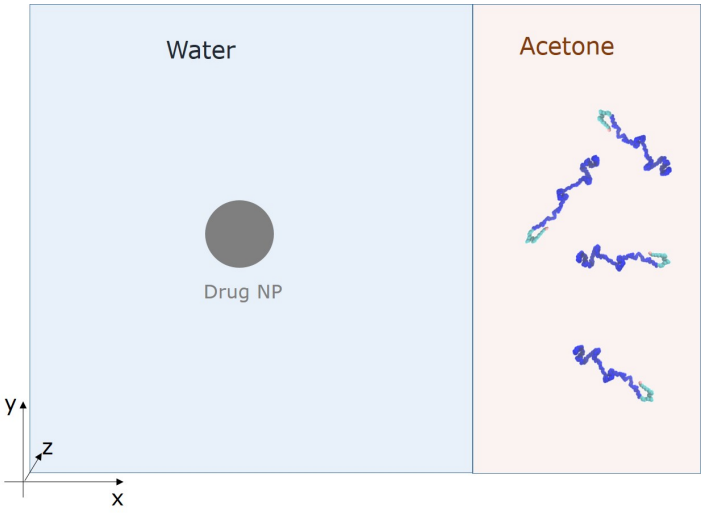


Fig. 2.6 Biphasic system for the simulation of the interfacial deposition.

The box was then expanded in the x direction in such a way to accommodate the acetone-polymer phase (figure 2.7), addressing two critical parameters: (a) the acetone:water molar fraction, (equation 3.1.1, $x_\alpha = 0.089$, corresponding to the experimental setup where 2ml of acetone are mixed with 5 ml of water) and (b) the polymer chains that needed to be as many as to coat all of the particles surface but still at a reasonable polymer:acetone concentration.

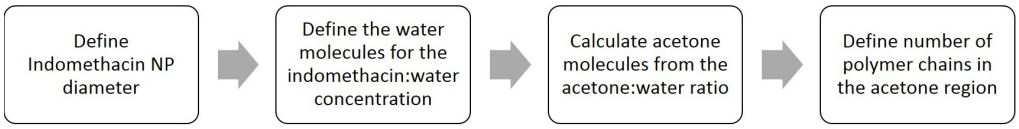


Fig. 2.7 Steps in order to calculate the amount of molecules for each of the simulations.

The complete numbers of the atoms and polymer chains included in each simulation can be found in tables 3.3 and 3.2.

2.1.2.4 Running Parameters

The GROMOS 53a6 and 54a7 force fields were selected [129]. The cut-off distance for the van der Waals and the electrostatic interactions was set

to 1 nm. All MD simulations were run in GROMACS (versions 4.6.5 and later 5.1.0) [130] using either resources of the High Performance Computing (HPC) cluster of the University of Nottingham or on UK National Supercomputer ARCHER [131]. Visualisation of the trajectories and visualisations used in this thesis were performed using VMD [132].

After the solvation of the biphasic box in GROMACS using the SPC water model [128], the atoms were relaxed by 10000 steps of EM with the steepest descent algorithm. Then each of the two phases were equilibrated separately, via NVT ensembles at 298 K (V-rescale thermostat) for 100ps and then in an NPT ensemble at 1 bar (Berendsen barostat) was applied to the whole system for another 100ps. Bonds to hydrogen atoms were constrained to allow a time step of 2 fs. All of the MD simulations were run with the same barostat and thermostat, under PBC. Long-range electrostatics were treated with PME [121, 122]. At the end of each equilibration step (EM, NVT, NPT) of the previous processes, the potential energies, temperature and pressure were checked retrospectively to ensure the proper equilibration of the system.

2.1.2.5 Tools used for the analysis of the simulations

Statistical properties of the polymers The residues of the polymers were defined as the hydrophilic (mPEG) and hydrophobic (PCL) block copolymers with the GROMACS module *gmx make_ndx*. In order to describe the collapse or the expansion of a polymer chain in a solvent, it is useful to calculate the end-to-end distances (R_{e-e}) and radius of gyration (R_{gyr}) (figure 2.8) and this was achieved using the *gmx polystat* module.

The radius of gyration of the polymers is dependent on solvent [133]. In a good solvent chains will remain expanded while in a bad solvent,

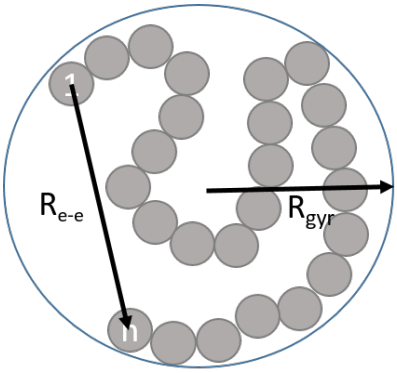


Fig. 2.8 The end-to-end distance (R_{e-e}) and radius of gyration (R_{gyr}) in a polymer chain.

the chains will collapse resembling a hard sphere. The radius of gyration of the polymer chains is:

$$R_{gyr} \sim N^{\nu} \tag{2.1.8}$$

where ν is an absolute number that relates to the solvent quality ($\frac{3}{5}$ for a good solvent and $\frac{1}{3}$ for a bad solvent [133]).

Solvent Mixing and Diffusion The *gmx density* module in GROMACS was used to calculate the distribution of the solvent molecules across a box direction in order to evaluate whether the two solvents have adequately mixed within the simulation time. The *gmx msd* module was used to calculate the diffusion coefficient D of acetone in water, which is discussed in more detail in section 3.1.1.

Other analysis tools The *gmx distance* and *gmx mindist* modules in GROMACS were used to calculate the distances between the centre of masses, and the number of contacts, retrospectively, of two groups of interest.

Solvent Evaporation Experimentally, the final aqueous nanosuspensions would be collected after the full evaporation of the acetone, usually achieved overnight. In order to replicate this computationally, acetone molecules were randomly replaced by water molecules, in small gradual acetone-removal steps. The system would then undergo the EM and equilibration steps of 250ps after which a 10ns MD run was produced, followed by another acetone replacement step.

2.2 Experimental work

All chemicals were bought from Sigma Aldrich unless stated otherwise. Monomethoxy poly(ethylene glycol) (mPEG) with molecular weights 350, 550, 750, 2000 g/mol, ϵ −caprolactone (ϵ-CL) and the catalyst 1,5,7−Triazabicyclo [4.4.0]dec−5−ene (TBD) were used as received and were kept under nitrogen atmosphere. Dichloromethane (DCM) and Chloroform ($CHCl_3$) HPLC grade were purchased from Fischer Scientific. Indomethacin (CAS 53-86-1, Lot #BCBK0293V) was purchased from Sigma Aldrich and was used in the milling or coating experiments as received.

2.2.1 Polymer Synthesis and Characterisation

2.2.1.1 Synthesis and purification of mPEG−*b*−PCL diblock copolymers

mPEG−*b*−PCL copolymers were synthesised via ring opening polymerisation (ROP) using the mPEG as the initiator (Figure 2.9) [134] and the organic catalyst 1,5,7−Triazabicyclo [4.4.0]dec−5−ene (TBD) [59, 135, 136]. All glass equipment (syringes and round bottom flasks) were kept

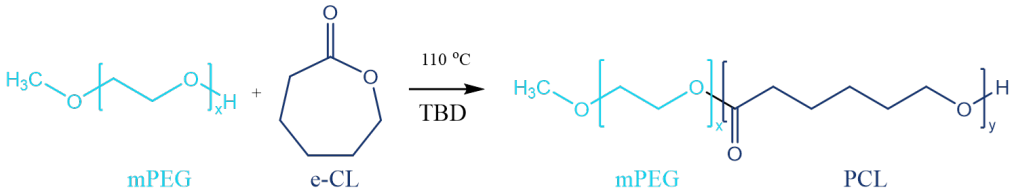


Fig. 2.9 Synthesis of mPEG−*b*−PCL polymers via Ring Opening Polymerisation. In light blue is the hydrophilic mPEG block, while in dark blue is the hydrophobic PCL.

in an oven overnight at 150^{o}C to remove any residual moisture. Prior to the reaction they were placed under a fume hood and a magnetic stirrer was added to the round bottom flask which was quickly capped with a rubber septum. A constant nitrogen flow was introduced to prevent the presence of moisture, and the flask was heated to 110^{o}C. The mPEG was added to the flask, (either with a syringe or prior to capping) and the system was left under nitrogen for an extra 20 minutes before the addition of the ϵ-CL. A fixed molar ratio of [mPEG]:[ϵ-CL] [1]:[40] was kept in all the reactions. The ϵ-CL was added drop-wise via a glass syringe and a sample was collected for the determination of the initial monomer units via ^{1}H NMR.

The reaction started with the addition of the catalyst (TBD dissolved in DCM, 2% mol with respect to ϵ-CL). Maximum conversion to polymer was achieved at 30 minutes when the reaction was terminated with the exposure of the system to air. The result was a very viscous polymer that after cooling to room temperature needed to be dissolved in chloroform for the following purification step. The polymers were purified via precipitation in cold methanol for the removal of any unreacted monomer and the catalyst.

All results for the polymer synthesis and characterisation are discussed in detail in section 4.1.

2.2.1.2 Polymer Characterisation

2.2.1.2.1 Proton Nuclear Magnetic Resonance (^1H-NMR) Proton nuclear magnetic resonance (^1H NMR) spectroscopy was used to determine the degree of polymerisation and the purity of the final polymers. All NMR samples were prepared with $CDCl_3$, run in a Bruker DPX UltraShield spectrometer (400 Hz) at 25^{o}C and were analysed with the MestReNova software (version 8.0.2) of MestReLab.

2.2.1.2.2 Gel Permeation Chromatography (GPC) Gel permeation chromatography (GPC) was employed to characterise further the molecular weight and the polydispersity index (PDI) of the polymers. GPC was carried out by using a PL50+ Polymer Laboratories system, employing two mixed bed (D) columns at 30^{o}C, using chloroform ($CHCl_3$) as the mobile phase, flow rate 1 mL min^{-1}, equipped with a refractive index detector. Polystyrene standards (Mn range: 443000-132 g mol^{-1}) were used to calibrate the GPC. Molecular weights and dispersity values were calculated using Polymer Labs Cirrus 3.0.

2.2.1.2.3 Water Contact Angle (WCA) measurements The contact angle between a water droplet and the surface of a material indicates the hydrophilic or hydrophobic characteristic of the surface [137]; high contact angle (θ>90^o) values correspond to hydrophobic surfaces while low contact angles (θ<90^o) to hydrophilic surfaces (figure 2.10).

The angles values were measured at 25^{o}C using a KSV Cam 200 (Instruments Ltd., Helsinki, Finland) equipped with a dedicated software (CAM200). Samples were prepared by coating glass microscope slides

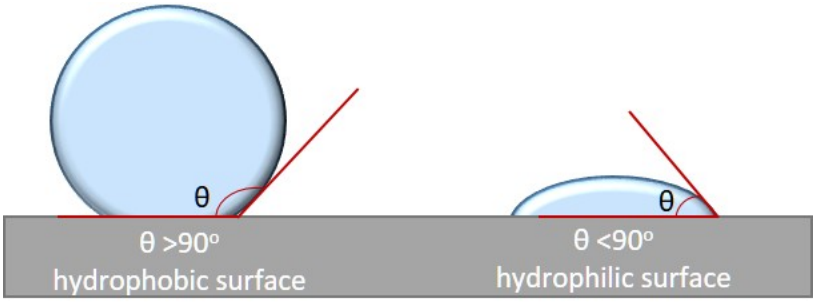


Fig. 2.10 Water contact angle measurements for the determination of the hydrophilicity or hydrophobicity of a surface.

with polymer thin films via solvent evaporation from 5% w/v solutions of polymers in acetone.

2.2.1.2.4 Attenuated Total ReflectanceInfrared spectroscopy (ATR-IR)

IFT-IR spectra were recorded with an Attenuated Total Reflection spectrophotometer (Agilent Technologies Cary 630 FTIR) equipped with a diamond single reflection ATR unit. Spectra were acquired with a resolution of 4 cm^{-1}, in the range 4000-650 cm^{-1} by recording 32 interferograms.

2.2.1.2.5 Differential Scanning Calorimetry (DSC)

DSC is a versatile tool to characterise polymers, as it measures enthalpy changes i.e. the heat required for a sample to undergo a physical phase transition (melting, glass transition among others).

Polymer and drug thermal properties were investigated by DSC (Q2000, TA Instruments, Leatherhead, UK) at a heating rate of 10 ^oC/min. Thermal Analysis Software (Version 4.5.05A) was used for data analysis.

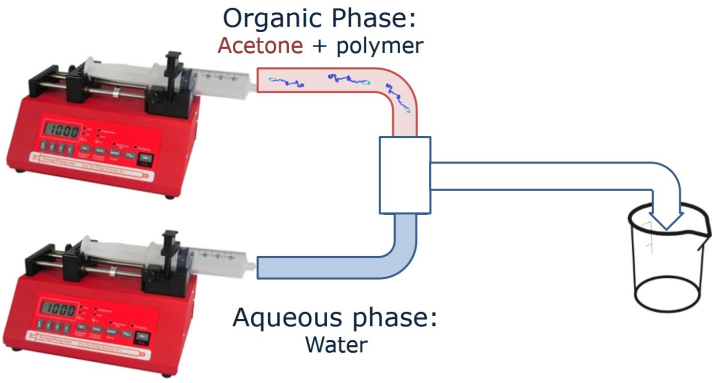


Fig. 2.11 Formation of polymer nanoparticles by the interfacial deposition method.

2.2.2 Nanoparticle preparation via the modified interfacial deposition method

2.2.2.1 Preparation of polymer nanoparticles

Unloaded polymer nanoparticles were prepared following an interfacial deposition method [1] previously adapted for the preparation of polymer-coated iron oxide nanoparticles (IONPs) [2]. The method is based on solvent displacement and is schematically described in figure 2.11.

Briefly, an acetone-polymer solution (2 ml) at various concentrations (10, 5, 1, 0.5, 0.1 and 0.05 mg/ml) was loaded in a glass syringe and used in the organic phase pump. In the aqueous phase, freshly filtered HPLC grade water (5 ml) was used. The two pumps started the mixing of the two phases simultaneously (organic phase flow rate 0.84 ml/min, aqueous phase flow rate 2.4 ml/min). The solvents were introduced to the connecting tubes (PEEK, organic solvent resistant, 0.25 mm internal diameter bought from Kinesis UK) and were interfacing via a T-connector (Kinesis). The mixture was then added drop-wise to a vial containing a magnetic stirrer. The resulting solution was stirred overnight for the evaporation of acetone and was collected for further analysis.

2.2.2.2 Preparation of drug nanosuspensions

The interfacial deposition method was modified by replacing the IONPs present in the aqueous phase with indomethacin NPs. Indomethacin (figure 2.12, M_w=357.79 Da, LogP=4.27, S_w=0.937 mg/L at 25 ^oC, solubility in acetone high [138, 139]) is a nonsteroidal anti-inflammatory drug that exhibits poor aqueous solubility. For this reason it was selected as a model hydrophobic drug.

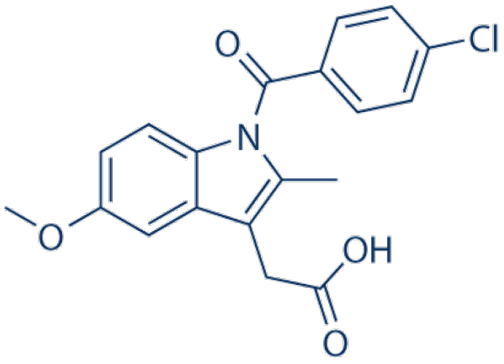


Fig. 2.12 Structure of indomethacin.

In order to create an indomethacin aqueous nanosuspension two top-down methods were selected, wet ball milling and cryomilling with sonication.

Wet Ball Milling (WBM) Nanosuspensions were prepared using a planetary micro mill (Pulverisette 7 Premium, Fritsch Co., Germany) with two grinding bowls of 80 ml capacity. In each milling bowl, milling beads (100 g, YTZ grinding beads, 0.6 mm, GSK Comet), sterile purified water (20ml) and indomethacin (1 g) were added in this order. Rotation speed of bowls (600 rpm), milling duration (12 cycles of altered bowl rotation direction) were selected following a protocol from Malamatari et al. [140]. Each milling cycle composed of 15 minutes rotation followed by 5 minute pause. In order to avoid overheating of the rotors, the milling vessels were

cooled down by immersing in ice for 10 minutes after the completion of 2 milling cycles. At the end of the 12 cycles, the nanosuspensions were left to reach room temperature, were collected with a pipette and were analysed by DLS for their size distribution. When used in the interfacial deposition experiments, these drug nanosuspensions were used immediately after their cool down, as the aqueous-drug bearing phase.

Cryomilling was performed by Ghaidaa Hameed, using a 6870 Freezer/Mill (SPEX, Metuchen, NJ). An electromagnetic coil shuttles an impactor bar back and forward inside the vial in order to pulverise the sample. Liquid nitrogen submerges the coil and vial to keep sample temperature at -196 C. 1 gram total weight of indomethacin was subjected to cryomilling for 150 minutes. This was done by pre-cooling the materials for 3 minutes then milling for 2 minutes at a frequency of 10 cycles per second. Throughout, there was a pause of 1 minute between cycles to minimise heat build-up in both sample and coils. After the cryomilling all samples were vacuum sealed inside a dry glove box to reduce the moisture uptake. This dry-box was supplied with argon to achieve a relative humidity about 7% which is the lowest possible in that system. The cryomilled indomethacin was characterised by XRPD, DSC and IR at different time points to assess the crystallinity of the powder (Appendix B).

When used in the interfacial deposition, both cryomilled indomethacin and commercially available indomethacin were used to prepare the drug nanosuspensions as follows: indomethacin (either cryomilled or as commercially available) was weighed in a round bottom flask and filtered HPLC grade water was added in order to achieve different concentrations (1, 0.5, 0.25, 0.1 mg/ml). The flask was capped with a rubber septum

and the solution was then sonicated for 15 minutes resulting in a milky suspension which was used as the aqueous phase in the syringe pumps.

2.2.2.3 Preparation of polymer-coated indomethacin nanoparticles

Polymer coated indomethacin nanoparticles were prepared with the same procedure as the polymer-only nanoparticles but with the addition of the drug-bearing aqueous phase as described above.

After the evaporation of acetone overnight, the resulting suspension was collected and an extra purification step was introduced to ensure the removal of any uncoated drug particles; the suspension was centrifuged (3 minutes at 2000 rpm) to sediment the uncoated free drug, which tended to aggregate. The supernatant containing the polymer coated drug nanoparticles was collected and was used either as collected for the size measurements or was lyophilised for the determination of the drug loading (section 2.2.3.7).

2.2.3 Nanoparticle Characterisation

2.2.3.1 Dynamic Light Scattering

Dynamic light scattering (DLS, figure 2.13) is a non-invasive technique for measuring the size of particles and molecules in suspension. Through DLS, the velocity of particles undergoing Brownian motion is measured. This velocity is defined by the translation diffusion coefficient D (equation 2.2.1) and depends on the size of the particles, the viscosity of the media and the temperature. By controlling the viscosity (η) and the temperature (T), one can measure the hydrodynamic diameter d_h of the measured particles, through the Stokes-Einstein equation:

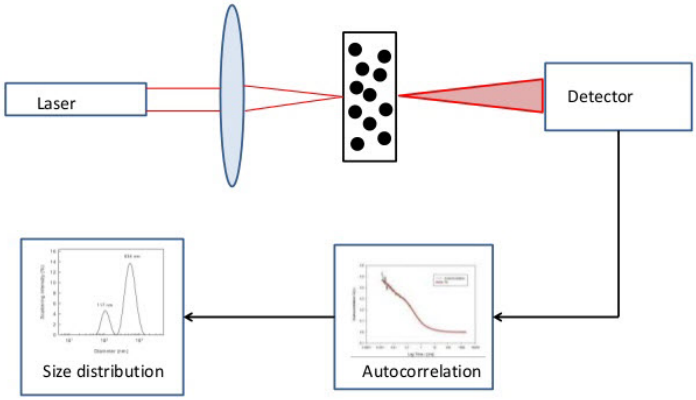


Fig. 2.13 Dynamic Light Scattering (DLS) Schematic. Taken from [141].

$$d_h = \frac{kT}{3\pi\eta D} \tag{2.2.1}$$

where k is Boltzmann's constant. DLS measurements were conducted at 25^{o}C, using a Malvern ZetaSizer Nano ZS at a scattering angle of 173^{o}C and laser of 633 nm. All samples were measured in triplicate for the report of the average values. Unless otherwise stated, the intensity distribution of the sizes is reported in this thesis.

2.2.3.2 Critical Aggregation Concentration

The critical aggregation concentration (CAC) is the minimum concentration above which polymer chains will collapse to form nanoparticle aggregates. The protocol used was provided by Dr. Francesca Mastrotto and was as follows; a suspension of polymer NPs (1 mg/ml) was diluted in water in a concentration range (300 - 0.1 μl/ml). Using the highest concentration (300 μg/ml) the attenuator of a Malvern ZetaSizer Nano ZS was selected and kept constant during the rest of the measurements. The count rate (kcps) was recorded for each of the decreasing polymer concentrations. The concentrations were plotted against the count rates

and the CAC was estimated as the crossover point of two extrapolated lines corresponding to the low and high concentrations.

2.2.3.3 Salt Stability

The colloidal stability of the NP formulations was investigated using increasing salt concentrations. Barium chloride ($BaCl_2$) in a range of concentrations (0.16 - 0.66 M) was added to 0.5 ml of the NP suspension and was left for 10 minutes. If a precipitation of the NPs was observed, then this was considered to be the maximum salt concentration at which the NPs were stable.

2.2.3.4 Zeta-potential

Assume a negatively charged particle in a liquid (figure 2.14). The liquid surrounding the particle exists as two parts (double layer); the inner region (Stern layer) where the positive ions are strongly bound, and an outer region (diffuse) where the ions are more loosely bound. The electric potential at the boundary of this double layer (slipping plane) is called the zeta (ζ) potential and is an indicator for the amount of effective charge present on the particle surface. It is often used in colloidal science as in indication for the electrostatic stability of particle suspensions; highly charged particles with a zeta potential higher than $|30|$ mV [14, 142]) will repel each other.

Zeta potential measurements were conducted at 25^oC, using a Malvern ZetaSizer Nano ZS. The nanoparticle suspensions were used without any further treatment and were run in triplicate for the report of the average values.

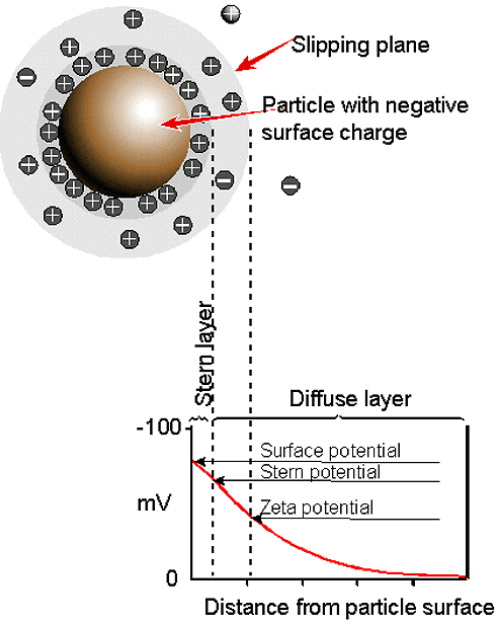


Fig. 2.14 Potentials at different distances from the surface of a negatively charged particle. Taken from [143].

2.2.3.5 Transmission Electron Microscopy

Transmission Electron Microscopy (TEM) operates on the same principle as a light microscope but uses electrons rather than light. A very thin sample is exposed to a high energy beam of electrons and the interactions between the electrons and the atoms can be used to observe features such as sizes, morphology, crystal structures. Due to the electrons' wavelength, TEM provide a better image resolution, many orders of magnitude better than that from a light microscope.

TEM samples were prepared as follows; the sample in aqueous suspension (13 μl) was added to a copper grid (Formvar/Carbon film 200 mesh Copper(100)). The sample was left on the grid for 10 minutes and then the excess was removed via a filter paper. Then, freshly prepared uranyl acetate (2%, 13 μl) was added on the grid and was left for 5 minutes before the removal of the excess with a filter paper. The grid was allowed to dry under a fume hood for a minimum of 30 minutes prior to use.

All TEM images were captured using the FEI Biotwin-12 TEM equipped with a digital camera at the Nanoscale and Microscale Research Centre (NMRC) of the University of Nottingham.

2.2.3.6 Polarised Optical Microscopy

Polarised Optical Microscopy (POM) uses plane polarised light to analyse birefringent samples like crystalline materials. The light is blocked by inserting a polarizer orientated at 90^o to the direction of the illumination. Crystalline material interacts strongly with a polarized light source generating evident contrast with the rest of the specimen. POM is an easy and quick tool to assess the crystallinity of a sample [137] and in the present work was used to validate the nanosize of the suspensions and the state of the indomethacin particles. An Advanced Polarising Microscope (Prior LuxPOLTM with 12V and 30W halogen lamp) was used. The nanosuspensions were added via a pipette on a glass slide and pictures were collected with and without the polariser.

2.2.3.7 Quantification of drug loading via UV-Vis

UV-Vis spectroscopy is a fast, simple and inexpensive method to determine the concentration of an analyte in solution, as long as the analyte can absorb light in the instrument's wavelength range. The solution of the sample is placed in a cuvette and this is exposed to a beam with a wavelength varying between 180 and 1100 nm (light intensity I_0). The sample absorbs part of this radiation (UV or visible) according to the concentration, the path length of the light through the cuvette and how well the analyte absorbs the light at a certain wavelength. The measured

light intensity I, will provide an indication of the concentration of the analyte via the transmittance $T = \frac{I}{I_0}$.

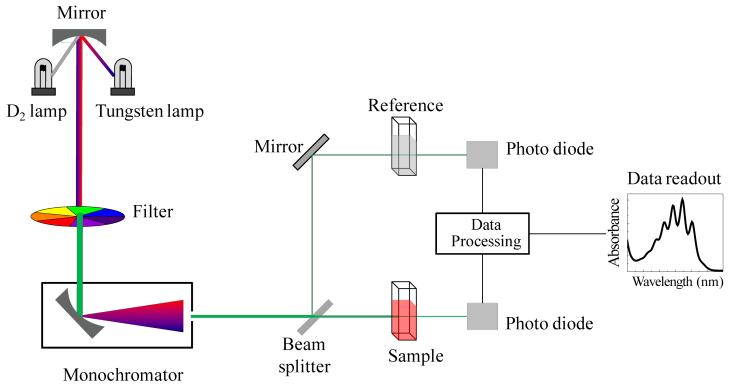


Fig. 2.15 UV-Vis schematic taken from [144].

The most-used term in UV-Vis spectrometry to indicate the amount of absorbed light is the absorbance, defined as: $A = -log10T = -log10(I/I_0)$. Beer-Lambert law gives the relation between the concentration and absorbance: $A = \epsilon lc$, where A is the absorbance, ϵ is the molar absorption coefficient of the analyte at a certain wavelength (l $mol^{-1}cm^{-1}$), l is the path length (cm) through the cuvette and c is the concentration of the analyte (mol l^{-1}).

UV-Vis measurements were performed in an Agilent UV-Vis spectrometer. The calibration curve for indomethacin was prepared in an acetone:methanol mixture (80:20) measuring the absorbance at 350nm (equation in Appendix B). The lyophilised samples were dissolved in the solvent mixture and their absorbance was measured. Drug loading and entrapment efficiency were calculated as follows:

$$\%Drug\ loading = \frac{amount\ of\ coated\ drug}{mass\ of\ NP} * 100 \qquad (2.2.2)$$

$$\%Entrapment\ efficiency = \frac{amount\ of\ coated\ drug}{initial\ amount\ of\ drug} * 100 \qquad (2.2.3)$$

CHAPTER 3

Computational Studies

The aim of this part of the PhD was to investigate the microscopic processes which may occur when coating a drug nanoparticle (NP) with a polymer, using conditions previously determined for the coating of iron oxide nanoparticles. Since the proposed experimental set-up involves a different polymer (mPEG-PCL rather than PGA) and a different moiety (indomethacin NPs rather than IONPs) to be coated, the following questions need to be considered:

- How does the organic solvent mix with the aqueous phase?
- How will the solubility of the drug in the organic solvent affect the coating mechanism?
- Will the system lead to the formation of polymer NPs and polymer-coated drug NPs?
- How will the drug molecules be arranged in the polymer-drug NP: will they be aggregated in the core or be dispersed into a polymer matrix ?

Using MD to address all of the above questions provides us with the opportunity to analyse in detail the behaviour of the drug NPs and the

polymers in the presence of both organic and aqueous environments, which will then lead to better understanding of the NP formation system.

The leading motivation for such modelling studies is to minimise the trial-and-error approaches that typically govern the experimental studies and to provide instead a formulation-by-design approach. Using all atom MD is non-trivial; the complexity of the systems means that the number of atoms that are included in the simulation is high, which means that the time needed to calculate all the forces in the system is also high. Access to high performance computing systems such as the UK national supercomputer ARCHER and the UoN High Performance Computing service (HPC Minerva) make such simulations possible. Although the field of biomolecular simulations has been well validated, all-atom modelling of polymer-based drug delivery systems is a novel field. As such, modellers in the field need to make careful selections of their systems and to adjust their models accordingly in order to achieve the best combination of computational needs and validity.

Although the simulation of pharmaceutical processes such as nanoprecipitation has been conducted before [93], a multiscale forcefield had to be developed in order to achieve the completion of the simulations in a reasonable time. However, by employing fully atomistic simulations one can achieve the more detailed models and this method was used here.

3.1 Diffusion of acetone in water.

The driving force of the interfacial deposition method is the diffusion of the two solvents. As this is crucial for the evolution of the system over time, the behaviour of the acetone and water models needed to be

optimised. Whilst other organic solvents have been successfully parameterised and their simulated physicochemical properties do not deviate greatly from the corresponding experimental values, acetone models and in particular the acetone-water diffusion, has been a long matter of discussion in the literature.

The first study to model acetone and water mixtures was presented in 1990 by Ferrario et al [145]; they proposed their own model of acetone, (named FHMK) while studying aqueous mixes of methanol, acetone and ammonia, and reproduced self-diffusion coefficients, reorientational correlation times and other thermodynamic properties.

During the parameterisation of the GROMOS53a6 forcefield, Oostenbrink et al in 2004 [126] parameterised a plethora of organic solvents (methanol, ethanol and acetone among others) in order to reproduce the free energy of hydration and solvation. They fitted the parameters firstly using cyclohexane for their simulations (resulting in the53a5 force field) and then adjusting them using the SPC [128] water model (53a6) When they tried to fit acetone, they found that there was a large deviation between the experimental (784 kg/m^3) and the simulated density (653 kg/m^3). Their next step was to evaluate the transferability of the parameters, via the calculation of the free enthalpies of solvation of both polar and apolar compounds in different solvents, (methanol, acetone, acetonitrile and DMSO). For the acetone model, they employed two previous models from literature:

- The OPLS acetone model, proposed by Jorgensen et al. [146]. Monte Carlo simulations were used and the geometries of the molecules were taken from gas-phase experimental data. This acetone model, named OPLSac for the following of the present work, had an over-

estimated dipole moment (2.96 D) in order to compensate the neglection of polarisation effects.

- The WS model, proposed by Weerasinghe and Smith in 2003 [147], was validated by reproducing the experimental values of the Kirkwood-Buff integrals in acetone-water mixtures. KirkwoodBuff integrals are related to properties that can be experimentally determined like partial molar volumes, compressibility and derivatives of the chemical potential of mixtures. For their studies they compared the WS model with the standard OPLSac and used three different water models (SPC/E, SPC and TIP3P) and different molar ratios. The WS model is a united atom model and has a larger dipole moment (3.31D) in comparison with the OPLSac.

Both of these acetone models were produced in order to be used in the OPLS and the WS forcefields respectively. When they were tested for the GROMOS53a6, their free enthalpies of solvation values deviated a significant amount from the experimental values. This observation was attributed by Geerke et al [148] to the overestimation of the van der Waals interactions between the acetone molecules. In the following years, other acetone models were developed, namely Perera [149], TraPPE-UA [150], CHARMM [151], and Kamath [152].

Continuing with the issue of problematic acetone models, Jedlovsky et al. [153], calculated the Helmholtz free energy of water and acetone (WS and Perera models), in neat condition and in various molar ratios mixtures only to find that the systems have a positive free energy difference and are thus thermodynamically unstable. Their conclusion was that at that time (2009), none of the existing acetone models, including the WS-SPC/E combination, could describe the miscibility of acetone in water.

In 2011, Pereyra et al. [154] performed simulations of water (TIP5P-E, [155]) with acetone (CHARMM27, [151]) in order to investigate the effect of the dipole moment, μ, of acetone. To reproduce experimental data for excess enthalpy in mixtures with varying acetone molar fraction, they scaled acetone charges with a factor α and found that in different molar fractions, different dipole moments are needed. Their acetone model, named PAC for the rest of this thesis, is based on the model that Martin et al. [156] proposed to study the vapour pressure and heat of vaporization, with a modified charge distribution. The charges of the acetone are scaled by a factor which was chosen in order to reproduce accurately the excess enthalpy for specific molar fractions (equation 3.1.1, x_α=0.5 and 0.2).

Another study for the mixing of acetone with water came from Pinke et al. [157] where the entropy, energy and Helmholtz free energy of mixing two neat systems was reproduced correctly for the entire composition range only for the PAC model with the TIP5P water [16]. The suggestion of the authors was that the PAC model would also be miscible with SPC and TIP4P water models.

More recently, Di Pasquale et al. [106] used the OPLS-all atom acetone model in mixtures of SPC water in order to study the aggregation of PCL chains and reported the aggregation of acetone molecules around the PCL chains. With all the above in mind, validation of the existing acetone models was considered vital in order to achieve a representation of the acetone-water diffusion. All the acetone models used here are described in the Appendix A.3.

3.1.1 Testing acetone models in GROMOS53a6

United atom topologies based on the acetone models of FHKM, WS, OPLS were created in GROMOS53a6, transferring the ϵ and σ parameters, following the procedure used by Geerke et al. [148]. At the same time an acetone topology using the ATB was obtained (Appendix A.1), which should be compatible with the selected forcefield. The experimental values for the diffusion coefficient were obtained from Tyn et al. [158], where the diffusion of solvents in binary systems was studied.

A small cubic box filled with acetone molecules was created with the experimental density (791 kg/m^3) and then it was placed in the centre of a larger box filled with water. The molar fractions of acetone in water (x_α) were calculated via:

$$x_\alpha = \frac{N_{acetone}}{N_{acetone} + N_{water}} \tag{3.1.1}$$

where N is the number of acetone or water molecules present in the system. The system was pre-conditioned following the procedure reported in section 2.1.2.4. The temperature was set at 298 K and the solvents were allowed to firstly mix for 5 ns, followed by another 10ns MD simulation. The final 10ns were analysed via *gmx msd* GROMACS module that derives the diffusion coefficient via the calculation of the mean square displacement of atoms from a set of initial positions.

Table 3.1 United atom acetone models: Diffusion in SPC water

Acetone model	Dipole moment μ (D)	Water molecules N_w	Acetone molecules N_a	Acetone Molar fraction x_α	Diffusion coefficient (Sim) $(10^{-9} m^2/s)$	Diffusion coefficient (Exp) $(10^{-9} m^2/s)$ [158]
OPLSac [146]	2.35	5782	216	0.036	0.1421 +/- 0.1146	1.20
FMHK [145]	2.70	5761	216	0.036	0.2032 +/- 0.1453	1.20
WS [147]	3.31	1981	818	0.292	1.3185 +/- 0.0782	0.59
ATB [124]	-	5000	818	0.140	1.5515 +/- 0.2520	0.70

The results, summarised in table 3.1, demonstrate that the OPLSac and the FHMK acetone models are immiscible in SPC water under GROMOS 53a6. Furthermore, due to the highly polar carbonyl group of acetone in the WS and ATB models, the diffusion constant is far from that of the experimental value, something that is in accordance with the observed trend in the literature.

As discussed previously, modelling acetone-water diffusion is very challenging and the modelling community still lacks an adequate acetone model to use in the GROMOS53a6 & 54a7 forcefields. However, as (a) the OPLSac and FHMK acetone models that have been used by Geerke et al. in GROMOS 53a6 [148] are immiscible with the SPC water model, (b) it was not the purpose of this work to parametrise the existing acetone models but to provide a qualitative description of an experimental technique and (c) the WS model was created and optimised to use in the OPLS forcefield, the ATB acetone was selected for the rest of the simulations.

3.2 Control simulations in pure solvents

In order to validate the behaviour of the molecular components in this work, it was necessary to perform a series of control simulations of the polymers and the drug NP in the presence of pure solvents. The systems were constructed following the procedure as described in section 2.1.2.4. Due to a lead from the parallel experimental work (discussed later in the experimental section) the behaviour of the mPEG$_{350}$-*b*-PCL$_{2000}$ polymer was prioritised.

3.2.1 mPEG$_{350}$-*b*-PCL$_{2000}$ in pure solvents

Five chains of mPEG$_{350}$-PCL$_{2000}$ were randomly placed in a cubic box (a= 12 nm) which was solvated using GROMACS module *gmx solvate* with the either the ATB acetone model or the SPC water model. The simulations ran for a minimum of 80 ns.

3.2.1.1 mPEG-*b*-PCL in the presence of acetone

Experimentally, acetone is a good solvent for mPEG-*b*-PCL copolymers, i.e. the polymer chains are expanded and this is reflected in the corresponding simulations (Figure 3.1). Radius of gyration and End-to-end distances were calculated and as can be seen in figure 3.2 the values fluctuate around the mean values over the course of the simulation, supporting that the polymers move freely in the space.

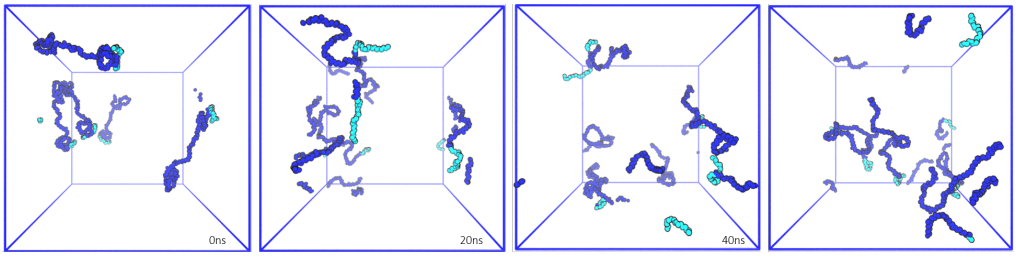


Fig. 3.1 Five mPEG$_{350}$ (in light blue)-*b*-PCL$_{2000}$ (in dark blue) chains simulated in pure acetone (not shown for clarity). The polymer chains remain untangled during the 80 ns simulation. PBC conditions apply, where the molecules can move across the end of the box.

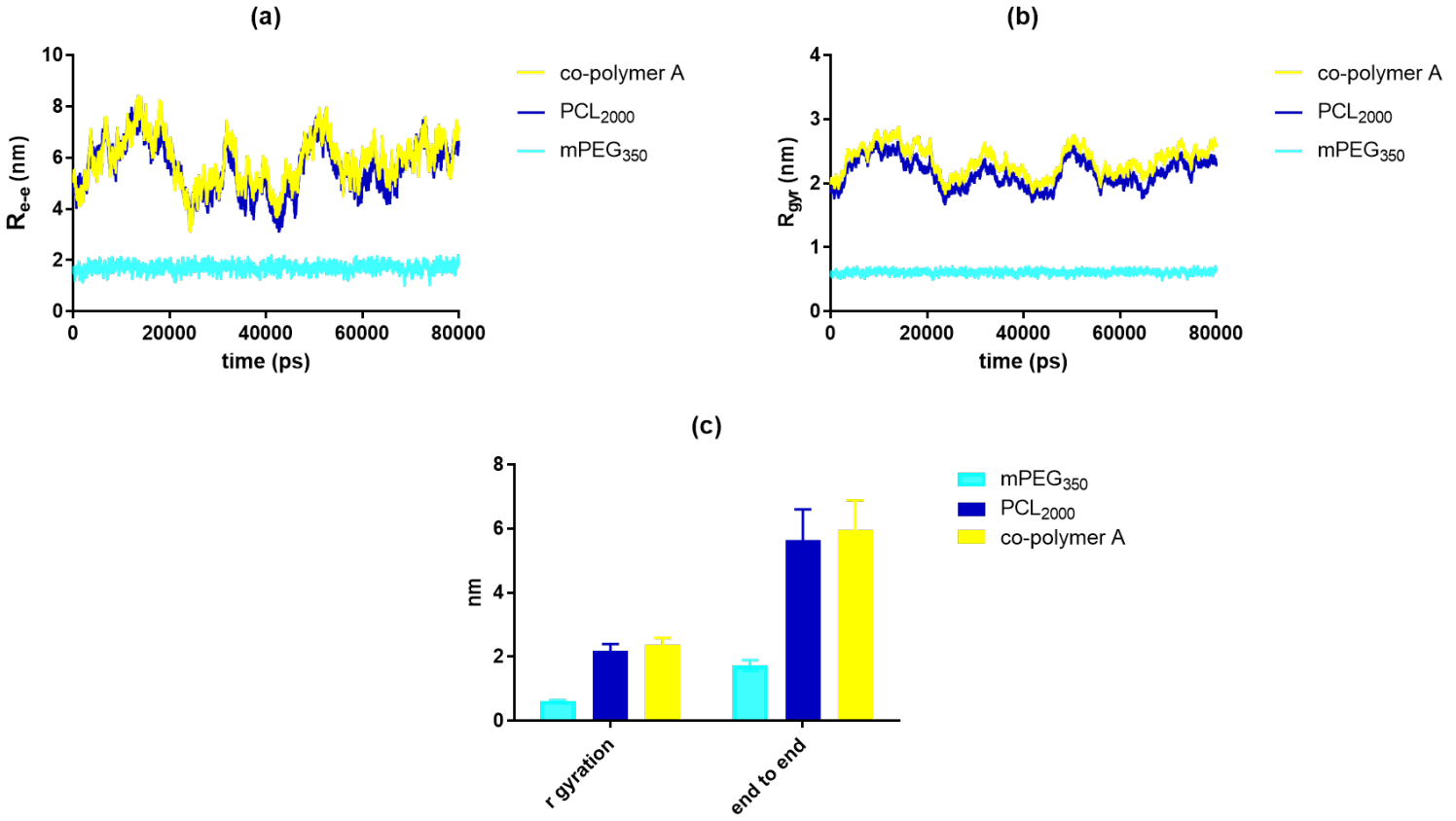


Fig. 3.2 End-to-End distances (a) and Radius of gyration (b) for the control simulation of 5 $mPEG_{350}$-*b*-PCL_{2000} polymers in pure acetone. Graph (c) gives the average values for each of the blocks and error bars correspond to the standard deviation of the measurements. Acetone is a good solvent for the above polymers so the radius of gyration and the end-to-end distances fluctuate over the course of the simulation.

As discussed, in a good solvent the polymer chains will remain expanded while in a bad solvent, the chains will collapse resembling a hard sphere. This trend was also verified by our simulations.

3.2.1.2 mPEG-*b*-PCL in the presence of pure water

Water is expected to be a poor solvent for $mPEG_{350}$-*b*-PCL_{2000}, as the PCL block is hydrophobic and collapses when in an aqueous environment. This is observed at a very early point of the simulation, resulting in single chain aggregates in less than 4 ns (figure 3.3). These single chains then lead to the formation of the two polymer aggregates and then one large polymer aggregate at 32 ns that contains all the chains. This agrees with the experimentally observed behaviour where mPEG-*b*-PCL copolymers will precipitate in water. Radius of gyration and End-to-end distances were calculated and as can be seen in figure 3.4, the values rapidly decrease over the first ns, supporting the aggregation of the polymers. The mean R_{e-e} for PCL has decreased from 5.6 nm in pure acetone to 1.7 nm when surrounded by water.

Fig. 3.3 Five $mPEG_{350}$ (in light blue)-*b*-PCL_{2000} (in dark blue) chains simulated in pure water (SPC model, not shown for clarity). PBC conditions apply, where the molecules can move across the end of the box. The formation of single polymer chain aggregates takes place during the first 4 ns of the simulation which later start interacting one with another, leading into the formation of one larger polymer aggregate (32ns).

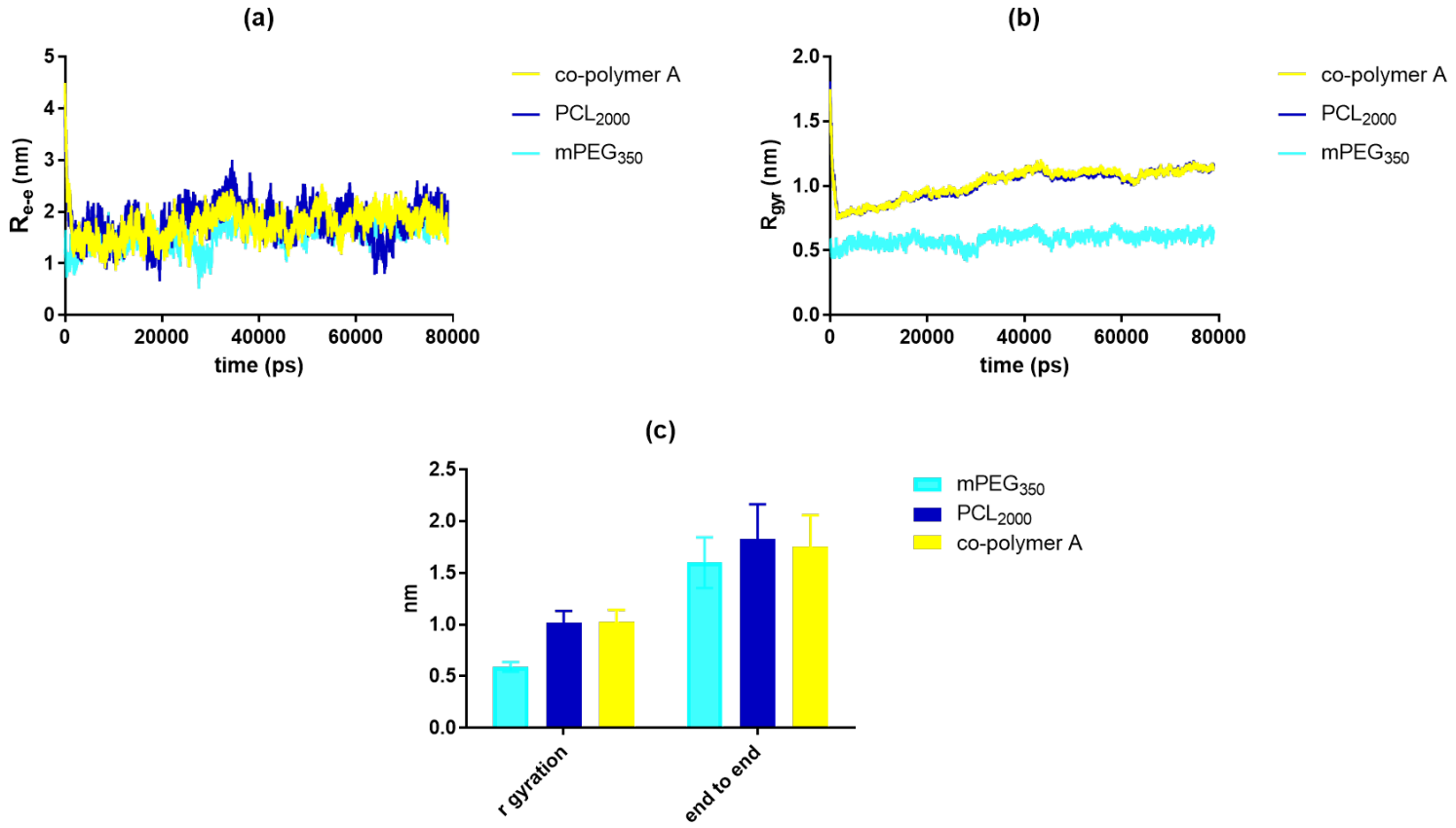


Fig. 3.4 End-to-End distances (a) and Radius of gyration (b) for the control simulation of 5 $mPEG_{350}$-*b*-PCL_{2000} polymers in pure water. Graph (c) gives the average values for each of the blocks and error bars correspond to the standard deviation of the measurements. Water is a good solvent for the $mPEG_{350}$ block of the polymers but a bad solvent for the PCL_{2000}. The radius of gyration and end-to-end distance are decreased immediately at the start of the simulation, when the single polymer chains are formed and then they plateau for the rest of the simulation.

3.2.2 Indomethacin NP in the presence of pure solvents

Indomethacin (figure 2.12) is a hydrophobic drug with low aqueous solubility (S_w=0.937mg/L [139]) but is highly soluble in acetone. Analogous with the control-polymer simulations, a spherical 5nm in diameter amorphous indomethacin NP, containing 145 molecules, was built in Packmol and was placed inside a cubic box (a=15 nm). The box was solvated in GROMACS with the selected solvent. The same equilibration and minimisation and MD run methods were used (section 2.1.2.4) and the simulations run for 60 ns.

3.2.2.1 Indomethacin NP in acetone

As expected from experiment, the indomethacin NP dissolves in the presence of acetone (figure 3.5). The individual drug molecules move freely in the organic solvent and the NP is almost completely broken down at 60 ns.

3.2.2.2 Indomethacin NP in the presence of water

The insoluble character of indomethacin in water is demonstrated (figure 3.6), where it is clear that the drug NP stays intact and moves as an aggregate around the aqueous environment. Some plasticity and movement of the molecules is observed as they rearrange their position around the surface of the NP, but their hydrophobic nature prevents the dissolution of the drug NP.

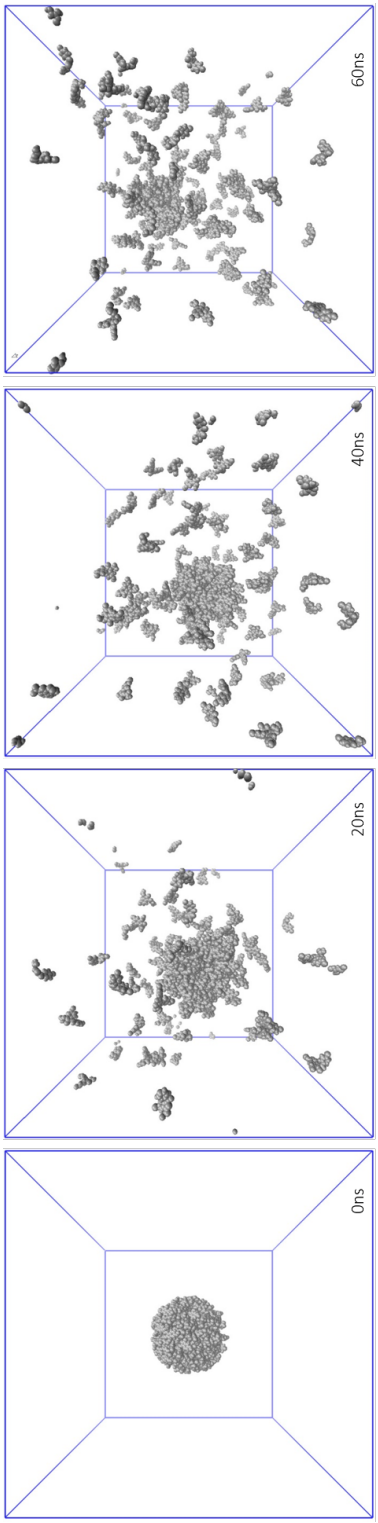


Fig. 3.5 A 5nm diameter indomethacin NP simulated in the presence of pure acetone. PBC conditions apply, where the molecules can move across the end of the box. The indomethacin NP is almost fully dissolved after 60 ns, displaying the high solubility indomethacin has in acetone.

Fig. 3.6 A 5nm diameter indomethacin NP simulated in the presence of pure water. PBC conditions apply, where the molecules can move across the end of the box. The indomethacin NP stays intact for the whole of the simulation, displaying a very poor aqueous solubility.

3.3 Modelling the interfacial deposition method

Experimentally, solvent displacement methods are used widely to produce drug loaded NPs [137, 80, 57]. In such systems, the polymer and the drug are dissolved in an organic solvent, which is then mixed with water. The mixing of the solvents is performed either via the drop-by-drop addition of the organic phase into the water (batch method), or by using mixing tubes (flow method). In both cases, the solvent displacement causes the hydrophobic part of the polymers to aggregate and form NPs.

Our system differs from the above in regards to the drug-bearing phase. It is usual to dissolve the hydrophobic drugs in the organic solvent, but as discussed in the Introduction of this thesis, such methods usually exhibit low yields and encapsulation efficiencies. Since our method was adapted from an existing iron oxide nanoparticle polymer coating procedure, we envisioned the drug particles to exist in the aqueous phase, in the form of an aqueous drug-suspension. At the same time as our model drug, indomethacin, is insoluble in water [138], our goal was to produce a nanosuspension of amorphous indomethacin NPs that would be used in the aqueous phase.

For this reason, the system was designed as a biphasic one (figure 2.6) and the procedure to build the simulation starting system is described in detail in section2.1.2.3. Every attempt was made to match realistic experimental conditions, however a compromise must be made to ensure that the system is large enough to be representative, but at the same time small enough for the simulation to be completed at a reasonable computational expense.

As the experimental method was initially proposed for the coating of the surface of iron oxide nanoparticles that are insoluble in acetone, a

series of simulations were performed in order to understand the effect of the co-existence of both the solvents would have on the polymers and the drug NP. The following simulation scheme was developed:

1. Formation of polymer NPs, in the absence of the drug NP (table 3.2 and section 3.4)

2. Investigation of the stability of the drug NP, in the absence of the polymer, as a negative control (section 3.5)

3. The complete system to investigate the formation of the polymer-drug NP (table 3.3 and section 3.6)

Each of the above 1 and 3 sets was created for all the four polymers ($mPEG_{350,550,750,2000}$-*b*-PCL_{2000}), resulting in overall 9 systems. In all the systems the polymer in acetone concentration is equal to 10 mg/ml. The concentration was the highest used during the parallel experimental work and was the starting point for the simulations.

Table 3.2 Systems for the formation of polymer NPs

System	Polymer	$N_{polymers}$	$N_{acetone}$	N_{water}	Total atoms	Simulation time (ns)	Acetone removal
A	$mPEG_{350}$-PCL_{2000}	10	29471	288979	986501	140	Yes
B	$mPEG_{550}$-PCL_{2000}	9	29471	255576	886123	10	-
C	$mPEG_{750}$-PCL_{2000}	8	29471	220578	781178	10	-
D	$mPEG_{2000}$-PCL_{2000}	6	29471	344547	1153163	10	-

Table 3.3 Systems for the Interfacial Deposition in the presence of an indomethacin NP

System	Polymer	$N_{polymers}$	$N_{acetone}$	N_{water}	$N_{indomethacin}$	Total atoms	Simulation time (ns)	Acetone removal
A$*$	$mPEG_{350}$-PCL_{2000}	31	68771	790732	145	2657273	330	Yes
B$*$	$mPEG_{550}$-PCL_{2000}	30	68771	632283	145	2182208	10	-
C$*$	$mPEG_{750}$-PCL_{2000}	27	68771	519571	145	1843847	10	-
D$*$	$mPEG_{2000}$-PCL_{2000}	18	68771	816341	145	2733806	10	-

3.4 Simulations for the formation of mPEG-*b*-PCL polymer nanoparticles

The four simulations that correspond to the formation of the polymer NPs (A, B, C, and D on table 3.2) were subjected to a 10 ns MD simulation after minimisation and equilibration (figure 3.7).

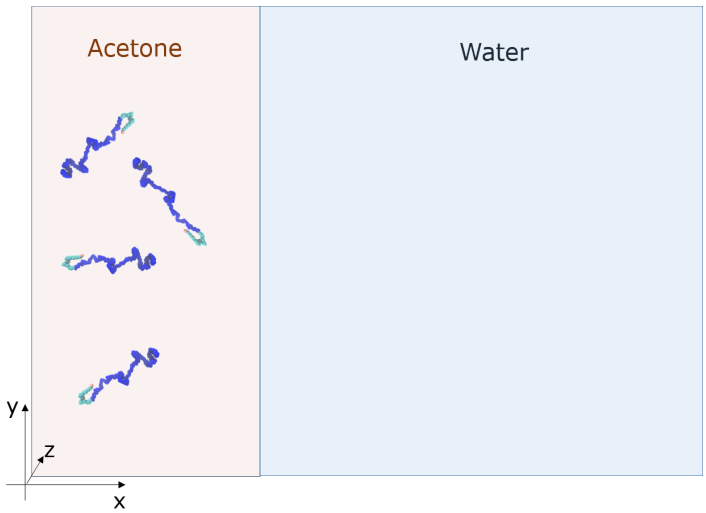


Fig. 3.7 Starting configuration for the simulations set for the formation of the polymer NPs (Systems A, B, C and D of table 3.2).

The system would be considered fully equilibrated once the acetone and the water have fully mixed. To determine this, the *gmx density* tool from GROMACS was used, where the x axis of the box is scanned to calculate the distribution of the acetone and water molecules across the system. From figure 3.8 it can be seen that there is still solvent separation after 10 ns and the system is not properly mixed.

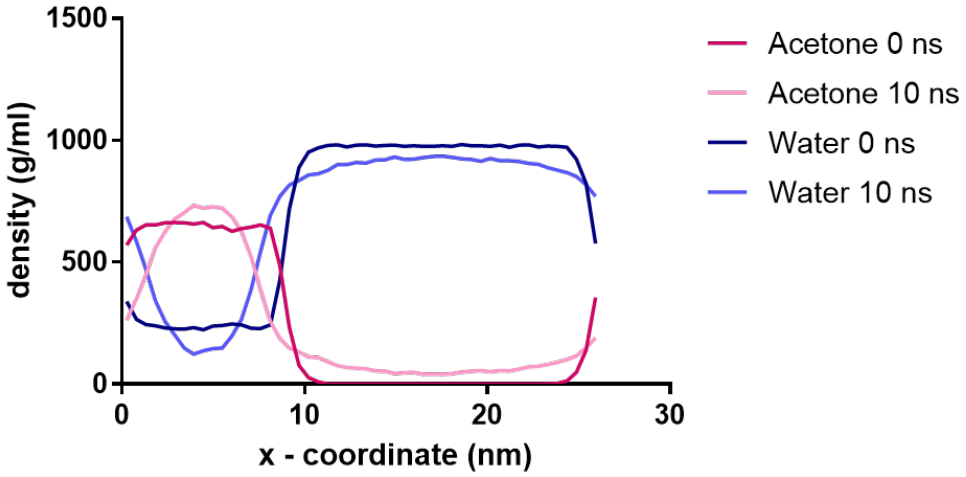


Fig. 3.8 System A: Simulation for the formation of $mPEG_{350}$-*b*-PCL_{2000} polymer NP: The spatial distribution of the acetone and water molecules across the x-axis of the simulated box in 10 ns reveal a solvent separation, i.e. the system is not fully equilibrated.

Although 10 ns were not enough for the mixing of the solvents, these set of simulations proved to be the starting point for the calculation of the static properties of the polymers during the interfacial deposition, using the tools as discussed in section 2.1.2.5. Figure 3.9 shows the static properties of the hydrophilic mPEG chains of the polymers during the first 10 ns of the simulations (Systems A, B,C and D of table 3.2).

As discussed (section 2.1.2.5), the radius of gyration of the polymers is proportional to number of monomers in the polymer, i.e. the molecular weight (eq. 2.1.8). The dependence of the distances to the molecular weight of the chain was verified by our simulations as it is clear that the larger the hydrophilic mPEG chain, the higher the radius of gyration and end-to-end distances it has.

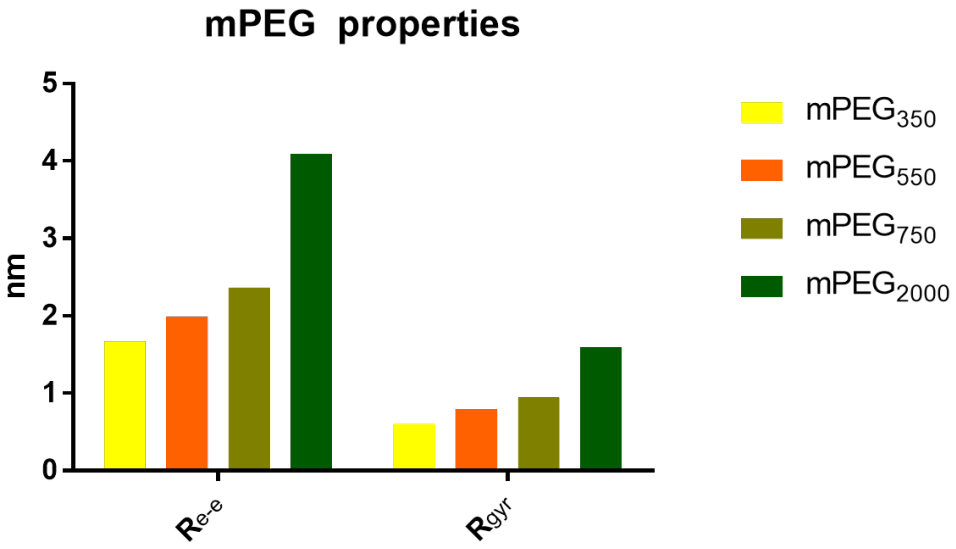


Fig. 3.9 Radius of gyration and end-to-end distances for the hydrophilic blocks of the polymers over the course of a 10ns simulation in the biphasic systems (Systems A, B, C and D, table 3.2). The larger the molecular weight of the polymer, the higher the radius of gyration and end-to-end distances.

Due to acetone-water phase separation at 10 ns it was initially planned to perform all of the four simulations simultaneously for a minimum of 100 ns. However, this was not possible with the computational resources that were then available; the Universitys HPC cluster was able to provide a 10 ns simulation in a week (without considering the queuing times), which meant that the completion of all the 9 simulations could take up to 90 weeks. This lead to the prioritisation of the systems, focusing on just the $mPEG_{350}$-*b*-PCL_{2000} polymer (system A) and using ARCHER, achieving performances of maximum 10 ns/day.

The system starts as in figure 3.10, with the polymers present in the acetone (pink) phase and the water molecules not shown for clarity. The simulations ran for 100 ns, followed by 4 simulation sets of 10 ns each, to mimic the evaporation of the acetone. In figure 3.11 snapshots illustrating the evolution of the system over the course of the first 100 ns of simulation are presented. Figure 3.12 shows the evolution of the system as acetone molecules (pink) are replaced by water molecules (not shown for clarity), mimicking the evaporation of the acetone that takes place in the wet-lab experiments.

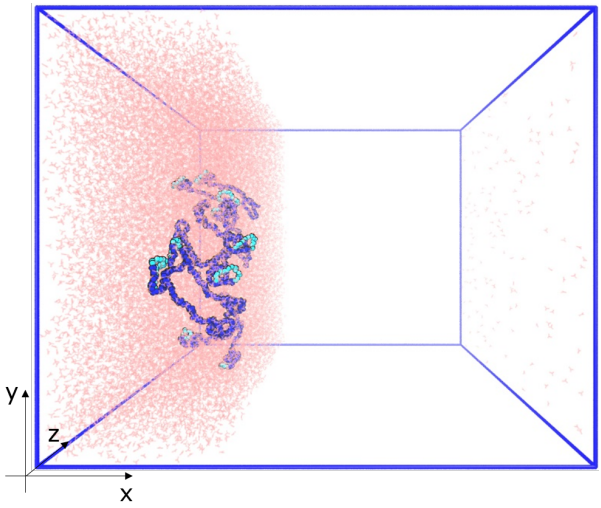


Fig. 3.10 System A: $mPEG_{350}$ (light blue)-*b*-PCL_{2000} (dark blue) polymer chains in the interfacial deposition simulation, for the formation of a polymer NP. The polymers are placed in the acetone (pink) region, while water is not shown for clarity.

Fig. 3.11 System A: $mPEG_{350}$ (light blue)-*b*-PCL_{2000} (dark blue) polymer chains in the interfacial deposition simulation, for the formation of a polymer NP. Snapshots taken at every 20 ns, solvents not shown for clarity. The polymer chains start to aggregate, as the presence of water in their surrounding environment increases. However their full aggregation is not facilitated due to the presence of the acetone.

Fig. 3.12 System A: mPEG$_{350}$ (light blue)-*b*-PCL$_{2000}$ (dark blue) polymer chains in the interfacial deposition simulation, for the formation of a polymer NP. Snapshots taken at the end of every 10 ns MD run where acetone molecules (pink) are replaced by water molecules, mimicking acetone's evaporation. A polymer NP is formed as the polymers aggregate in the increasing aqueous environment. Water is not shown for clarity.

The PCL chains start to aggregate, as the polymers are exposed to more water molecules. However due to the presence of the acetone in the system, their full aggregation is not facilitated and the polymer NP has not formed after the end of 100 ns simulation. However, during the gradual acetone-replacement steps (evaporation), the absence of the good solvent-acetone leads the hydrophobic PCL_{2000} blocks of the polymer chains to aggregate, leading to the formation of a polymer NP of 3.4 nm diameter.

In order to provide a quantitative description of the polymers aggregation, the static properties of the polymers were calculated for the whole of the 140 ns of the simulation and are presented in figure 3.13.

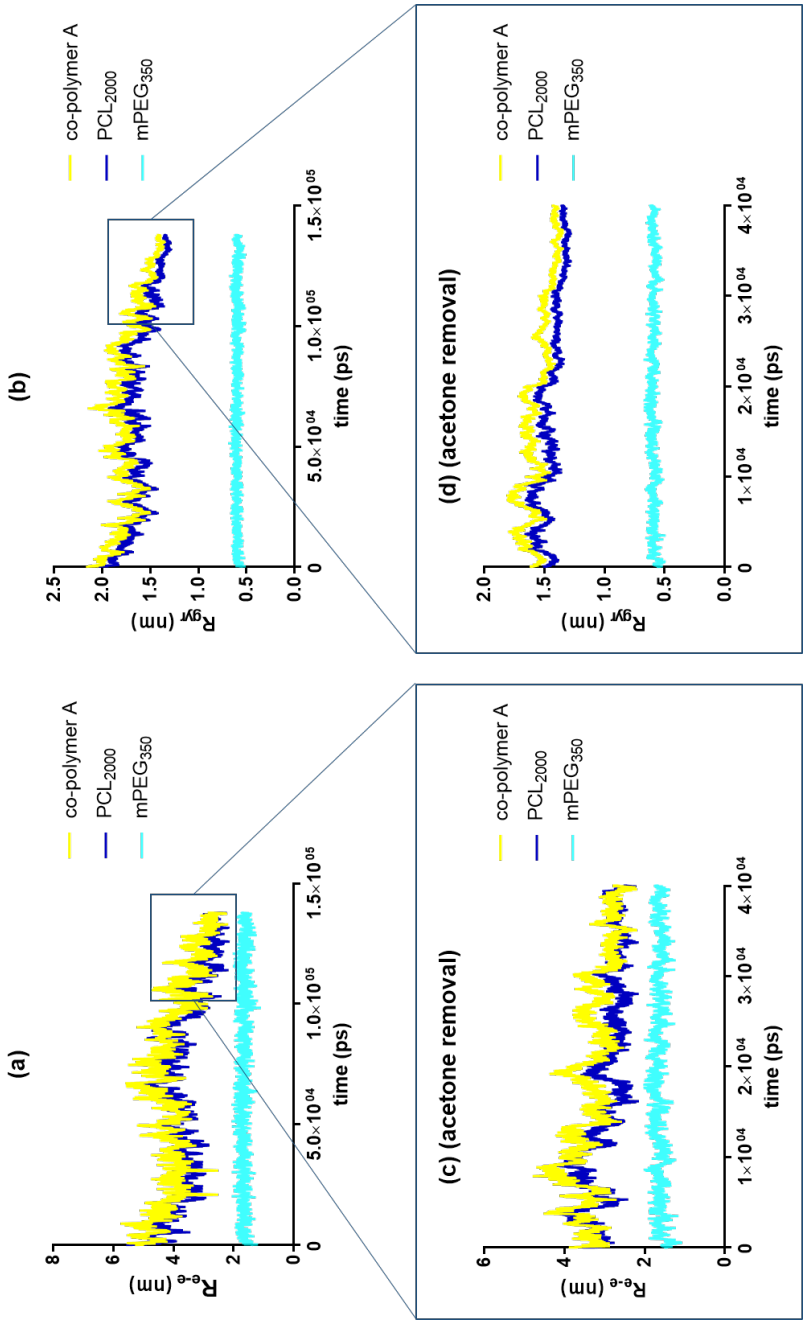


Fig. 3.13 System A analysis: mPEG$_{350}$-*b*-PCL$_{2000}$ polymer chains in the interfacial deposition simulation for the formation of a polymer NP. End-to-end distances ((a), (c)) and Radius of gyration ((b), (d)) for the different blocks of mPEG$_{350}$-*b*-PCL$_{2000}$ polymer chains for the complete simulation of 140 ns (top row) and the acetone evaporation steps during the last 40 ns (bottom row). The hydrophobic PCL$_{2000}$ block starts to aggregate during the replacement of the acetone molecules, thus reducing its spatial conformation.

The hydrophilic $mPEG_{350}$ blocks of the polymers remain flexible during simulation, as both water and acetone are good solvents for these chains. The hydrophobic PCL_{2000} starts to collapse i.e. to reduce the radius of gyration and end-to-end distance during the first 25 ns of the simulation, as the presence of the water molecules is increased in the acetone region. After that, the distances plateau for the rest 75 ns indicating that the chains remain on average on the same conformation, due to the acetone's presence. This was illustrated before in the snapshots of figure 3.11, where although the polymers have aggregated, they haven't yet formed a NP. However, during the last 40 ns that correspond to the acetone evaporation, the PCL_{2000} blocks clearly reduce their spatial conformation as they collapse to form a polymer NP of 3.4 nm diameter.

3.5 Simulation of indomethacin in the absence of polymer

A control simulation was performed in order to investigate the behaviour of the indomethacin drug NP in the absence of the polymer. A 5nm in diameter amorphous indomethacin NP was placed in the aqueous cubic box (a=26.7 nm) while the acetone region was polymer-free (b=11 nm, total acetone region volume of 11x26.7x26.7 nm^3). The simulation ran for a total of 100 ns.

Figure 3.14 illustrates the evolution of the simulation. The drug NP stayed intact till 70ns. Then it started to slowly swell up and dissolve, due to the increased presence of the acetone around it.

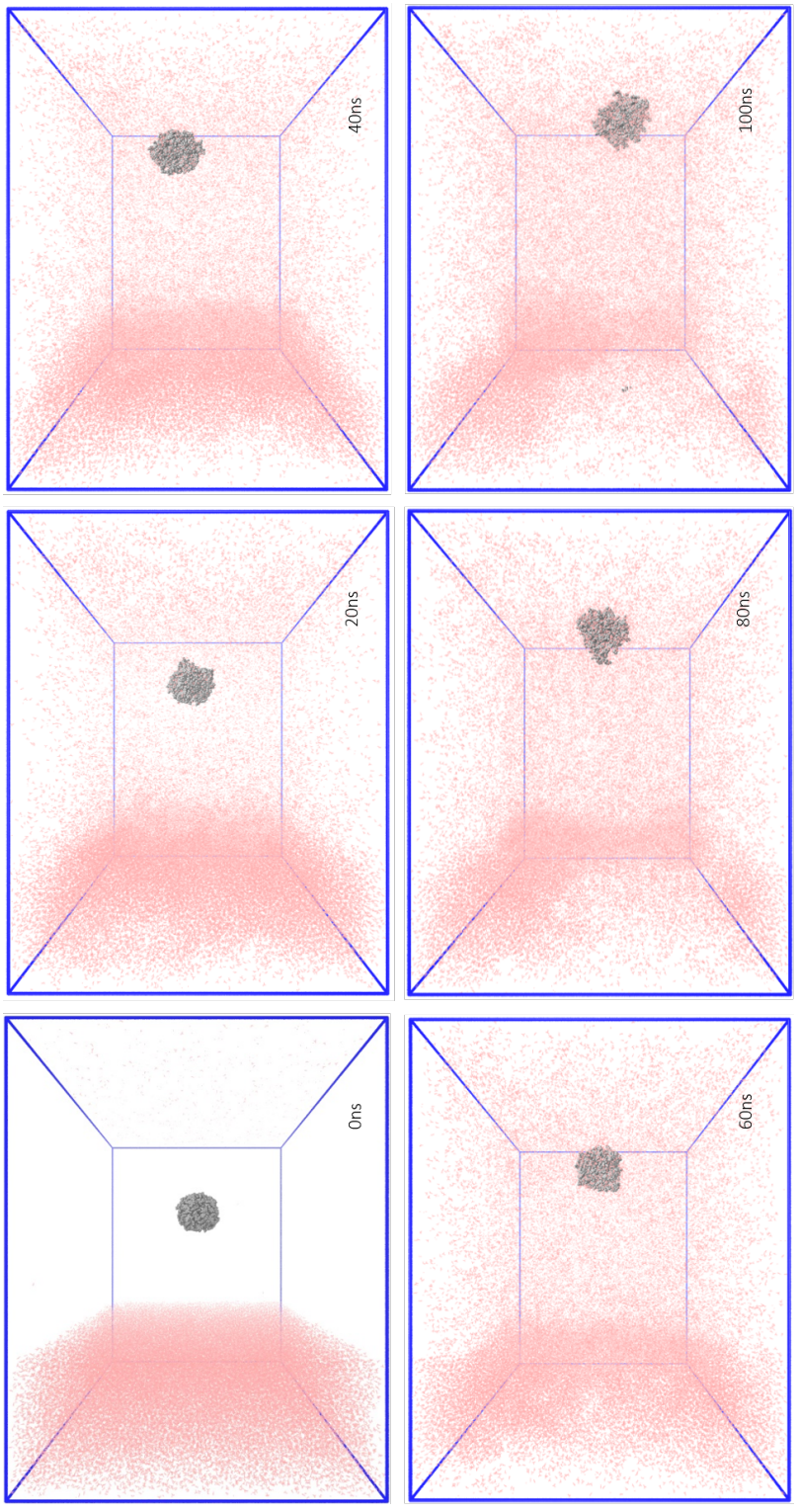


Fig. 3.14 Control simulation of the indomethacin NP (grey) to evaluate the NP's stability in the biphasic system. The drug NP stays intact till 70 ns, however as the acetone's (pink) presence increases in the NP's surrounding environment, the NP starts to swell up and to slowly dissolve. Water is not shown for clarity.

3.6 Simulation for the formation of polymer-drug nanoparticles

A 5nm in diameter amorphous indomethacin NP was placed in the aqueous cubic box (a=26.7 nm) while 31 mPEG$_{350}$-*b*-PCL$_{2000}$ polymer chains (10 mg/ml) were inserted in the acetone region (b=11 nm, volume of 11x26.7x26.7 nm^3). The simulation box contained more than 2.6 million atoms, which made the simulations very slow (figure 3.15). The simulation ran for 281 ns, followed by 5 simulation sets of 10 ns each, to mimic the evaporation of the acetone (total simulation time for system A* 330 ns).

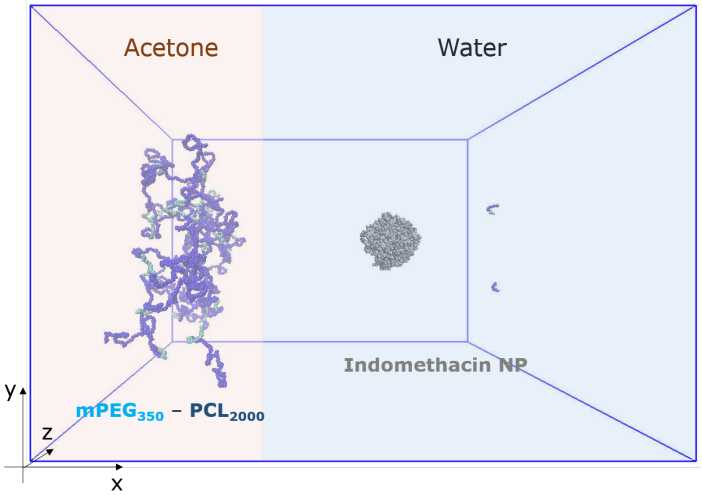


Fig. 3.15 System A* for the formation of polymer-drug NP. The starting point of the simulation of mPEG$_{350}$ (light blue)-*b*-PCL$_{2000}$ (dark blue) in the acetone region, in the presence of the amorphous indomethacin NP (grey) in the aqueous phase.

In figures 3.16 and 3.17, snapshots at different time points of the simulation are presented.

Fig. 3.16 System A*: Interfacial deposition simulation of $mPEG_{350}$ (light blue)-*b*-PCL_{2000} (dark blue) polymer chains in the presence of a 5 nm indomethacin NP (grey). Solvents are not shown for clarity. PBC conditions apply, where the molecules can move across the end of the box. Snapshots taken at various time points of the simulation. The polymer chains start to aggregate slowly as the acetone diffuses towards the water region. The indomethacin NP stays intact in the aqueous region till it reaches close proximity with the polymer chains and gets dissolved at 108 ns.

Fig. 3.17 System A*: Interfacial deposition simulation of $mPEG_{350}$ (light blue)-*b*-PCL_{2000} (dark blue) polymer chains in the presence of a 5 nm indomethacin NP (grey). Solvents are not shown for clarity. PBC conditions apply, where the molecules can move across the end of the box. Later snapshots over the course of the 280 ns simulation; the polymer chains strongly interact with the indomethacin molecules but the presence of the acetone inhibits the formation of a dense polymer-drug NP.

As the acetone diffused towards the water region, the polymer chains started to aggregate, while the drug NP moved intact around the water region. However, at around 100 ns the drug NP reached close proximity to the polymer and dissolved. In order to identify the exact time point where the interactions between the polymer chains and the indomethacin NP occurred, the number of contacts and the distance between the PCL blocks and the indomethacin molecules were calculated and are presented in figure 3.18.

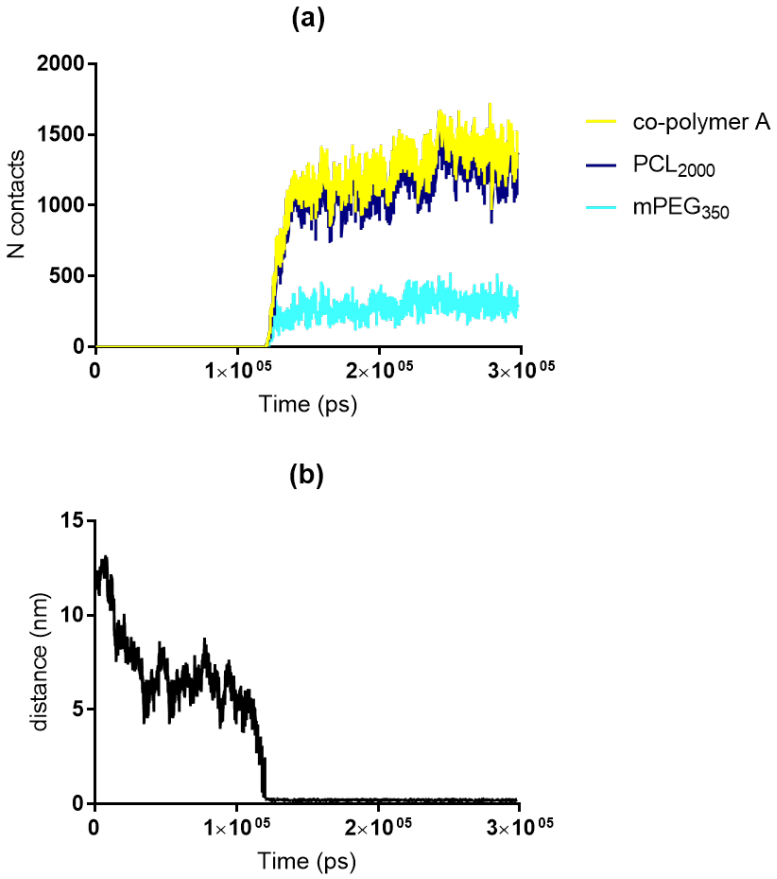


Fig. 3.18 System A*: (a) Number of contacts between the indomethacin molecules and the blocks of the $mPEG_{350}$ (light blue)-*b*-PCL_{2000} (dark blue) polymer chains. The increase after the contact occurs at 108 ns, demonstrates the dynamic interaction between the indomethacin molecules and the polymer chains. (b) Distance between the centre of mass of the indomethacin NP and the PCL chains, which becomes zero when indomethacin interacts with the polymers.

The decrease in the distance between the moieties show clearly the point where the NP started to interact with the polymers (108 ns). The number of contacts increased drastically during the first 15 ns after the first contact however they plateaued for the rest of the simulation. This graph has provided a quantitative description of figure 3.17, where an active interaction between the polymer and the drug molecules for a long period in the presence of the acetone is illustrated.

The complete dissolution of the indomethacin NP was not witnessed during the control simulation and thus suggests that there is a synergistic effect between the polymer and the acetone that breaks down the drug NP. At the same time, as both the indomethacin NP and the polymer chains are soluble in acetone, and the acetone is still present, the formation of a dense polymer-drug NP is inhibited.

In order to evaluate the mixing of the solvents, the simulation box was scanned in the x-axis at the start and the end of the simulation (figure 3.19). A satisfactory distribution was achieved at 280 ns, i.e. the solvents were mixed and the system has reached full equilibration.

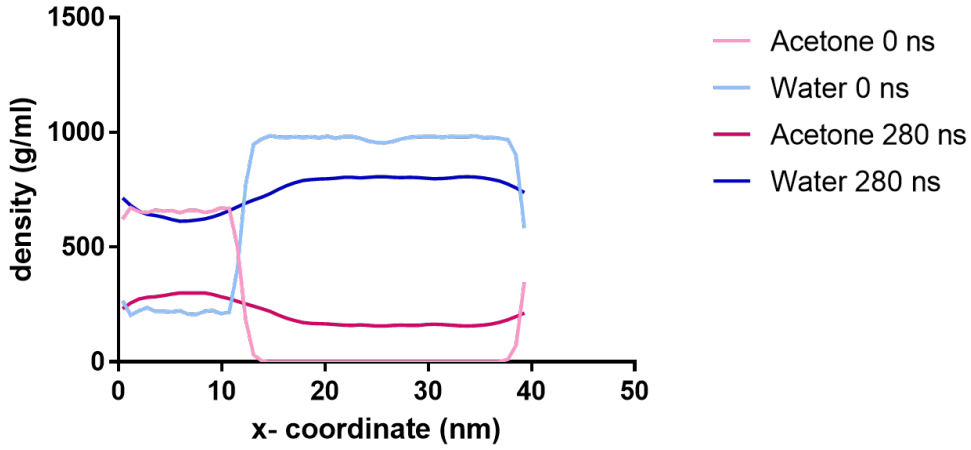


Fig. 3.19 System A*: Interfacial deposition simulation for the formation of a polymer-drug NP. The spatial distribution of the acetone and water molecules across the x-axis of the simulated box at the start and at 28- ns of the simulation. A satisfactory distribution of the solvent molecules across the box is achieved, and the system is considered fully equilibrated.

As performed before, the acetone molecules were replaced with water molecules to simulate the evaporation of the organic solvent. Snapshots at the end of each 10 ns simulation runs are presented in figure 3.20

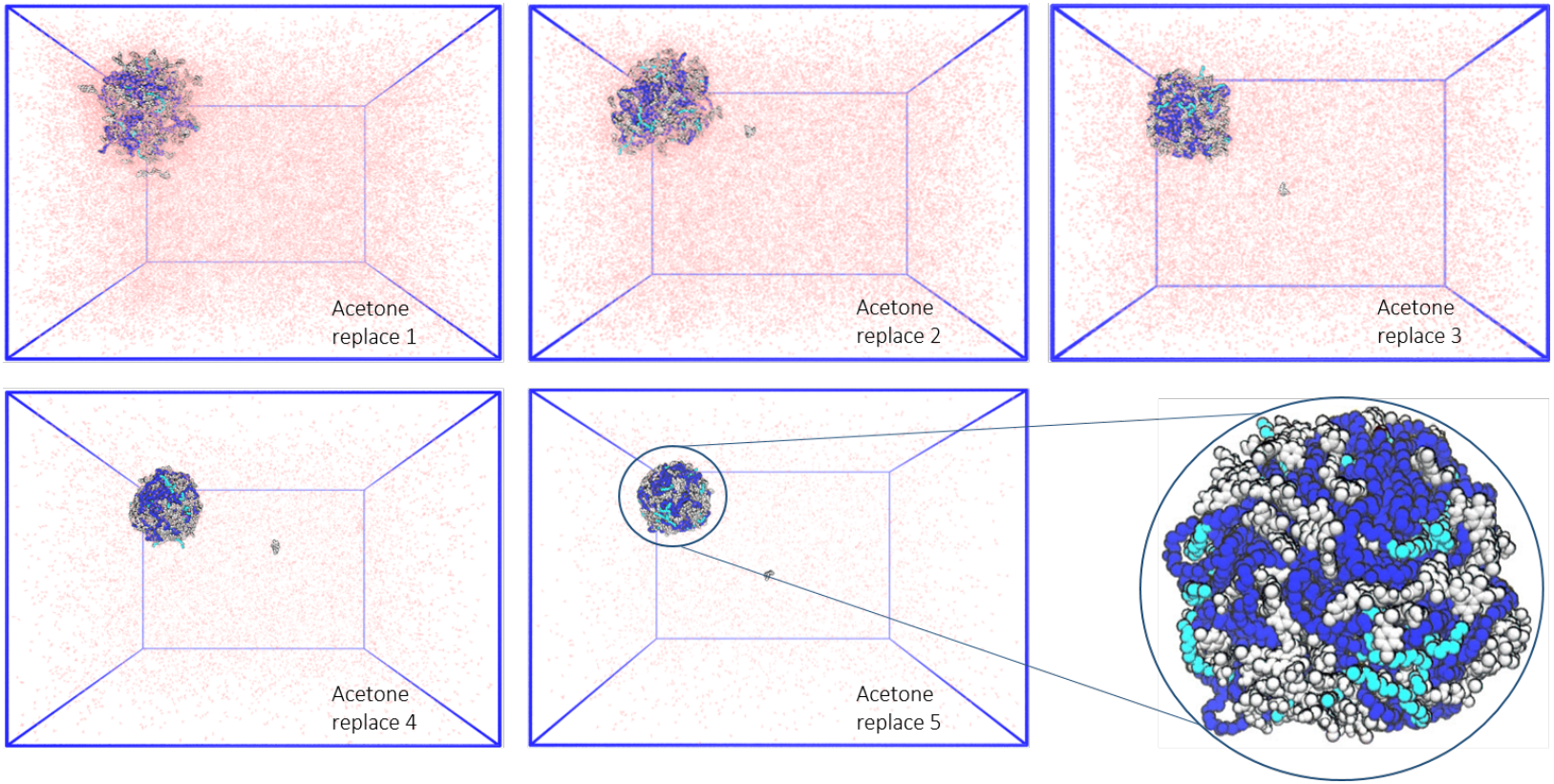


Fig. 3.20 System A*: Acetone (pink) replacement during the interfacial deposition simulation of $mPEG_{350}$ (light blue)-*b*-PCL_{2000} (dark blue) polymer chains in the presence of indomethacin (grey). Water is not shown for clarity. PBC conditions apply, where the molecules can move across the end of the box. Snapshots after each 10 ns MD run simulating acetone's "evaporation". The polymer chains and the indomethacin molecules aggregate and form a dense polymer-drug NP of 7 nm diameter.

Once the acetone molecules started to be replaced by water molecules the polymers and drug particles started to interact strongly and a particle started to form; a polymer-drug NP of 7 nm in diameter was obtained. This resulting NP, after nearly 330 ns of simulation, does not resemble the ideal coated NP as envisioned in the Introduction of this thesis. The mPEG chains were entangled with the drug molecules and since the drug NP had dissolved completely during the first 110 ns of the simulation, the drug molecules were dispersed uniformly inside the NP.

144 indomethacin molecules were incorporated by the polymer chains resulting in a 99.3% of yield in respect to the drug. Only one indomethacin molecule remained unattached to the polymer-drug NP and was moving in the aqueous region. The fate of this indomethacin molecule is debatable: it is possible that it would become incorporated at a longer simulation time if it reached to close proximity with the polymer-drug NP, or it could remain free in the aqueous region. The latter scenario also correlates with some of the experimental work presented in the next chapter, where the uncoated drug particles would precipitate. With the same rationale, had the starting indomethacin NP been larger, the simulation could have resulted in two different NP populations; one polymer-drug NP and one uncoated pure drug NP.

In order to provide a quantitative description of the polymers aggregation, the static properties of the polymers were calculated for the whole of the 330 ns of the simulation and are presented in figure 3.21.

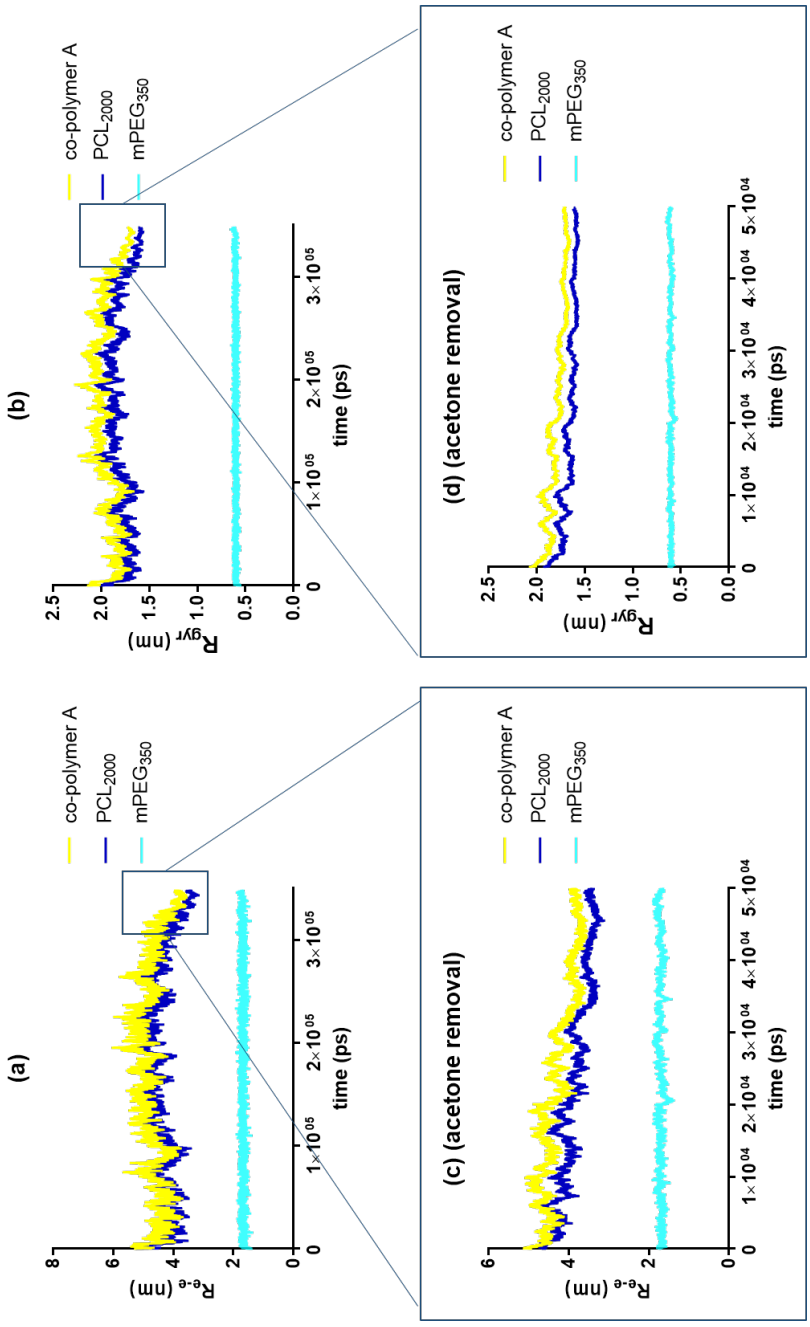


Fig. 3.21 System A*: End-to-end distances ((a), (c)) and Radius of gyration ((b), (d)) for the different blocks of $mPEG_{350}$-*b*-PCL_{2000} polymer chains for the complete simulation (top row) and the acetone evaporation steps (bottom row). The hydrophobic PCL starts to aggregate thus reducing its spatial conformation.

Similar to the results from the drug-free simulation for the formation of the polymer NP (System A, section 3.4), the hydrophilic $mPEG_{350}$ chains remain flexible throughout the simulation as both water and acetone are good solvents for them. The PCL_{2000} chains are flexible as well during the mixing of the two solvents, however during the evaporation of the acetone they aggregate and thus both the radius of gyration and the end-to-end distances decrease.

3.7 Discussion

In this chapter all-atom MD simulations were employed to model the coating method of a drug NP, via a modified interfacial deposition method.

Interfacial deposition is based on solvent displacement and as such, the diffusion of the organic solvent into the anti-solvent region greatly affects the NPs formed. The nature of the organic phase and its importance on the NP formation has been discussed in the Introduction of this thesis.

Since the diffusion of the acetone in water is such a critical parameter, prior to modelling the interfacial deposition, different acetone models were evaluated for their diffusion with SPC water model. The acetone model selected, based on parameters of the force field used in this work (GROMOS53a6) demonstrated a higher diffusion rate compared with the experimental value. This observation means that the phenomena leading the formation of any NPs via MD simulations are accelerated and thus it could be that the phenomena observed in the present work could require larger simulation times with the use of a less diffusive acetone model. However, to our knowledge, the field of MD is still missing an acetone model, able to mix with water in all molar fractions [106, 154, 153].

Whilst acknowledging the inadequacies of the acetone model used, the physical representation of the system from the simulations is satisfactory. The simulations have reproduced successfully the expected experimental behaviour of the pure systems i.e. the dispersive behaviour of the mPEG-*b*-PCL polymers and the indomethacin NP in pure solvents.

When mPEG-*b*-PCL chains are introduced into the biphasic system, it was observed that the PCL chains started to aggregate as the aqueous environment surrounding the polymers increased. However, the

hydrophobic effect leading to the formation of a polymer NP was inhibited by the presence of the acetone molecules in the simulations: acetone molecules were clustering around the polymer chains, not allowing their full aggregation, an observation which was previously reported by Di Pasquale et al. [106].

Experimentally, the evaporation of the organic solvent started immediately after the interfacial deposition method has been performed. In order to replicate this in the simulations a gradual removal of acetone molecules was adopted, via their replacement with water molecules. Due to the increasing aqueous environment, the polymers aggregated resulting into a polymer NP of 3.4 nm diameter. This polymer NP consisted of a tightly and randomly aggregated polymer chains, with PEG chains entangled even in the core of the NP. This morphology was not expected; as discussed in the Introduction, polymer NPs are typically envisioned to have a very tight hydrophobic core while the hydrophilic PEG chains are on the surface of the NP forming a corona. The difference between the expected NP morphology could be attributed to the small length of the $mPEG_{350}$ chains. Had the simulations been performed with $mPEG_{2000}$ it is possible that a different NP morphology would be obtained, due to the steric behaviour of the larger PEG chains.

31 polymer chains were used in the acetone region, corresponding to a 10 mg/ml polymer concentration in acetone. This was the highest amount of polymer used in the experimental chapter, and for $mPEG_{350}$-*b*-PCL_{2000} this concentration resulted into the formation of stable polymer NPs as will be discussed in the next chapter. Usually, in MD simulations, the solutes' concentrations are not in the same order of magnitude as the experimental values: when they are underestimated it is due to the increase in the computational cost [93] while when overestimated it is in

order to increase the success rate. In this work all the MD simulations were performed using concentrations within one order of magnitude of the actual concentrations used in the experiments. This is a success of the present work, as the phenomena that take place during the formation of the NPs can not be falsely attributed to the over/under estimation of the concentrations used.

In order to investigate the coating procedure a drug NP was presented in the aqueous phase. This NP containing 145 indomethacin molecules had a 5nm diameter and was formed as amorphous. This corresponded in a 4 mg/ml indomethacin in acetone concentration which is still in the same order of magnitude with the experimental work. The size of the starting indomethacin NP was at this scale as increasing the diameter even by 1 nm the computational cost would increase.

During the mixing of the solvents in the presence of both the polymers and the drug NP, the polymer chains behaved as in the simulation described above, while the insoluble in water indomethacin NP remained intact for the first 100 ns. However when the drug NP reached in close proximity, the polymer chains facilitated by the constant presence of acetone molecules around them, dissolved the NP and kept interacting dynamically with them for more than 150 ns. This interaction justifies our selection to use MD simulations to model interfacial deposition as a compliment to the experimental studies as in the macroscopic experimental world such a phenomenon is not possible to be observed.

The aggregation of the chains and the drug molecules into a dense NP was again inhibited by the presence of the acetone. Once it was removed, a polymer-drug NP of 7 nm diameter was formed with a 99.3% yield in drug incorporation; 144 drug molecules dispersed into the poly-

mer matrix, and only one indomethacin molecule was unbound. The morphology of this NP also differed from the one that was hypothesised in the beginning, as there was a homogeneous distribution of all the moieties in sphere.

From a NP preparation perspective, this is the first time an unbiased simulation resulted into the self-assembly of a polymer-drug NP, something that reportedly was missing from the field [85].

In regards to modelling solvent-displacement processes, computational fluid dynamics (CFD) have been employed before by DiPasquale et al. [82, 83], Bally et al. [159] and Lince et al.[160]. CFD provide invaluable information over parameters like solvents' velocities and molar fractions, mixer geometries and are able to predict the final NP size based on population balance equations. However, such methods fail to describe the morphology of the NPs. All-atom MD simulations in this work both simulated the solvent displacement and provided a description of the NP with atomistic detail.

At the same time, in other MD NP-formation studies, the NPs are preformed utilising linkers in the particles' surfaces [109, 113] thus simulating a biased system. In regards to the solvents used, usually in the literature polymers and drugs are simulated in pure solvents (water in most cases) [83, 102, 101] and/or single polymer chains are used [83, 106, 102] in order to make the systems faster and less computationally needy.

The NPs formed in this work are not covalently bonded; the individual polymers and drug molecules are dynamic, thus with the start of the simulations the systems were allowed to evolve in the closest and most unbiased way possible.

Table 3.4 Radius of gyration (nm) of PCL_{2000} block compared with the existing literature and models.

x_α	Present work	Di Pasquale et al. [106] calculated from eq.3.7.1	Huynh et al. [107]
0	0.949	0.612	1.331
0.08945	1.682	0.836	-
1	2.189	2.508	-

From a quantitative point of view, we were able to calculate the static properties of the polymers during the interfacial deposition and in the presence of pure solvents. Relevant data in the literature were provided by the studies of Huynh et al. [107] and Di Pasquale et al. [106].

Huynh et al. [107] studied the effect of mPEG-PCL blocks' chain length in the formation of micelles, under the OPLS forcefield. They performed all their simulations in water and reported that the PCL blocks aggregated within the first 15 ns which is in agreement with the present work. In another work, Di Pasquale et al. [106] performed all-atom simulations, using the OPLS forcefield of PCL in various molecular weights, and in different acetone-water molar ratios, and reported the static properties of PCL in them. The authors of that work presented the following equation to calculate the radius of gyration of the PCL blocks:

$$R_{gyr} = [0.0064exp(-3.15x_\alpha)]M_w^{0.60+0.90x_\alpha-0.30x_\alpha^2} \qquad (3.7.1)$$

where x_α is calculated from equation 3.1.1 and M_w is the molecular weight of the PCL block. Combining the information from the above works, the radius of gyration was calculated for PCL_{2000} via the *gmx polystat* GROMACS module analysing the trajectories from the pure solvents simulations (water x_α=0, acetone x_α=1) and from the simulation for the formation of the polymer NP (System A, x_α=0.08945). Results are summarised in the table 3.4.

Reasons for the difference in the values reported could be different acetone models and forcefields, number of MD timesteps or the fact that the number of polymer chains used are different in all the works.

However, the fact that similar results for the static properties of the polymers were obtained under different forcefields, strengthens the point raised earlier in this thesis; there is no universal empirical forcefield to describe all the interactions that take place in the nanoscale. For example, although the OPLS forcefield has been used a lot in the past, in a very recent work, Goliaei et al. [115] studied the behaviour of Poloxamer molecules using a slightly modified GROMOS53a6 forcefield and reproduced successfully observations that before were available only via coarse graining simulations.

Another key point raised via this work is that using ATB-created files for GROMOS53a6 has proven to be a fast and versatile approach, that has facilitated the all-atom simulations.

CHAPTER 4

Experimental Studies

Interfacial deposition has been used in the past to coat IONPs with a thin polymer (PGA) layer [2]. One of the main aims of this work was to investigate the translation of this technique to coat the surface of drug NPs. mPEG-*b*-PCL was chosen as the polymer to be used in this NP preparation process, as the components are biocompatible and the blocks are used in approved formulations. The hydrophobic PCL block of the polymers is biodegradable and is expected to bind to the drug NP's surface while the length of the hydrophilic mPEG block can be optimised to control the steric interactions between the NPs. Some of the main considerations during the experimental work were the following:

- Would the process be transferable from an insoluble inorganic NP to a solvent soluble drug NP?
- Would the mPEG-*b*-PCL copolymers in the present work have the same coating ability as the PGA used in previous studies?
- What is the best way to create drug NPs suitable for this process?

In this chapter all of the above raised points needed to be addressed. Firstly, mPEG-*b*-PCL diblock copolymers were synthesised in four differ-

ent hydrophilic:hydrophobic ratios. It was decided that the hydrophobic PCL block would be kept at a constant molecular weight in order to evaluate the effect the hydrophilic mPEG block would have on the stability of the resulting NP suspensions. The polymers were fully characterised for their physical and thermal properties via ^{1}H NMR, DSC, ATR-IR and WCA (section 4.1).

As a next step, the pre-existing interfacial deposition method was optimised, resulting in a flow method (section 4.2.1), to produce polymer NPs. The idea was that these polymer NPs would act as a control to distinguish the drug-coated NPs from any polymer NPs which may be formed in this process. The range of the polymer concentrations needed for the coating studies was defined and the morphology and sizes of the polymer NPs were studied via DLS and TEM (section 4.2.2).

The best way to produce an aqueous suspension of indomethacin particles is to use in the aqueous phase was investigated. Two milling methods, wet-ball milling and cryomilling were used and the state of the resulting indomethacin was investigated by DSC and ATR-IR. The indomethacin NP suspension was further characterised by TEM, POM and DLS (section 4.2.3).

The stability of the drug nanoparticles during the coating method in the absence of the polymer was examined. This also served as a negative control to distinguish the pure drug NPs from the polymer-coated ones. The resulting suspension was characterised by DLS, POM and TEM for the size and morphology of the particles as well as by UV-VIS for the quantification of the drug amount in the final suspension (section 4.2.4).

Finally, the polymer-coating of indomethacin NPs was explored, for all the four polymers in a range of polymer concentrations and in different

indomethacin suspensions. DLS, POM and TEM were employed for the size and morphology of the polymer-coated drug NPs while UV-VIs was used for the quantification of drug loading and encapsulation efficiency. (4.2.5)

4.1 Polymer Synthesis and Characterisation

The polymers were synthesised as described in section 2.2.1.1. The chain propagation and formation of mPEG-*b*-PCL diblock copolymers was studied via ^{1}H NMR. Figure 4.1 shows a typical spectrum of mPEG$_{350}$-*b*-PCL$_{2000}$ copolymer. The proton signal at δ 4.2-4.27 ppm corresponds to the CH_2 methylene protons adjacent to the ester bond to the PCL component (i.e. the last PEG unit connected to the CL chain) (peak b′) allows the calculation of the degree of polymerisation (DP) and thus the number of the repeated CL units [52]. The molecular weight of the polymer was calculated by the integration of peak c after setting peak b to the unit of 1, i.e. following the equation:

$$M_{n(NMR)} = M_{n(mPEG)} + 114.14 * DP \tag{4.1.1}$$

The two triplets in the region 3.2-3.3 ppm correspond to the catalyst TBD and they are absent after the purification by precipitation in cold methanol.

PEG350PCL: ^{1}H NMR (figure 4.1) (400 MHz, $CDCl_3$, , ppm): 1.41 (m, 34, $CH_2CH_2CH_2$), 1.68 (m, 68, $CH_2CH_2CH_2$), 2.33 (t, 34, $COCH_2$), 3.40 (s, 3, PEGCH_3), 3.67 (m, 24, OCH_2CH_2O), 4.08 (t, 34, $CH_2CH_2CH_2O$), 4.25 (t, 2, CH_2CH_2OCO). The polymers have also been characterised by ATR-IR

(figure 4.2) ATR-IR: υ (cm^{-1}) 3447, 2937, 2889, 2866, 1718, 1473, 1418, 1395, 1366, 1288, 1234, 1171, 1107, 1065, 1047, 957, 935, 733.

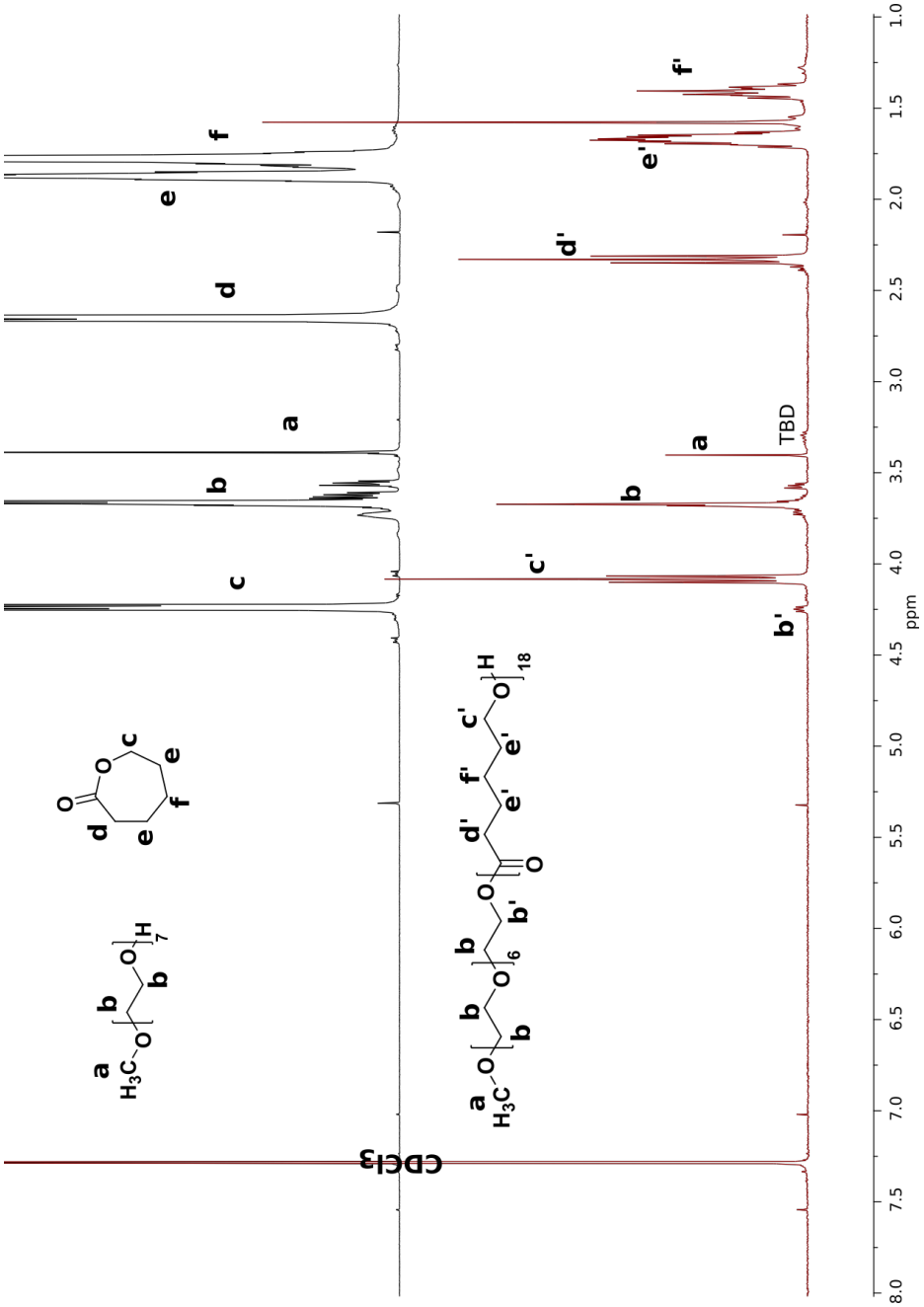


Fig. 4.1 ^{1}H NMR spectra of PEG350PCL at the end of the reaction (30 minutes).

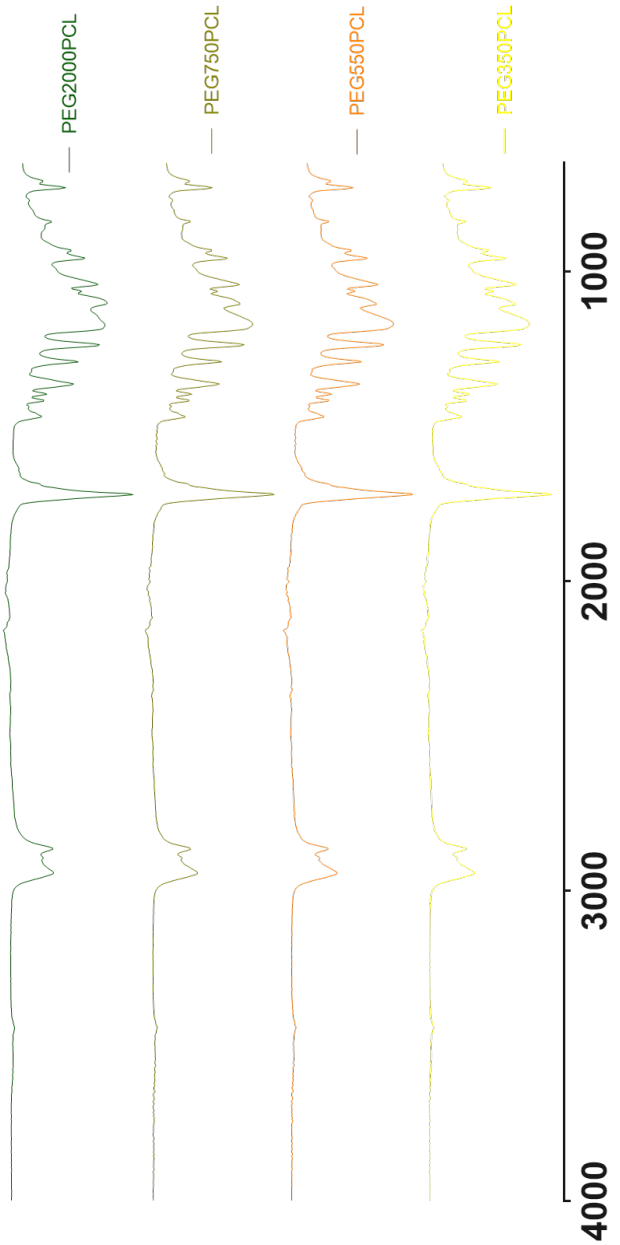


Fig. 4.2 ATR-IR spectra of mPEG-b-PCL polymers.

The properties of the polymers after their characterisation via NMR and GPC are summarised in table 4.1. The hydrophobic segment of the polymers is very close to the targeted value of 2000 Da. The observed difference between the reported GPC and the calculated NMR molecular weights can be attributed to the behaviour of both PCL and mPEG blocks in the mobile phase of the GPC (chloroform). The polystyrene standards that have been used for the calibration demonstrate a different behaviour in comparison to PCL, while the hydrophilic PEG-counterpart is highly flexible and most likely exhibits a higher hydrodynamic volume. All the GPC traces can be seen in Appendix B.1 .

Table 4.1 Polymer and monomer characterisation by ^{1}H NMR [a], GPC [b] and DSC

Abbreviation	Polymer	NMR		GPC		DSC	
		M_nPCL [a]	M_nPolymer [b]	M_n	PDI	T_m (^{o}C)	ΔH (J/g)
PEG350PCL	$mPEG_{350}$-PCL_{2000}	1940	2290	7384	1.60	50.21	78.7
PEG550PCL	$mPEG_{550}$-PCL_{2000}	2055	2605	6823	1.60	55.71	82.25
PEG750PCL	$mPEG_{750}$-PCL_{2000}	1940	2690	7601	1.43	50.05	73.97
PEG2000PCL	$mPEG_{2000}$-PCL_{2000}	2169	4169	10957	1.49	59.10	82.5
	$mPEG_{350}$			389	1.18	-6.83	49.12
	$mPEG_{550}$			684	1.14	14.37	129.6
	$mPEG_{750}$			976	1.12	29.67	145.4
	$mPEG_{2000}$			3307	1.07	51.94	171.7
	ϵ-CL			120	1.01	-1.3	119.2

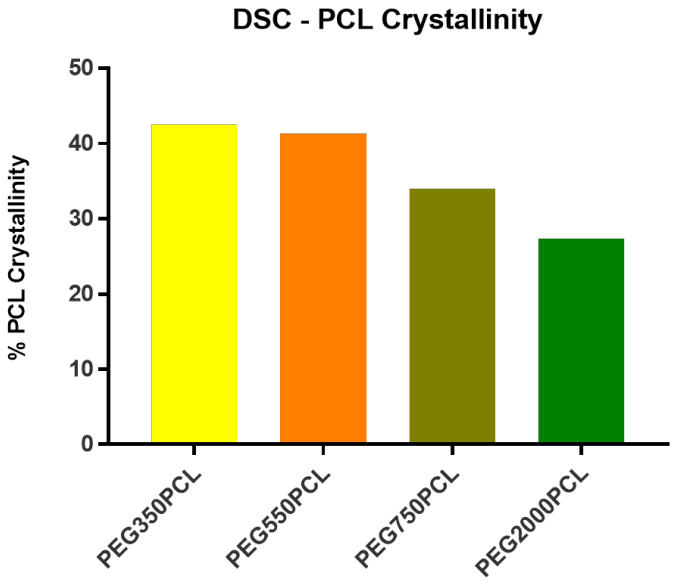


Fig. 4.3 Analysis of ΔH measurements from DSC revealed a decrease in the percentage of crystallinity of the PCL block of the copolymers with an increase of the length of the hydrophilic block.

DSC measurements The thermal transitions of the polymers were studied by DSC (appendix section B.2). As seen in table 4.1, the mPEG initiators demonstrate an increase in their melting points, consistent with the increase of their molecular weight [161]. Melting points of the polymers are in the range of 50 -59 ^{o}C, but no trend due to the increase in mPEG content is observed in the final copolymers, due to their semi-crystalline nature. No glass transition was detected for any of the block-copolymers, but it should be mentioned that $mPEG_{350}$ displayed a glass transition at -31.7 ^{o}C (appendix, figure B.5).

Further analysis of the ΔH from the DSC revealed a trend in the crystallinity of PCL block of the copolymers, presented in figure 4.3. It is clear that the increase in the molecular weight of mPEG affected the crystallinity of the PCL block of the polymers.

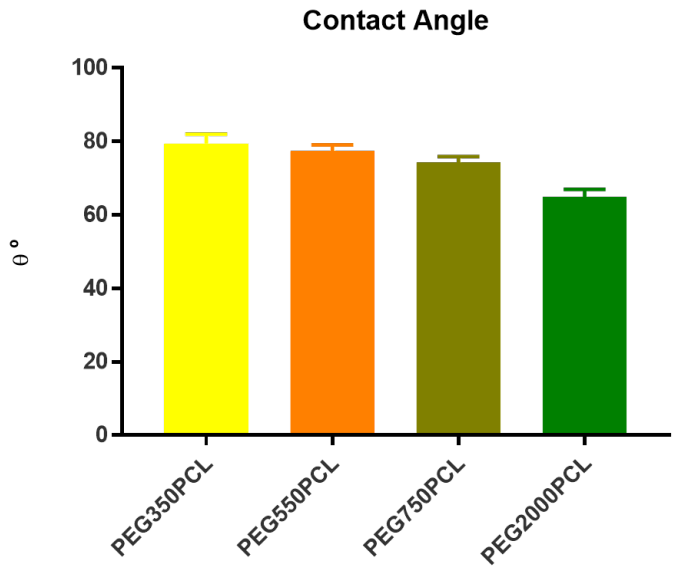


Fig. 4.4 Water contact angle measurements for the assessment of the wettability properties of the polymers. Error bars correspond to the standard deviation calculated from four measurements. The θ values decrease with the increase of the hydrophilic block reflecting the increased hydrophilicity of the polymers.

Water contact angle measurements Water contact angle measurements were performed on polymer-coated glass cover slips to evaluate the wettability properties of the polymers. Figure 4.4 illustrates the findings which demonstrated that the increase of the length of the hydrophilic mPEG resulted in a decrease of the contact angle. This observation reflects the increasing hydrophilic character of the polymers and can be interpreted by the spatial arrangement of the polymers with their hydrophilic part arranged towards the environments moisture. This becomes clear with the behaviour of the largest PEG2000PCL polymer that is very flexible and demonstrates the lowest θ and the smallest particle sizes during NP formation (discussed later).

4.2 The coating process

4.2.1 Derivation of the coating process

In a typical nanoprecipitation method, the solute is dissolved in the presence of a stabilising molecule (i.e. polymer) in a favourable solvent, which is then added into a miscible solvent that acts as a non-solvent for both the solute and the stabiliser [77]. In the case of Flash Nanoprecipitation (FNP) [79], this is done by mixing the two streams in a confined space providing supersaturation conditions in order both the solute and the stabiliser to precipitate simultaneously. As the precipitation occurs, the stabiliser has a double role; it acts as an inhibitor to the uncontrollable growth of the solute particles but it also provides steric stabilisation of the final particles [77]. This method has been used in the literature to produce β-carotene-PEG-PCL [78], itraconazole-poloxamer 407 [80], and other polymer NPs [162, 163].

The final NP population is dependent on the solvents miscibility and molar ratios, the nature and the length of the hydrophobic and hydrophilic blocks of the polymeric stabilisers, as well as the mixing times and flow ratios. CFD simulations have been performed to establish the solvent/non solvent ratio with good agreement between experiments and simulations by Di Pasquale et al. [83, 82]. Previous work in our group has also used FNP to produce thermoresponsive NPs to target cancer cells [164].

However in this present work, the FNP was adapted to the pre-existing IONP coating method (interfacial deposition) where the IONPS are present in the aqueous environment. The use of the pump system enhances the reproducibility of the experiments as well as facilitating the

optimisation of the process by allowing control over parameters like flow rates and mixing tube diameters.

4.2.2 Formation of polymer nanoparticles

In order to distinguish the polymer-coated drug NPs from polymer NPs, the formation of polymer micelles was investigated for all the polymers, following the protocol as described in section 2.2.2.1. Firstly, the PEG2000PCL was selected to investigate the size of the polymer NPs as a function of the starting polymer amount present in the acetone region. The results are summarised in figure 4.5 and an example of the raw data can be seen in figure 4.6.

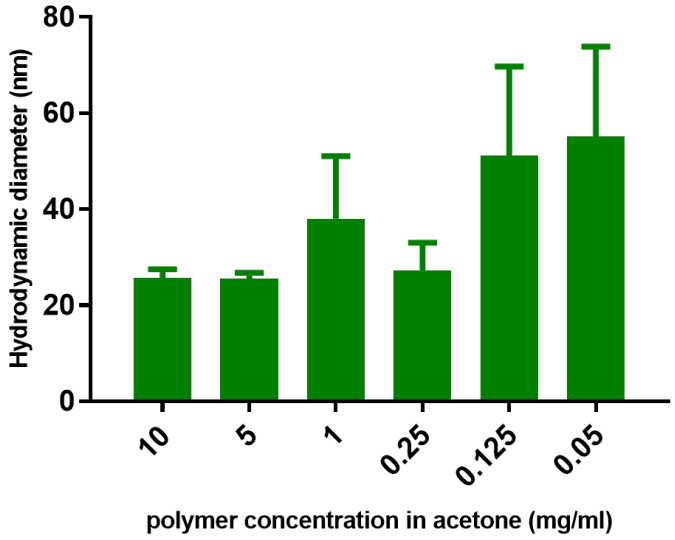


Fig. 4.5 Hydrodynamic diameter (DLS, Number distribution) of the PEG2000PCL polymer NPs in a range of different polymer in acetone concentrations (mg/ml). Error bars correspond to the SD as measured by the instrument. Hydrodynamic diameter of PEG2000PCL polymer NPs varies according to the concentration from 25 to 50nm.

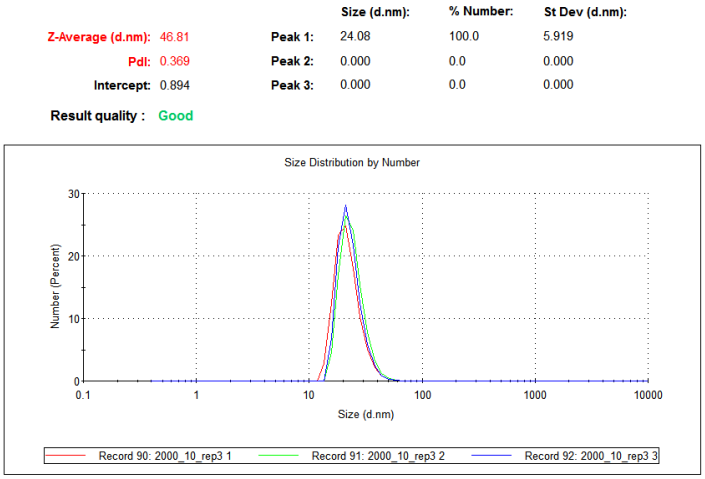


Fig. 4.6 Hydrodynamic diameter (DLS, Number distribution) of the PEG2000PCL polymer NP prepared from a starting 10 mg/ml polymer in acetone concentration.

The hydrodynamic diameter of the polymer NPs formed with the PEG2000PCL varied from 25nm for the high polymer in acetone concentrations and increased to 40 - 50nm in lower concentrations.

The higher polymer in acetone concentrations (10, 5 and 1 mg/ml) were used for the formation of polymer NPs with the rest of the polymers and results are illustrated in figure 4.7.

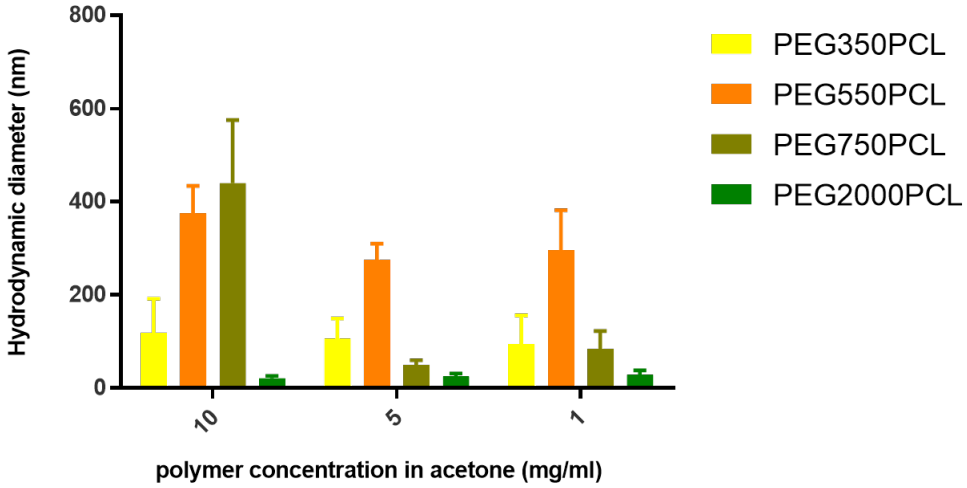


Fig. 4.7 Hydrodynamic diameter (DLS) of polymer NPs in a range of high polymer in acetone concentrations (mg/ml). Error bars correspond to the SD as measured by the instrument. NPs formed with PEG550PCL and PEG750PCL were unstable, aggregated and finally sedimented within 24 hours.

Large particles were formed for the PEG550PCL and PEG750PCL that sedimented within 24 hours; this led to the decision to use concentrations in the range of 1-0.05 mg/ml for the rest of the polymers.

The results showing the hydrodynamic diameters of the polymer NPs for the lower polymer in acetone concentrations (1, 0.5, 0.1 0.05 mg/ml) are illustrated in figure 4.8.

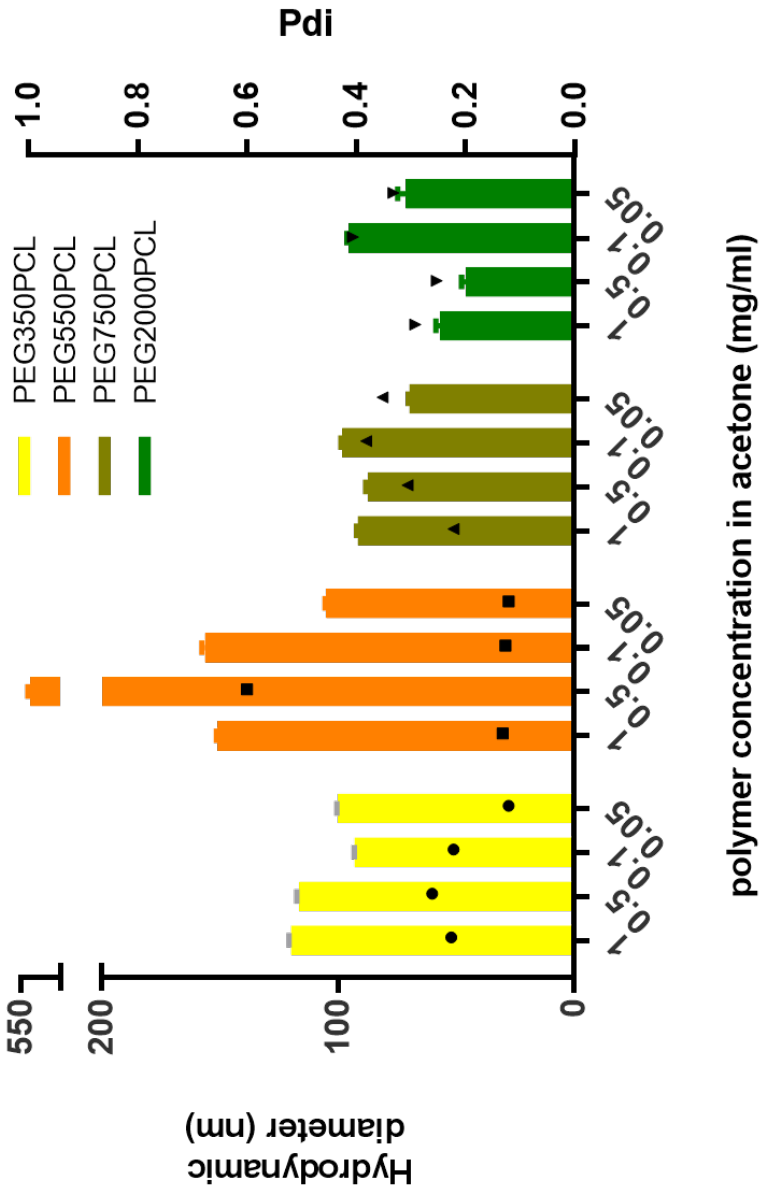


Fig. 4.8 Hydrodynamic diameter (DLS) of polymer NPs of all the four diblock copolymers in different polymer in acetone concentrations (mg/ml). Error bars correspond to the SD of 3 measurements. Black filled symbols (dots, squares and triangles) correspond to the polydispersity index values (right graph bar) as reported from the measurements.

As can be seen, PEG350PCL has demonstrated PDI values less than 0.25, indicating a single NP population. PEG550PCL formed the largest NPs with diameters more than 150nm (with the exception of 0.05 mg/ml where a 100nm distribution was recorded). It also showed single peaks of NPs with PDIs less than 0.2 with the exception of the NPs formed at 0.5 mg/ml which precipitated after a while. PEG750PCL formed NPs of less than 100nm in diameter but the increased PDI values in the lower concentrations (between 0.30-0.38) could be indicating stability issues. As was expected, PEG2000PCL has demonstrated the smallest NPs distribution in all the concentrations, with sizes ranging from 80nm (0.1 mg/ml) down to 50nm (0.5 mg/ml) in diameter.

The reproducibility of the method was also considered; preparation of 3 batches of the PEG350PCL at 0.05 mg/ml polymer:acetone concentration successfully reproduced the same size distribution via DLS (appendix, figure B.16).

Zeta potential measurements were performed to evaluate the surface potential of the polymer NPs (figure 4.9).

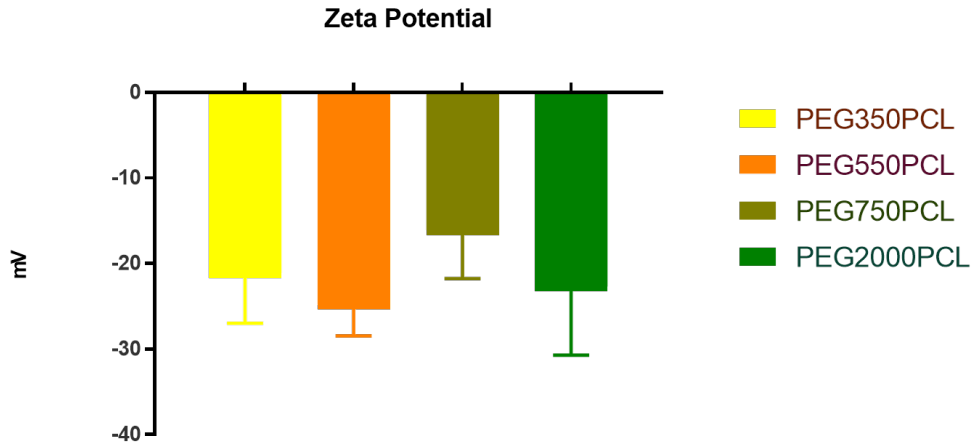


Fig. 4.9 Zeta potential of the polymer NPs, in water. Error bars correspond to the SD of 3 measurements. The NP populations exhibit a values larger than -20 mV with the exception of PEG750PCL (-16 mV).

All the polymer NPs with the exception of PEG750PCL (-16.1 mV) have demonstrated zeta potential values larger than -20 mV. Zeta potential values less than |30| mV suggest borderline unstable behaviour [143] for NP populations whose stability depends on electrostatic forces. However the polymer NPs produced in this work were sterically stable due to the length of the hydrophilic mPEG block.

In order to evaluate the NP stability further, a salt concentration test was performed using barium chloride ($BaCl_2$) at the NPs produced with the lowest polymer in acetone concentration (0.05 mg/ml); the increase in the ionic strength of the solution destabilises both electrostatic and sterically stabilised particles, causing the precipitation of unstable populations. The polymer NPs started precipitating when the salt molarity reached 0.66 M (data not shown), indicating a stable population of NPs.

The physical stability of the NPs were also assessed. When kept under typical lab conditions, the NPs exhibited the same particle distribution after 1 month (data shown in appendix B.5.4).

In order to evaluate the minimum amount of polymer needed to form a NP, the critical aggregation concentration (CAC) was determined by DLS (appendix B.5.5). For all the polymers, the CAC was calculated to be in the range 5-10 μg/ml, suggesting that the aggregation of the NPs is dominated by the hydrophobic collapse of the PCL block, which has almost the same length in all the polymers synthesised. As seen from the control simulations in chapter 3.2.1.2, the polymer chains collapse almost immediately in the presence of water, before forming a polymer aggregate-NP.

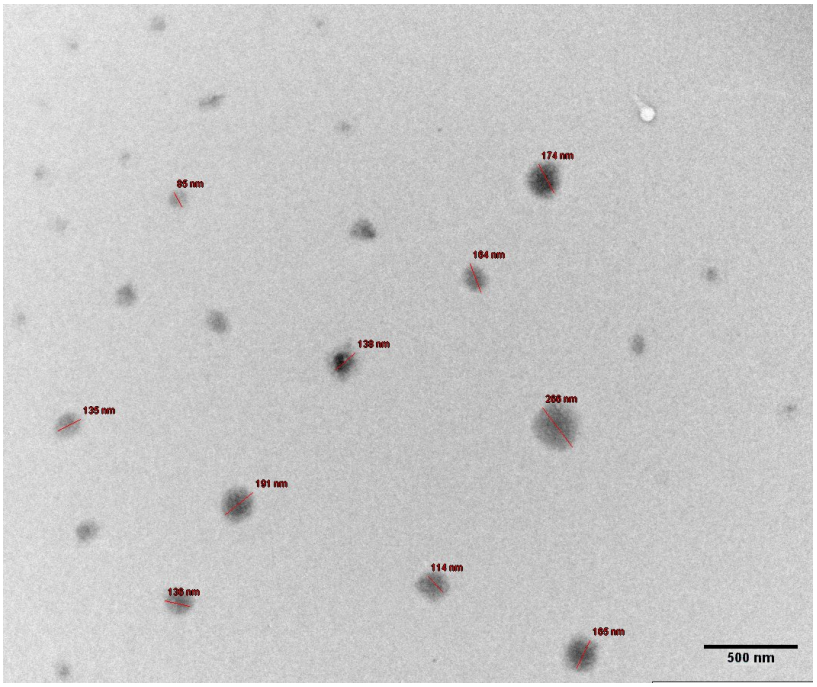


Fig. 4.10 TEM image of the PEG350PCL NPs formed at 0.05 mg/ml starting concentration in acetone. (Size range 143.5±47.4 nm, Scale bar 500 nm).

Finally, TEM was used to study the morphology of the polymer NPs. Figure 4.10 shows a clear distribution of spherical PEG350PCL NPs, with particle sizes of 143.5±47.4 nm.

4.2.3 Production of drug particles for the aqueous phase

As discussed in the introduction of this thesis, more than 70% of the new potential small drug molecules have poor aqueous solubility and/or dissolution [7, 72]. Indomethacin exhibits poor aqueous solubility and has been used as a model hydrophobic drug in many studies [76, 75, 66, 1, 165].

The initial approach in order to test the transferability of the coating method was to replace the IONPs with indomethacin NPs, i.e. to produce an aqueous suspension of indomethacin NPs to be used in the aqueous phase, preferably in an amorphous state. The amorphous state was desired as amorphicity would increase the aqueous solubility of the drug and it was thought that this would be preferable for the method. In order to achieve this, two top-down methods for the production of indomethacin NPs were considered; wet-ball milling and cryo-milling.

4.2.3.1 Wet ball milling

Wet ball milling (WBM) is the most frequently used method to produce drug nanocrystals [5]. WBM is a top-down method that is very versatile as it can be used for almost any API [6] producing nanosuspensions with particle sizes ranging between 100-300nm [5]. However, WBM involves the milling of the API in the presence of an anti-solvent and one or more stabilisers. Since the approach taken on the present work was to minimise the amount of stabilisers/excipients that would be present in the final polymer-coated formulation, WBM was used without excipients in order to create a pure drug aqueous suspension.

Initial experiments were performed in GlaxoSmithKline, in the absence of a surfactant, by milling indomethacin with water as the anti-solvent as discussed in chapter 2.2.2.2. However, the procedure required a lot of time as the system needed to cool down after each set of runs. In the absence of surfactants, a foam top layer was created in the milling pots (figure B.9 in experimental appendix), resulting in extensive drug losses. The resulting indomethacin aqueous suspension showed a very fast sedimentation rate (figure B.10 in experimental appendix) and did not result in a successful nanoparticle suspension for our purposes. As the presence of an added polymer-stabiliser would affect the coating method, a second option, cryomilling, was considered.

4.2.3.2 Cryomilling

Cryomilling of indomethacin resulted in an amorphous powder which gradually converted to a crystalline material. In all the different steps its state was characterised using DSC and XRPD (data in B.4). However indomethacin started recrystallising within 24 hours after the cryomilling. The coating experiments took place 3 weeks after the cryomilling and thus the state of the indomethacin resembled the commercial crystal one.

4.2.3.3 Aqueous indomethacin suspension

The cryomilled indomethacin powder was used to produce the aqueous drug suspension as described in section 2.2.2.2. The hydrodynamic diameter of the suspension was measured by DLS prior to the the coating experiments (figure 4.11).

A population of sub-micron particles with an average diameter of 712($\pm$357) nm with quite high PDI value (0.377) was observed . The

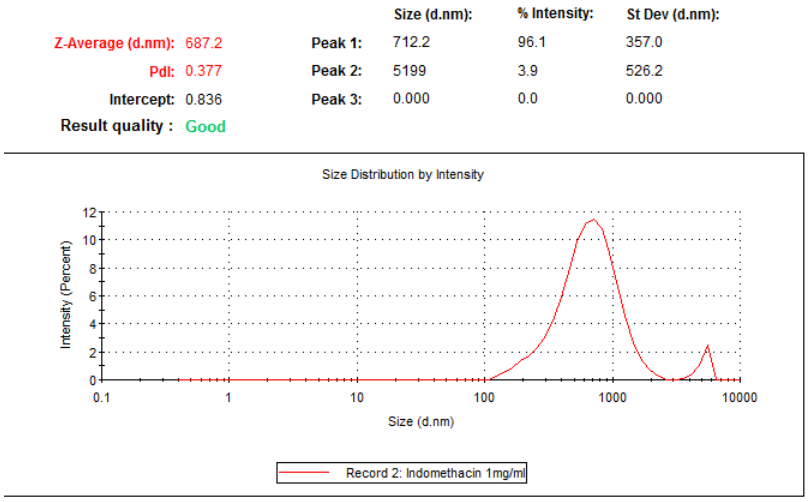


Fig. 4.11 DLS distribution of indomethacin particles as used in the aqueous phase (1mg/ml). The peak is the average intensity distribution of three measurements. The sonnicated indomethacin particles demonstrate a population of sub-micron particles of 712($\pm$357) nm diameter (PDI 0.377).

large PDI value was indicative of the instability of the suspension, which had a tendency to precipitate. Further analysis of the suspension by POM (figure 4.12) and TEM (figure 4.13) showed large aggregates with clear sharp crystal planes. These suspensions were used in the interfacial deposition as the aqueous drug-rich phase.

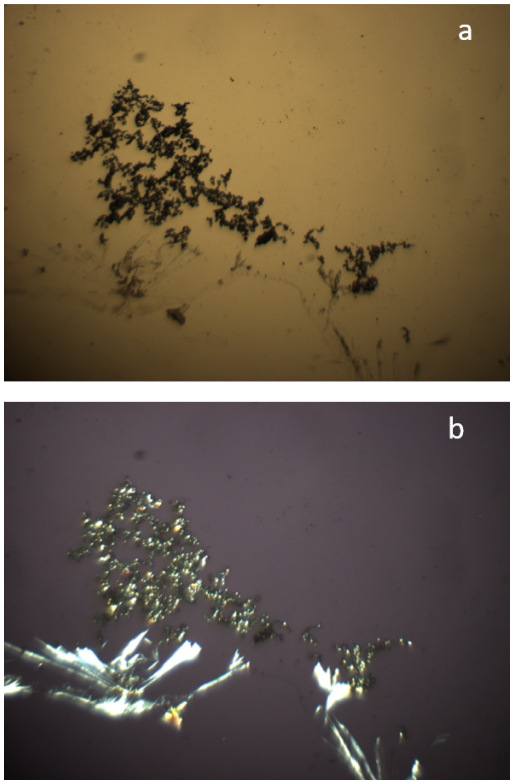


Fig. 4.12 POM image of indomethacin particles as used in the aqueous phase; (a) without and (b) with the polariser. Indomethacin is clearly crystalline. (Magnification 10x).

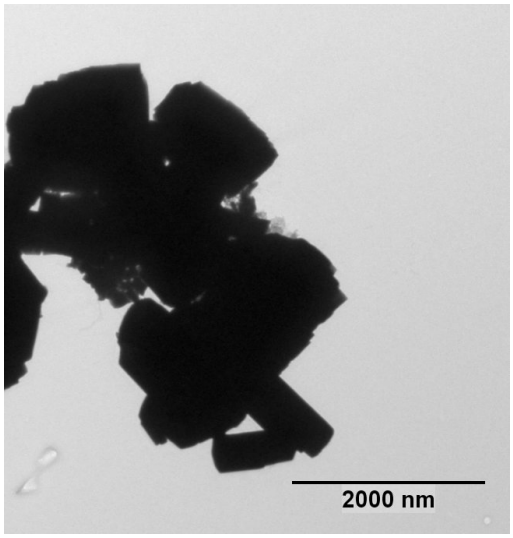


Fig. 4.13 TEM image of indomethacin particles as used in the aqueous phase; the indomethacin demonstrates well defined crystal planes. (Scale bar 2 μm).

4.2.4 Formation of drug nanoparticles via the interfacial deposition method

In order to assess the fate of the indomethacin particles in the aqueous suspension when exposed to acetone, a negative control experiment was planned, in the absence of the polymer. The drug suspension was exposed to acetone under a flow in the syringes, and the suspension formed was analysed via DLS. The combined data for all the concentrations used are presented in figure 4.14.

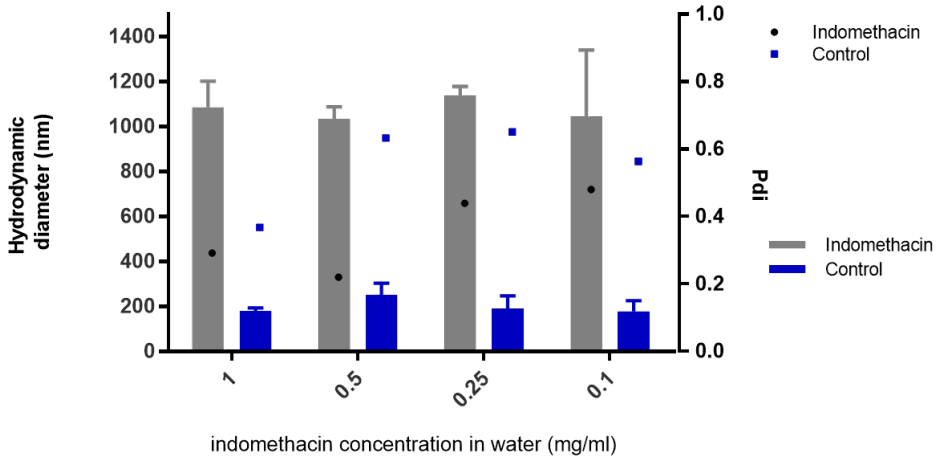


Fig. 4.14 Hydrodynamic diameter (via DLS) of indomethacin particles as used in the aqueous phase (grey) and after their exposure to pure acetone during the interfacial deposition (blue). The peak and error bars correspond to the average intensity distribution and SD of three measurements. A clear size reduction has been achieved in the absence of the polymer resulting in pure-drug NP suspensions.

After the exposure of the micron-size indomethacin particles to pure acetone, a suspension of pure drug NPs was obtained. The highest concentration (1 mg/ml) showed a distribution of 181 ($\pm$10)nm and the smallest PDI (0.38). When lower drug concentrations were used for the aqueous phase (0.5, 0.25 and 0.1 mg/ml), the PDI of the control population

increased significantly and the NP suspensions were no longer stable as they sedimented quickly. There is a clear reduction in the particles' size distribution that can be attributed to the high solubility indomethacin has in acetone; it is possible that the large particles have partially dissolved and during the evaporation of the acetone nucleation started forming indomethacin NPs.

The highest concentration (1 mg/ml) was used in the following coating experiments as it demonstrated the lowest PDI.

4.2.5 Formation of polymer-coated drug nanoparticles

When the coating method was performed with PEG350PCL (0.05 mg/ml in acetone) in the presence of the drug suspension (1 mg/ml), fine translucent nanosuspensions were formed. DLS analysis is shown in figure 4.15 where the peak corresponding to the polymer-coated NPs (blue) is shown in comparison with those of the starting indomethacin population (red) and the polymer NP (green).

The nearly micrometer sized population of drug particles (red) has disappeared and a single NP peak was obtained (diameter of 250 nm, blue peak in figure 4.15). This peak was also different from the polymer NP one (diameter of 100 nm, green peak in figure 4.15).

The same behaviour was observed for all the different polymer in acetone concentrations selected and for all the polymers as well (figure 4.16).

As illustrated in figure 4.16, all the polymers (0.05 mg/ml polymer in acetone concentration) resulted in the formation of polymer-coated indomethacin NPs with size distributions in the range of 150-260 nm.

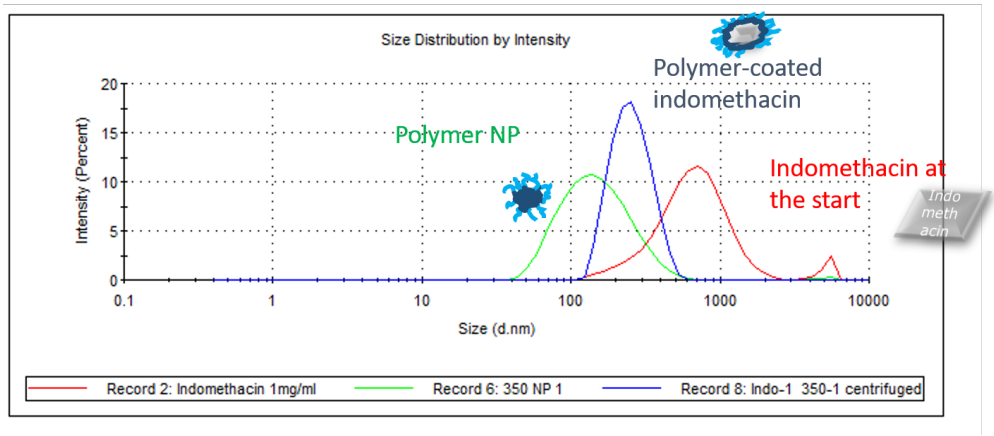


Fig. 4.15 Overlay of 3 DLS samples to show 3 different NP populations: PEG350PCL polymer NPs (green, 0.05 mg/ml), indomethacin sonicated as used in the aqueous suspension (red, 1mg/ml) and the result, polymer-coated indomethacin NP (blue). Each peak corresponds to the average intensity distribution of three measurements.

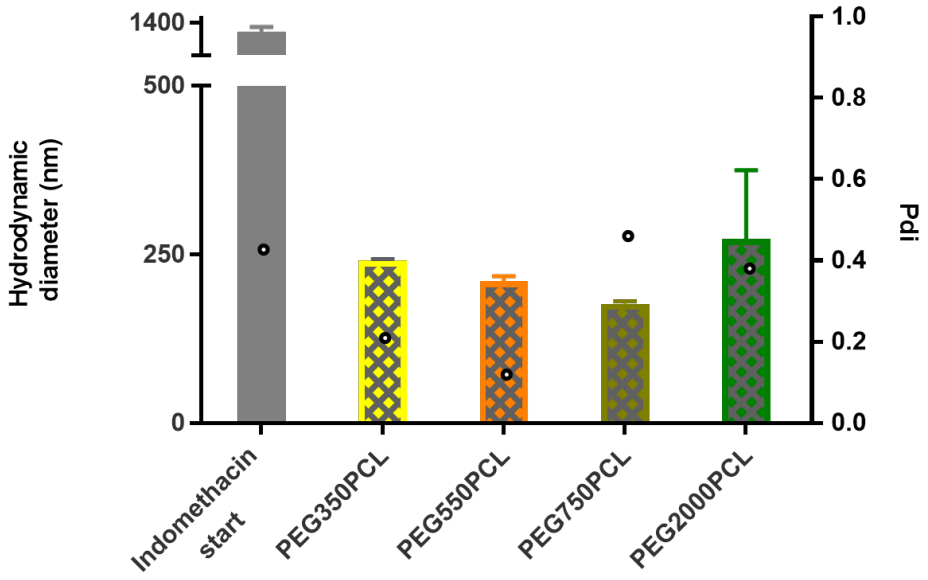


Fig. 4.16 Hydrodynamic diameter and PDIs (DLS) of polymer-coated indomethacin NPs; indomethacin 1 mg/ml in water, polymers 0.05 mg/ml in acetone. The polymer coated NPs demonstrate sizes significantly smaller than the starting indomethacin population suggesting a new population. Circular dots correspond to the PDI value of the sample.

However larger PDIs for the PEG750PCL and PEG2000PCL lead us into focusing the future experimental work on PEG350PCL and PEG550PCL coated drug NPs.

A small purification step via centrifugation was also introduced to remove any uncoated drug particles. Indeed, after the centrifugation the PDI of the DLS measurements improved (figure 4.17) and any drug aggregates were removed and were not detectable by POM (figure 4.18).

TEM was employed to visualise the polymer-coated drug NPs (figure 4.19).

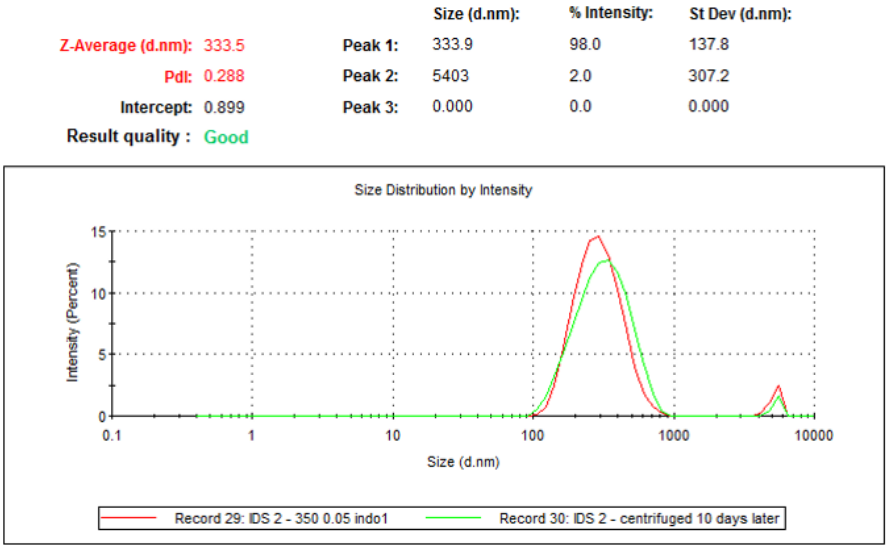


Fig. 4.17 DLS measurement of the PEG350PCL-coated indomethacin NP population, before (red line) and after (green line) the centrifugation/purification process. Peak corresponds to the average of 3 measurements.

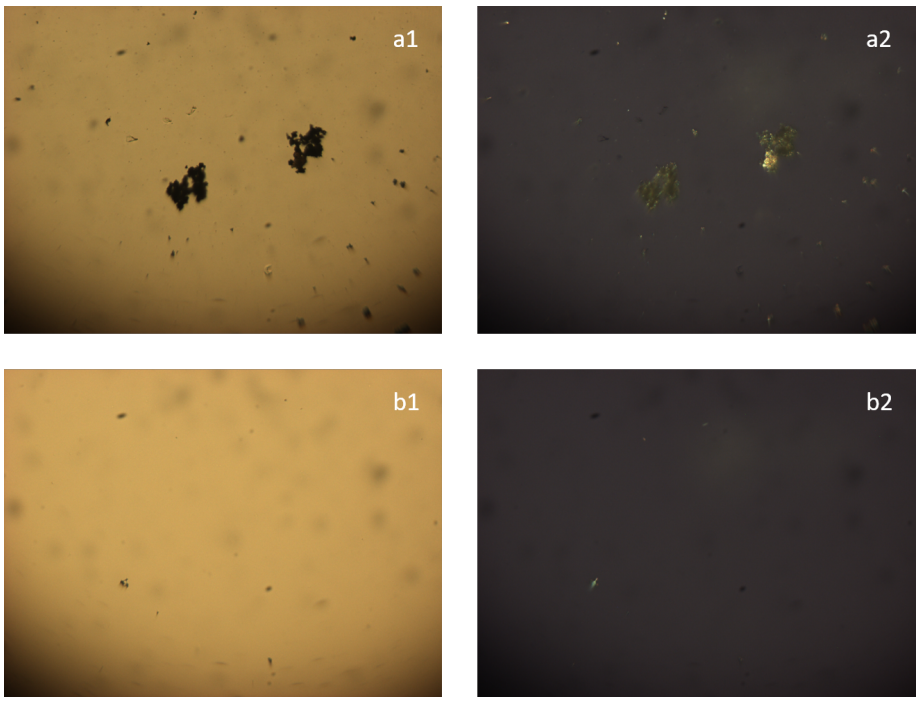


Fig. 4.18 POM images of the PEG350PCL-coated indomethacin NPs. (a1) and (a2) prior to centrifugation/purification, where uncoated drug particles form aggregates, and (b1), (b2) after the purification where no crystals are observed. (Magnification 10x)

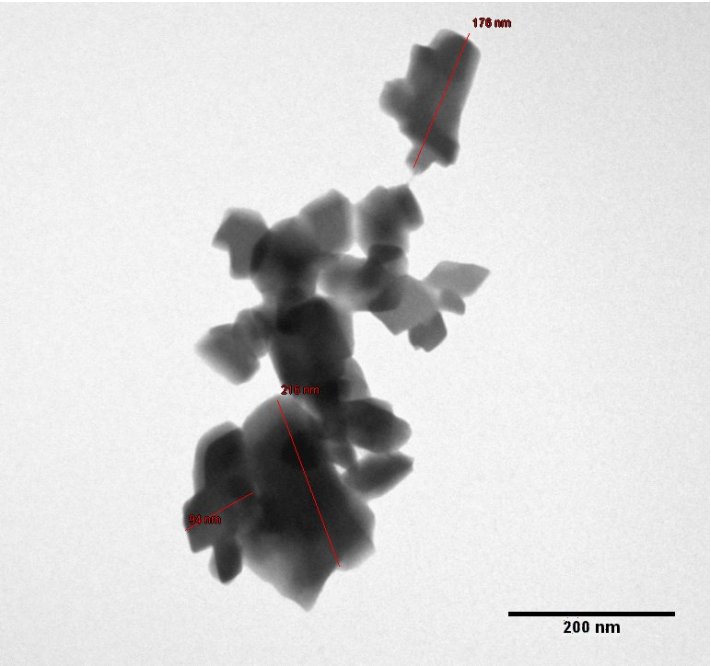


Fig. 4.19 TEM image of the polymer-coated indomethacin NPs in the lowest PEG350PCL concentration used (0.05mg/ml). Scale bar corresponds to 200 nm. The core consists of crystalline indomethacin, while a very thin polymer coating has smoothed the surface of the drug. (Scale bar 200nm).

As can be illustrated in figure 4.19, the particles differ significantly from the starting indomethacin suspension (figure 4.13), both in size and in morphology as they are smaller and do not exhibit the same sharp crystal edges. Although they appear as if they have aggregated, this may be at least partially due to the TEM sample preparation method; preparing TEM samples involves dropping and drying a solution on a grid (drop-cast method). However, the drop cast method induces agglomeration [34, 166] so the agglomerates seen in the TEM images could be an artefact due to the preparation method.

When larger amounts of polymer were used (PEG350PCL 1mg/ml) the surrounding polymer coating was significantly thicker as can clearly be illustrated in figure 4.20.

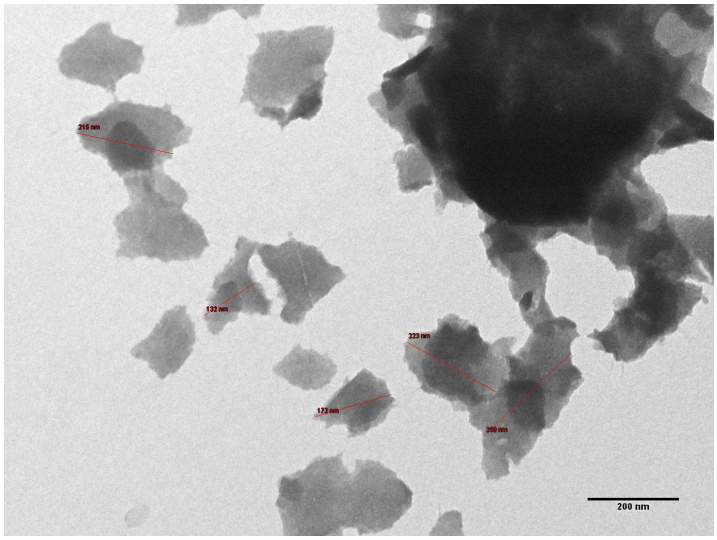


Fig. 4.20 TEM image of the polymer-coated indomethacin NPs in the highest PEG350PCL concentration used (1 mg/ml). Scale bar corresponds to 200 nm. The core consists of crystalline indomethacin while the polymer coating is evidently thicker than in figure 4.19. (Scale bar 200nm).

The reproducibility of the method was also considered; preparation of 5 batches of PEG350PCL-coated indomethacin NPs successfully reproduced the same size distribution via DLS (figure B.17 in the experimental appendix).

At the same time, two unpaired t-tests were performed using the sizes of three batches of the indomethacin control population (polymer-free) and the polymer NP population (drug-free) versus the polymer-coated drug NPs. The results are summarised in figure 4.21.

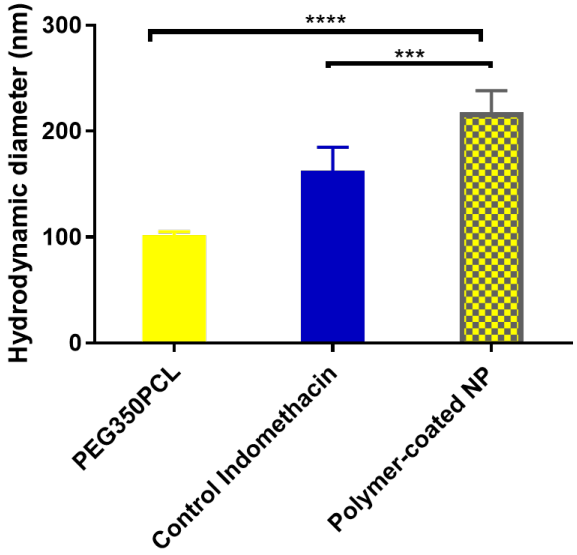


Fig. 4.21 Unpaired t-tests to demonstrate the statistical difference ($p<0.0001$) between the drug-free polymer NPs versus the polymer-coated drug NPs, ($p<0.0001$) and the polymer-free drug NPs versus the polymer-coated drug NPs ($p=0.0006$). Indomethacin (1 mg/ml) was mixed with PEG350PCL (0.05 mg/ml). Error bars correspond to the SD of 9 measurements.

The three populations, i.e. drug-free NPs (yellow), polymer-free NPs (blue) and polymer-coated drug NP (yellow/grey) have sizes that are significantly different: ($p<0.0001$) between the drug-free polymer NPs versus the polymer-coated drug NPs, ($p<0.0001$) and the polymer-free drug NPs versus the polymer-coated drug NPs ($p=0.0006$). This strengthened the point that the populations created were single peaks as measured by DLS, and different from the control ones.

In order to investigate the effect the initial drug concentration in water would have in the formation of the polymer-coated drug NPs of different concentrations of indomethacin (1, 0.5, 0.25, 0.1 mg/ml) were used in the aqueous phase (figure 4.22).

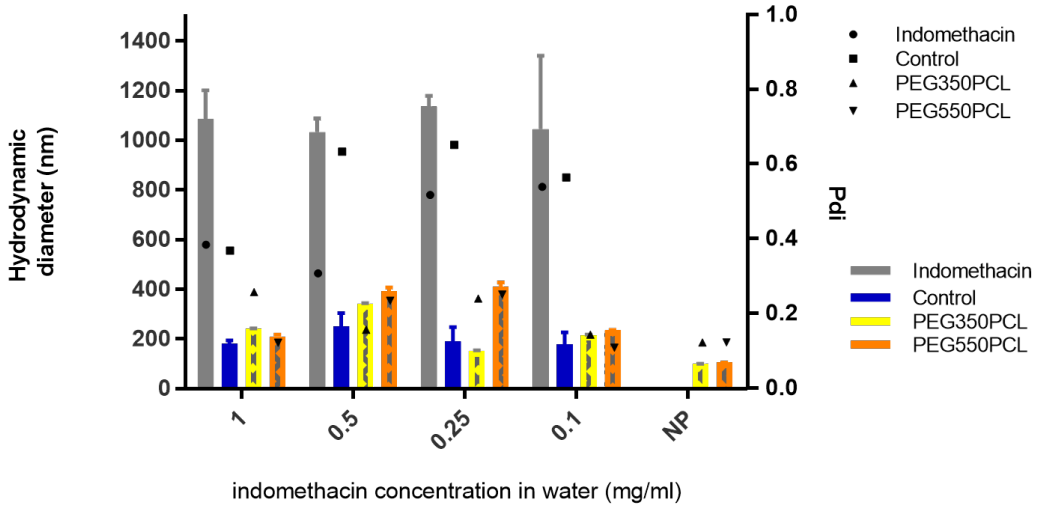


Fig. 4.22 Hydrodynamic diameter and PDIs (DLS) of polymer-coated indomethacin NPs using different indomethacin concentrations and PEG350PCL, PEG550PCL (0.05 mg/ml in acetone) for the coating. In grey, the sonicated indomethacin population, prior to the interfacial deposition, in blue, the control polymer-free indomethacin NPs, while yellow and orange the polymer-coated drug NPs of PEG350PCL and PEG550PCL respectively. The error bars correspond to the SD of 3 measurements.

As was demonstrated in figure 4.22 there was no apparent trend in the use of smaller drug amounts either of the different polymers. However, as the drug amount decreased, the PDI of the control population increased, as the suspension was very unstable and precipitated faster than the typically used 1 mg/ml.

Finally UV-Vis was employed to measure the drug loading and the yield of the method. The results for PEG350PCL and indomethacin (1 and 0.5 mg/ml) are summarised in table 4.2.

Table 4.2 UV-Vis measurements for the determination of drug loading and the entrapment efficiency of the method when using indomethacin in the aqueous phase (1 and 0.5 mg/ml).

PEG350PCL (mg/ml)	Indomethacin (mg/ml)	Drug loading (%)	Entrapment efficiency (%) (eq. 2.2.3)	Entrapment efficiency * (%) (eq. 4.2.1)
1	1	13.79	16.0	95.53
	0.5	9.76	21.63	69.10
0.5	1	23.17	15.32	91.47
	0.5	20.14	26.48	77.39
0.1	1	64.39	18.41	109.88
	0.5	57.70	27.29	77.74
0.05	1	78.27	18.31	99.02
	0.5	71.42	25.19	80.46

The drug loading reached up to 78% for the smallest polymer concentration used (0.05 mg/ml) which is very high compared to the traditional batch NP preparation methods (<25%, [167]). Similar results were found for the other polymers as well when 0.05 mg/ml was used as the polymer in acetone concentration (PEG750PCL 77.96%, PEG2000PCL 72.06%).

While the entrapment efficiency did not exceed 18% when a 1 mg/ml indomethacin feed was used, the efficiency rose up to 27% when 0.5 mg/ml was used. However, if equation 2.2.3 is modified to account for the actual drug amount that has been calculated from the polymer-free control NPs (i.e. equation 4.2.1), then higher percentages were found.

$$\%Entrapment\ efficiency^{*} = \frac{amount\ of\ coated\ drug}{amount\ of\ control\ drug} * 100 \qquad (4.2.1)$$

This change was deemed necessary due to drug losses in the syringe loading and the pumping phase; altough this was not quantified during the experiments, it is estimated that approximately 50% of the initial drug amount is lost in these two phases. It is anticipated that this could be improved using of a continuous flow pump rather than a syringe one.

4.3 Discussion

In this section the successful production of polymer-coated drug NPs has been presented. A modified interfacial deposition method has been used to deliver a fast, reproducible and stable polymer-coated drug nanosuspensions that consist of a drug nanocrystal core. The minimal amount of polymers used resulted in impressive drug loadings and high entrapment efficiencies.

The polymers used in this work are biocompatible, and approved by the FDA. The polymerisations were fast and very efficient, resulting in well defined, easy to tune diblock copolymers whose physicochemical properties were determined.

To our knowledge, this is the first time that such a variety of smaller mPEG chains is used. Zhou et al. [48] reported the formation of polymer microspheres using mPEG chains in the range of 1000-6000 Da via a double emulsion method, but the size of the particles was unfavourable for the needs of the present work.

Regarding the physicochemical properties of the polymers, the degree of crystallinity of PCL was found to be dependent on the length of the mPEG block present in the copolymer, a result that is in accordance with the existing literature [49, 60].

Indomethacin is not a new drug but due to it's low aqueous solubility it has been used as a model drug in various studies. Indomethacin loaded NPs have been produced using mPEG-PCL copolymers in the past [66, 168, 53, 76, 75], yet most of these studies employed more traditional NP production methods.

Regarding the solvents, and the molar fractions used we followed the pre-existing work on polymer-coated IONP [2]. Acetone is generally considered to be a safe solvent option easily removed from formulations and at the same time it miscible with water at all molar fractions. The selection of the solvent is a non-trivial issue as it has been reported from De Oliveira et al. [67] that water-solvent miscibility affect the size of the polymer NPS formed via solvent displacement methods.

In order to discuss about the efficacy of the present polymer-coated drug NP preparation method, one needs to establish the criteria under which this will take place. The most comparable techniques are WBM and FNP; the former is a top-down method using an anti-solvent to mill drug powders in the presence of a stabiliser, while the latter is a bottom-up approach based on the nucleation of drug molecules in the presence of surfactant. Since the present method combines elements of the two, a comparison over related studies needs to be performed.

When comparing the polymer-coating technique presented in this thesis with WBM, the most critical parameters that need to be taken into consideration are:

- the amount of polymer used and the drug loading
- the quality of the dispersions of the polymer-coated drug NPs produced
- the time needed for the production of the polymer-coated drug NPs

When Liu et al. [75] used WBM, to produce indomethacin nanosuspensions, it was reported that the best combination was achieved when indomethacin was milled at a 80%wt (to drug amount) ratio with amphiphilic block co-polymer Pluronic F68 (M_w 8400 Da). The results after

10 milling cycles were particles of 400 nm and a PDI of 0.34. In another study [76], the binding efficiency of indomethacin to different polymers was under evaluation, assessing the effect the structure and the M_w of the polymer used as a stabiliser in WBM would have. It was reported that the highest affinity was exhibited with the L64 stabiliser, that has a M_w of 2900 Da and a lower hydrophilic:hydrophobic ratio. This falls into agreement as a trend with the results presented in this thesis where the best coating of the drug NPs was achieved with PEG350PCL that has the smallest hydrophilic:hydrophobic ratio. Nevertheless, it was also reported that the L64-indomethacin particles were more likely to aggregate due to the thinner layer and thus were unstable. In the light of our results, this could be due to a large indomethacin core that could not be sufficiently covered by the L64 polymers. However, the amount of polymer added in the WBM and the high PDI of the suspensions do not appeal as an optimal solution to produce polymer-drug NPs.

Although WBM is scalable and well established in the pharmaceutical industry, it is very time consuming and requires high polymer amounts to stabilise the NPs [72]. It has also been reported that the beads can cause contamination [169, 25]. Our modified interfacial deposition is fast, and utilises very small amount of polymers to achieve the coating.

The present coating method resembles FNP, but as discussed before, it differs in the drug-bearing phase; in FNP the API is dissolved in the solvent while in the present work the drug is already in the form of microparticles in the aqueous phase. Some vital parameters that affect the performance of FNP have also been found to be critical in this work. Regarding the solvents, the miscibility between the two phases is important [67], as well as the solvent:antisolvent ratio as low ratios are

required to produce effective NPs with good dispersivity [77]. Although acetone hasn't been reported to be used in FNP, it's low boiling point, full miscibility with water at all molar ratios and polar nature makes it an ideal solvent. Regarding the selection of the hydrophobic block of the polymers used in FNP, it has been discussed that larger hydrophobic blocks i.e. polymers with large M_w, provide less nucleation sites, leading to larger particle sizes [77, 70].

Another important contribution that derived from the coating method is the the high drug loadings. By using the modified interfacial deposition, we achieved drug loadings up to 78% which is a significant increase over the reported results achieved via usual nanoprecipitation techniques (less than 25%, [170, 171, 167]).

High drug loadings (up to 86%) have been reported by Matteuci et al. [172] where a batch antisolvent precipitation was used to form sub 300nm itraconazole using poloxamer 407 as a stabiliser. However, these high drug loadings are unrealistic from a formulation viewpoint, as the group performed all experiments at 3^oC to avoid particle growth, while the size measurements were conducted just 30s after the precipitation. In comparison, in the present work, the DLS measurements were taken at several time points over a longer timescale, all experiments were performed at room temperature and the high drug loadings correspond to stable NP suspensions.

Another study reporting high drug loadings was performed by Zhu [173], where FNP was used to prepare β-carotene loaded polymer NPs. Different diblock copolymers were used and the FNP took place in a small chamber at high velocity; this caused turbulent mixing and in return the polymers and β-carotene precipitated quickly leading to the formation of

NPs. A drug loading of 83% was observed when PLGA(10K)-PEG(5K) was used, however the measurement was calculated indirectly via the weight calculation of the precipitated NPs and refers to an amorphous β-carotene load. When PEG(5k)-PCL(12k) was used in the same study, the NPs formed were only temporarily stable something attributed to the crystallisation of the PCL block that caused a change in the particle morphology. In comparison with the work presented, the smaller PCL chains have not caused any instability issues. At the same time, the amorphicity of the drugs in NPs can cause further instability and impurity issues, while in the present work the polymer-coated indomethacin NPs have crystalline cores, enhancing their nanoparticulate stability and behaviour.

The present modified interfacial deposition method combines both top-down and bottom-up characteristics; we have utilised the presence of the organic phase to partially dissolve the micron sized drug NPs that are present in the aqueous phase, until the polymer chains reach in close proximity. After the acetone evaporated, the coated drug NPs are separated from the less stable uncoated drug NPs using a gentle centrifugation step, and the resulting coated population is stable.

Modified interfacial deposition proved to be a fast, reproducible, cost effective, easily scalable technique used to coat the surface of the drug NPs with a thin polymer layer. To our knowledge this is the first time such a combinatorial method has been used for this cause but we believe that the potential it has within the pharmaceutical industry is enormous, as it can possibly be applicable to other hydrophobic APIs.

CHAPTER 5

Conclusions and Future Work

5.1 Overview and Final Discussion

This work has combined both theoretical and practical approaches in order to investigate the formation of polymer-coated drug NPs. A flowchart summarising the two routes and their parallel evolution through this project is illustrated in figure 5.1. Starting from an existing method to polymer-coat IONPs, it was asked whether the IONPs could be replaced by drug NPs. In parallel, MD simulations were set to replicate the experimental procedure, polymers were synthesised, and characterised. It was important to use an appropriate acetone model for the simulations as the solvent's diffusion is one key parameter affecting the NP formation. Additionally, polymer NPs were formed both computationally and experimentally, laying the ground for the polymer-drug NPs.

The result of this work is a novel, fast and reproducible experimental method to produce polymer-coated drug NPs, complimented with pioneering and unbiased MD simulations that provide an atomistic description of the formation and the morphology of the NPs.

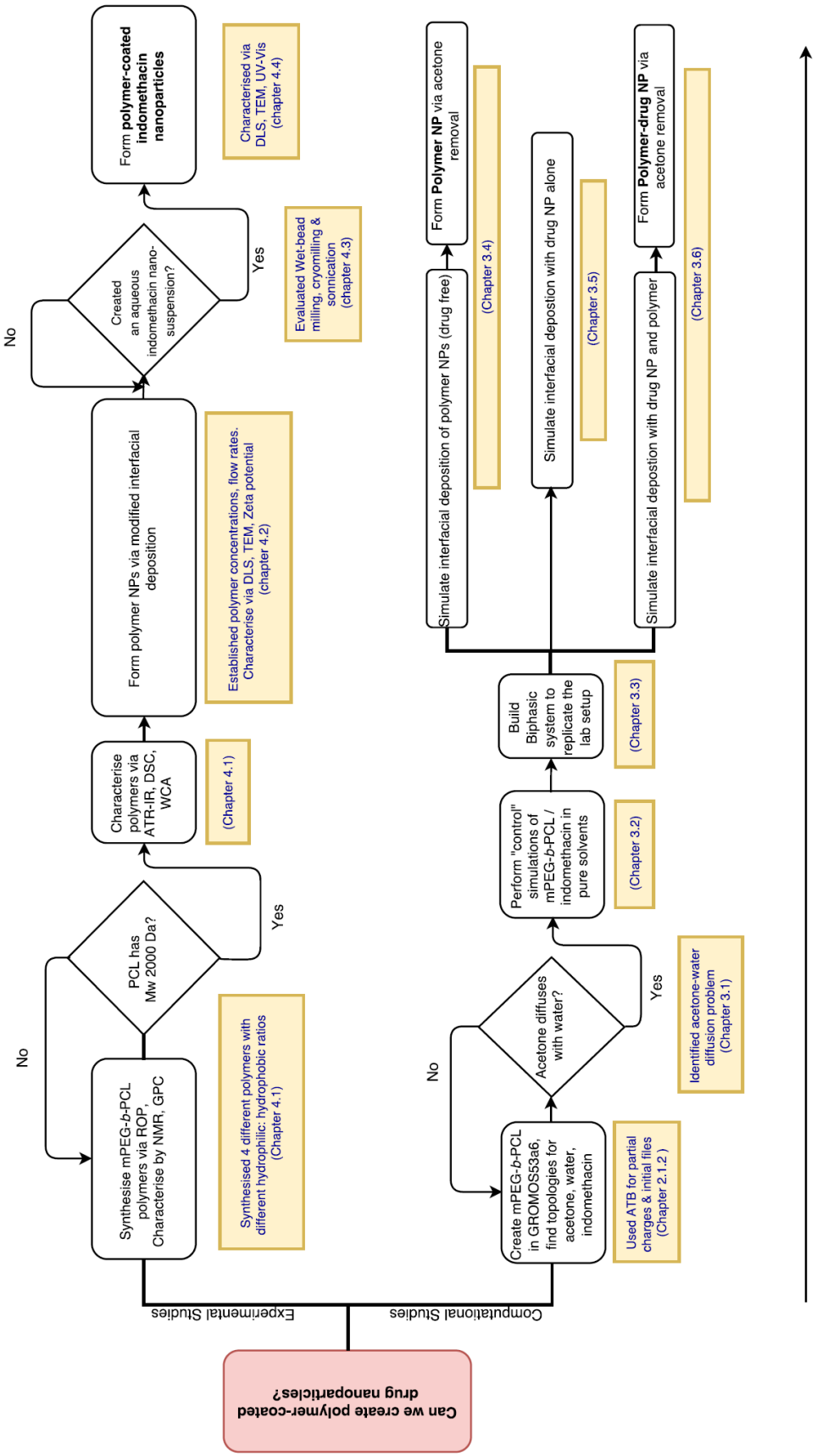


Fig. 5.1 Thesis map and flowchart, demonstrating the parallel work undertaken during this PhD showing how the timelines of the two tracks coincided. Some key points with reference to the relevant chapter are described in the yellow boxes.

In comparison with existing NP formulation techniques, the present method utilised both bottom-up and top-down characteristics. The drug underwent comminution via sonnication while a flow nanoprecipitation method was used to coat the NPs. To our knowledge this is the first time an insoluble drug was used in the anti-solvent phase during the nanoprecipitation process.

In an attempt to interpret the interactions that take place based on the information collected from both the experimental and the computational studies, a graphical illustration is presented in figure 5.2.

Micron-sized indomethacin particles are present in the aqueous phase. Once they are exposed under flow to acetone and polymers, their fate depends on their initial size: larger particles will have their surface dissolved, while smaller particles will dissolve completely to indomethacin molecules. This size reduction is not solemnly due to the presence of the acetone as the MD simulations have demonstrated that the polymers dissolve the indomethacin NPs as well. Also, in the light of the morphology of the polymer-drug NP as produced via MD, it is plausible to assume that the polymers could form a saturated surface, where polymer chains are entangled with dispersed indomethacin molecules, while the core of the drug NP's remains crystalline.

The fate of the dissolved indomethacin molecules could be similar, as under the right environment they could undergo nucleation forming NPs. The absence of a second size peak in the DLS measurements indicates that even if micellisation occurs during flow, the polymers will de-micellise and will preferably coat the drug NPs' surface.

In the final nanosuspension, the nanosized indomethacin particles are polymer-coated and thus sterically stable. On the contrary, the un-

coated indomethacin molecules or particles, will undergo Ostwald ripening, forming larger aggregates that can be separated from the coated population.

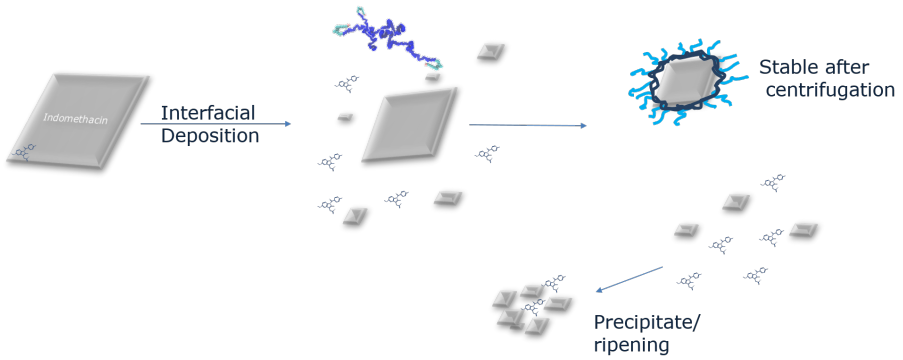


Fig. 5.2 Interpretation of the phenomena that take place during the modified interfacial deposition. A population of micron-sized indomethacin particles in an aqueous environment is exposed to a flow of polymer and acetone. The drug particles are either broken down, or dissolved due to the synergistic effect of the acetone and the polymers. The polymers are able to coat the surface of the drug NPs, making a population that can be stable due to steric interactions, while the rest of the uncoated drug particles aggregate and finally precipitate during centrifugation.

The high drug loadings, the reproducibility and the simplicity of the technique make it very promising to use in other formulations. If a different API is used and a polymer-coated NP population is achieved, then we would not be off from achieving the third question stated in the Introduction: we could delivery different APIs with the same formulation.

5.2 Future Work

From the computational perspective, the formation of the polymer NP and the polymer-drug NP via all-atom simulations were novel and this was something reportedly missing from the field [85].

MD is an atomistic microscope; it sheds light into fundamental interactions that take place in the nanoscale. In the light of the experimental results, it would be ideal to use a crystal indomethacin NP in the aqueous phase. The amorphous indomethacin NP was used as it was considered to be the most representative aqueous suspension that would be created experimentally; amorphous hydrophobic APIs offer higher dissolution rates leading to improved bioavailability. In reality, the amorphous preparations prepared were so unstable that they rapidly crystallised, and the final polymer-coated indomethacin NPs had a crystalline core. Crystalline materials have the advantage that they are more stable than the amorphous ones and so do not change properties during storage. It is possible that in the time needed for the polymer to aggregate that the crystalline indomethacin NP wouldn't dissolve, thus leading to the expected surface coating.

It would be also very interesting to continue the simulations with the rest of the polymers, to study the effect the large PEG chain would have on the NP. However a multiscale model would have to be employed in order to accelerate the simulations; ideally the interactions between the solvents could be calculated using coarse-grained methods, while we would keep the atomistic detail on the polymer and the drug interactions. Such models are non-trivial and require a lot of effort and validation, thus delaying their publication.

In order to evaluate the NP agglomeration, a methodology as proposed by Salerno et al. [109] could be utilised to study the interaction between the NPs: once the polymer-drug NP is formed via MD, it can be placed in proximity to another identical NP and the forces between the NPs can be calculated. Via such an approach the tendency to agglomerate or not could be investigated and translated to formulation stability.

Another point is that such simulations can be used to study the coating of other hydrophobic drugs or even the combinations of different polymers and drugs. If the simulations were a bit faster, then MD could be used to get vital information over the physical interactions between the moieties that take place in such interactions, thus reducing the expensive -and time consuming - trial-and-error approaches that exist in labs worldwide.

From the experimental side of the project, the work presented in this thesis has demonstrated a lot of potential; If the syringe pumps are substituted with a more automated system like a constant flow system, and the drug suspension in the beginning is constantly agitated, then it is the strong belief of the writer that well defined aqueous drug-nanosuspensions will be created, with high drug loadings and higher entrapment efficiencies than the ones presented.

At the same time, the method could easily be scaled up and could be expanded to other amphiphilic polymers and class III drugs (low solubility. high permeability). Preliminary work with PEG350PCL and felodipine (data not presented) showed that an investigation over the ideal polymer concentration is needed, but the results were promising.

It is the combination of both of the aspects of the pharmaceutical field that lead us towards a formulation-by-design approach; using computational techniques that are strongly influencing and influenced by parallel experimental work in order to understand and design better formulations.

References

[1] H Fessi et al. "Nanocapsule formation by interfacial polymer deposition following solvent displacement". In: *International Journal of Pharmaceutics* 55.1 (1989), R1–R4.

[2] Ahmed Abushrida. "Formulation of novel polymer coated iron oxide nanoparticles". In: *PhD thesis* (2011).

[3] Leo Y T Chou, Kevin Ming, and Warren C W Chan. "Strategies for the intracellular delivery of nanoparticles". In: *Chem. Soc. Rev.* 40.1 (2011), pp. 233–245. DOI: 10.1039/C0CS00003E.

[4] J E Kipp. "The role of solid nanoparticle technology in the parenteral delivery of poorly water-soluble drugs." eng. In: *International journal of pharmaceutics* 284.1-2 (Oct. 2004), pp. 109–122. ISSN: 0378-5173 (Print). DOI: 10.1016/j.ijpharm.2004.07.019.

[5] Jan P Möschwitzer. "Drug nanocrystals in the commercial pharmaceutical development process". In: *International Journal of Pharmaceutics* 453.1 (2013), pp. 142–156. ISSN: 0378-5173. DOI: http://dx.doi.org/10.1016/j.ijpharm.2012.09.034.

[6] Eugene R. Cooper. "Nanoparticles: A personal experience for formulating poorly water soluble drugs". In: 141.3 (Feb. 2010), pp. 300–302. DOI: 10.1016/j.jconrel.2009.10.006.

[7] C A Lipinski et al. "Experimental and computational approaches to estimate solubility and permeability in drug discovery and development settings". In: *Advanced Drug Delivery Reviews* 46.1-3 (2001), pp. 3–26. DOI: 10.1016/s0169-409x(00)00129-0.

[8] Elaine M Merisko-Liversidge and Gary G Liversidge. "Drug nanoparticles: formulating poorly water-soluble compounds." eng. In: *Toxicologic pathology* 36.1 (Jan. 2008), pp. 43–48. ISSN: 1533-1601 (Electronic). DOI: 10.1177/0192623307310946.

[9] Volkmar Weissig, Tracy K Pettinger, and Nicole Murdock. *Nanopharmaceuticals (part 1): products on the market*. eng. 2014. DOI: 10.2147/IJN.S46900.

[10] Daniel Bobo et al. "Nanoparticle-Based Medicines: A Review of FDA-Approved Materials and Clinical Trials to Date." eng. In: *Pharmaceutical research* 33.10 (Oct. 2016), pp. 2373–2387. ISSN: 1573-904X (Electronic). DOI: 10.1007/s11095-016-1958-5.

[11] J Jiang, G Oberdörster, and P Biswas. "Characterization of size, surface charge, and agglomeration state of nanoparticle dispersions for toxicological studies". In: *Journal of Nanoparticle Research* 11.1 (2009), pp. 77–89.

[12] B Derjaguin and L Landau. "Theory of the stability of strongly charged lyophobic sols and of the adhesion of strongly charged-particles in solutions of electrolytes". English. In: *Progress in Surface Science* 43.1-4 (1993), pp. 30–59. DOI: 10.1016/0079-6816(93)90013-l.

[13] J Th G Overbeek. "Recent developments in the understanding of colloid stability". In: *Journal of Colloid and Interface Science* 58.2 (1977), pp. 408–422. DOI: http://dx.doi.org/10.1016/0021-9797(77)90151-5.

[14] E J W Verwey. "Theory of the Stability of Lyophobic Colloids". In: *The Journal of Physical and Colloid Chemistry* 51.3 (1947), pp. 631–636. DOI: 10.1021/j150453a001.

[15] H C Hamaker. "The London - Van Der Waals attraction between spherical particles". English. In: *Physica* 4 (1937), pp. 1058–1072. DOI: 10.1016/s0031-8914(37)80203-7.

[16] Yuncheng Liang et al. "Interaction forces between colloidal particles in liquid: Theory and experiment". In: *Advances in Colloid and Interface Science* 134135 (2007), pp. 151–166. DOI: http://dx.doi.org/10.1016/j.cis.2007.04.003.

[17] C Kiparissides and O Kammona. "Nanoscale carriers for targeted delivery of drugs and therapeutic biomolecules". English. In: *Canadian Journal of Chemical Engineering* 91.4 (2013), pp. 638–651. DOI: 10.1002/cjce.21685.

[18] Gerhard Scheuch et al. "Clinical perspectives on pulmonary systemic and macromolecular delivery". In: *Advanced Drug Delivery Reviews* 58.9-10 (2006), pp. 996–1008. DOI: 10.1016/j.addr.2006.07.009.

[19] C Kleinstreuer, Z Zhang, and J F Donohue. *Targeted drug-aerosol delivery in the human respiratory system*. 2008.

[20] *Lungs and Breathing*. DOI: https://medlineplus.gov/lungsandbreathing.html.

[21] Mark M Bailey and Cory J Berkland. "Nanoparticle Formulations in Pulmonary Drug Delivery". In: *Medicinal Research Reviews* 29.1 (2009), pp. 196–212. DOI: 10.1002/med.20140.

[22] D A Groneberg et al. "Fundamentals of pulmonary drug delivery". In: *Respiratory Medicine* 97.4 (2003), pp. 382–387. DOI: http://dx.doi.org/10.1053/rmed.2002.1457.

[23] Lianjun Shi, Carl J Plumley, and Cory Berkland. "Biodegradable Nanoparticle Flocculates for Dry Powder Aerosol Formulation". In: *Langmuir* 23.22 (2007), pp. 10897–10901. DOI: 10.1021/la7020098.

[24] Adriana L Da Silva et al. "Nanoparticle-based therapy for respiratory diseases". In: *Anais da Academia Brasileira de Ciências* 85 (2013), pp. 137–146.

[25] Jian Zhang et al. "Formation, characterization, and fate of inhaled drug nanoparticles". In: *Advanced Drug Delivery Reviews* 63.6 (2011), pp. 441–455. DOI: 10.1016/j.addr.2010.11.002.

[26] M P Timsina et al. "Drug delivery to the respiratory tract using dry powder inhalers". In: *International Journal of Pharmaceutics* 101.1-2 (1994), pp. 1–13.

[27] W. Ostwald. "Studien über die Bildung und Umwandlung fester Körper." In: *Zeitschrift für physikalische Chemie* 22 (1897), pp. 289–330.

[28] Jun Hu et al. "Spherical agglomerates of pure drug nanoparticles for improved pulmonary delivery in dry powder inhalers". In: *Journal of Nanoparticle Research* 15.4 (2013). DOI: 10.1007/s11051-013-1560-2.

[29] Suzanne M D'Addio and Robert K Prud'homme. "Controlling drug nanoparticle formation by rapid precipitation". In: *Advanced Drug Delivery Reviews* 63.6 (2011), pp. 417–426. DOI: http://dx.doi.org/10.1016/j.addr.2011.04.005.

[30] O Schmid et al. "Dosimetry and toxicology of inhaled ultrafine particles". English. In: *Biomarkers* 14 (2009), pp. 67–73. DOI: 10.1080/13547500902965617.

[31] J Heyder et al. "Deposition of particles in the human respiratory tract in the size range 0.005-15 μm". In: *Journal of Aerosol Science* 17.5 (1986), pp. 811–825.

[32] N Tsapis et al. "Trojan particles: large porous carriers of nanoparticles for drug delivery". eng. In: *Proc Natl Acad Sci U S A* 99.19 (2002), pp. 12001–12005. DOI: 10.1073/pnas.182233999.

[33] J Wang et al. "Measurement of Nanoparticle Agglomerates by Combined Measurement of Electrical Mobility and Unipolar Charging Properties". English. In: *Aerosol Science and Technology* 44.2 (2010), pp. 97–108. DOI: 10.1080/02786820903401427.

[34] N Hondow et al. "Quantitative characterization of nanoparticle agglomeration within biological media". English. In: *Journal of Nanoparticle Research* 14.7 (2012), p. 15. DOI: 10.1007/s11051-012-0977-3.

[35] M Seipenbusch et al. "Interparticle forces in silica nanoparticle agglomerates". English. In: *Journal of Nanoparticle Research* 12.6 (2010), pp. 2037–2044. DOI: 10.1007/s11051-009-9760-5.

[36] Haoyang Haven Liu et al. "Analysis of Nanoparticle Agglomeration in Aqueous Suspensions via Constant-Number Monte Carlo Simulation". In: *Environmental Science & Technology* 45.21 (2011), pp. 9284–9292. DOI: 10.1021/es202134p.

[37] R Bhavane, E Karathanasis, and A V Annapragada. "Agglomerated vesicle technology: a new class of particles for controlled and modulated pulmonary drug delivery". In: *Journal of Controlled Release* 93.1 (2003), pp. 15–28. DOI: 10.1016/s0168-3659(03)00359-6.

[38] Rohan Bhavane, Efstathios Karathanasis, and Ananth V Annapragada. "Triggered release of ciprofloxacin from nanostructured agglomerated vesicles". In: *International Journal of Nanomedicine* 2.3 (2007), pp. 407–418.

[39] Nashwa El-Gendy, Warangkana Pornputtapitak, and Cory Berkland. "Nanoparticle agglomerates of fluticasone propionate in combination with albuterol sulfate as dry powder aerosols". In: *European Journal of Pharmaceutical Sciences* 44.4 (2011), pp. 522–533. DOI: 10.1016/j.ejps.2011.09.014.

[40] H F Salem et al. "Nanosized rods agglomerates as a new approach for formulation of a dry powder inhaler". In: *International Journal of Nanomedicine* 6 (2011), pp. 311–320. DOI: 10.2147/ijn.s14309.

[41] Schalk J Strydom et al. "Self-assembled macromolecular nanocoatings to stabilize and control drug release from nanoparticles". In: *Powder Technology* 256 (2014), pp. 470–476. DOI: http://dx.doi.org/10.1016/j.powtec.2014.01.088.

[42] Nobuhiro Nishiyama and Kazunori Kataoka. "Current state, achievements, and future prospects of polymeric micelles as nanocarriers for drug and gene delivery". In: *Pharmacology & Therapeutics* 112.3 (2006), pp. 630–648. DOI: 10.1016/j.pharmthera.2006.05.006.

[43] Kazunori Kataoka, Atsushi Harada, and Yukio Nagasaki. "Block copolymer micelles for drug delivery: design, characterization and biological significance". In: *Advanced Drug Delivery Reviews* 47.1 (Mar. 2001), pp. 113–131. ISSN: 0169409X. DOI: 10.1016/S0169-409X(00)00124-1.

[44] T Riley et al. "Physicochemical evaluation of nanoparticles assembled from poly(lactic acid)-poly(ethylene glycol) (PLA-PEG) block copolymers as drug delivery vehicles". In: *Langmuir* 17.11 (2001), pp. 3168–3174. DOI: 10.1021/la001226i.

[45] Cinzia Garofalo et al. "Different insight into amphiphilic PEG-PLA copolymers: influence of macromolecular architecture on the micelle formation and cellular uptake". eng. In: *Biomacromolecules* 15.1 (Jan. 2014), pp. 403–415. ISSN: 1525-7797. DOI: 10.1021/bm401812r.

[46] Mikhail Yu. Kozlov et al. "Relationship between Pluronic Block Copolymer Structure, Critical Micellization Concentration and Partitioning Coefficients of Low Molecular Mass Solutes". In: *Macromolecules* 33.9 (May 2000), pp. 3305–3313. ISSN: 0024-9297. DOI: 10.1021/ma991634x.

[47] Alexander V Kabanov, Elena V Batrakova, and Valery Yu Alakhov. "Pluronicő block copolymers as novel polymer therapeutics for drug and gene delivery". In: *Journal of Controlled Release* 82.2-3 (Aug. 2002), pp. 189–212. ISSN: 01683659. DOI: 10.1016/S0168-3659(02)00009-3.

[48] Shaobing Zhou, Xianmo Deng, and Hua Yang. "Biodegradable poly(ϵ-caprolactone)-poly(ethylene glycol) block copolymers: characterization and their use as drug carriers for a controlled delivery system". In: *Biomaterials* 24.20 (2003), pp. 3563–3570. DOI: http://dx.doi.org/10.1016/S0142-9612(03)00207-2.

[49] C He et al. "Study of the synthesis, crystallization, and morphology of poly(ethylene glycol) - Poly(ϵ-caprolactone) diblock copolymers". In: *Biomacromolecules* 5.5 (2004), pp. 2042–2047.

[50] Marian E Gindy et al. "Preparation of Poly(ethylene glycol) Protected Nanoparticles with Variable Bioconjugate Ligand Density". In: *Biomacromolecules* 9.10 (2008), pp. 2705–2711. DOI: 10.1021/bm8002013.

[51] T K Dash and V B Konkimalla. "Poly-epsilon-caprolactone based formulations for drug delivery and tissue engineering: A review". eng. In: *J Controlled Release* 158.1 (2012), pp. 15–33. DOI: 10.1016/j.jconrel.2011.09.064.

[52] S Meerod et al. "Magnetite nanoparticles stabilized with polymeric bilayer of poly(ethylene glycol) methyl ether-poly(ϵ-caprolactone) copolymers". English. In: *Polymer* 49.18 (2008), pp. 3950–3956. DOI: 10.1016/j.polymer.2008.07.003.

[53] So Yeon Kim et al. "Methoxy poly(ethylene glycol) and -caprolactone amphiphilic block copolymeric micelle containing indomethacin.: II. Micelle formation and drug release behaviours". In: *Journal of Controlled Release* 51.1 (1998), pp. 13–22. DOI: http://dx.doi.org/10.1016/S0168-3659(97)00124-7.

[54] Dirk Pfefferkorn et al. "Crystallization and melting of poly(glycerol adipate)-based graft copolymers with single and double crystallizable side chains". In: 51.21 (Nov. 2013), pp. 1581–1591. ISSN: 08876266. DOI: 10.1002/polb.23373.

[55] Benjamin S Schuster et al. "Nanoparticle diffusion in respiratory mucus from humans without lung disease". In: *Biomaterials* 34.13 (2013), pp. 3439–3446. DOI: http://dx.doi.org/10.1016/j.biomaterials.2013.01.064.

[56] X Wei et al. "Biodegradable poly(ϵ-caprolactone)-poly(ethylene glycol) copolymers as drug delivery system". In: *International Journal of Pharmaceutics* 381.1 (2009), pp. 1–18. DOI: 10.1002/jps.21694.

[57] Chunhua Shen, Shengrong Guo, and Chengfei Lul. "Degradation behaviors of monomethoxy poly(ethylene glycol)-b-poly(epsilon-caprolactone) nanoparticles in aqueous solution". In: *Polymers for Advanced Technologies* 19.1 (2008), pp. 66–72. DOI: 10.1002/pat.975.

[58] C F Lu et al. "Synthesis and aggregation behavior of four types of different shaped PCL-PEG block copolymers". In: *Polymer International* 55.6 (2006), pp. 694–700. DOI: 10.1002/pi.2034.

[59] Luis Simón and Jonathan M Goodman. "The Mechanism of TBD-Catalyzed Ring-Opening Polymerization of Cyclic Esters". In: *The Journal of Organic Chemistry* 72.25 (2007), pp. 9656–9662. DOI: 10.1021/jo702088c.

[60] B Bogdanov et al. "Synthesis and thermal properties of poly(ethylene glycol)-poly(e-caprolactone) copolymers". In: *Polymer* 39.8-9 (1998), pp. 1631–1636.

[61] M L Forrest et al. "Paclitaxel prodrugs with sustained release and high solubility in poly(ethylene glycol)-b-poly(ϵ-caprolactone) micelle nanocarriers: Pharmacokinetic disposition, tolerability, and cytotoxicity". In: *Pharmaceutical Research* 25.1 (2008), pp. 194–206.

[62] A S Mikhail and C Allen. "Poly(ethylene glycol)- b -poly(ϵ-caprolactone) micelles containing chemically conjugated and physically entrapped docetaxel: Synthesis, characterization, and the influence of the drug on micelle morphology". In: *Biomacromolecules* 11.5 (2010), pp. 1273–1280.

[63] Young Hyo Kim et al. "Structural Characteristics of Size-Controlled Self-Aggregates of Deoxycholic Acid-Modified Chitosan and Their Application as a DNA Delivery Carrier". In: *Bioconjugate Chemistry* 12.6 (2001), pp. 932–938. DOI: 10.1021/bc015510c.

[64] Suksiriworapong, Jiraphong, J Sripha K. ;Kreuter, and V.B. ;Junyaprasert. "No Title". In: *Journal of Pharmaceutical Science* 37.1-2 (2010), pp. 17–27.

[65] I G Shin et al. "Methoxy poly(ethylene glycol)/epsilon-caprolactone amphiphilic block copolymeric micelle containing indomethacin. I. Preparation and characterization." eng. In: *Journal of controlled release : official journal of the Controlled Release Society* 51.1 (Jan. 1998), pp. 1–11. ISSN: 0168-3659 (Print).

[66] So Yeon Kim et al. "Indomethacin-loaded methoxy poly(ethylene glycol)/poly(ϵ-caprolactone) diblock copolymeric nanosphere: pharmacokinetic characteristics of indomethacin in the normal SpragueDawley rats". In: *Biomaterials* 22.14 (2001), pp. 2049–2056. DOI: http://dx.doi.org/10.1016/S0142-9612(00)00393-8.

[67] A M de Oliveira et al. "Physicochemical aspects behind the size of biodegradable polymeric nanoparticles: A step forward". English. In: *Colloids and Surfaces A: Physicochemical and Engineering Aspects* 436 (2013), pp. 1092–1102. DOI: 10.1016/j.colsurfa.2013.08.056.

[68] Vivek K. Pawar et al. "Engineered nanocrystal technology: In-vivo fate, targeting and applications in drug delivery". In: *Journal of Controlled Release* 183 (2014), pp. 51–66. ISSN: 01683659. DOI: 10.1016/j.jconrel.2014.03.030.

[69] D Douroumis and A Fahr. "Stable carbamazepine colloidal systems using the cosolvent technique". In: *European Journal of Pharmaceutical Sciences* 30.5 (2007), pp. 367–374. DOI: 10.1016/j.ejps.2006.12.003.

[70] S M D'Addio et al. "Effects of block copolymer properties on nanocarrier protection from in vivo clearance". English. In: *Journal of Controlled Release* 162.1 (2012), pp. 208–217. DOI: 10.1016/j.jconrel.2012.06.020.

[71] Yuqi Zhou et al. "State of the art of nanocrystals technology for delivery of poorly soluble drugs". In: *Journal of Nanoparticle Research* 18.9 (2016), pp. 1–22. ISSN: 1572-896X. DOI: 10.1007/s11051-016-3575-y.

[72] Bernard Van Eerdenbrugh, Guy Van den Mooter, and Patrick Augustijns. "Top-down production of drug nanocrystals: Nanosuspension stabilization, miniaturization and transformation into solid products". In: *International Journal of Pharmaceutics* 364.1 (2008), pp. 64–75. DOI: http://dx.doi.org/10.1016/j.ijpharm.2008.07.023.

[73] J Lee, J.-Y. Choi, and C H Park. "Characteristics of polymers enabling nano-comminution of water-insoluble drugs". In: *International Journal of Pharmaceutics* 355.12 (2008), pp. 328–336. ISSN: 0378-5173. DOI: http://dx.doi.org/10.1016/j.ijpharm.2007.12.032.

[74] D Zhang and L Zhang. "Binding to semiflexible polymers: A novel method to control the structures of small numbers of building blocks". In: *Soft Matter* 10.38 (2014), pp. 7661–7668. DOI: 10.1039/c4sm00885e.

[75] Peng Liu et al. "Nanosuspensions of poorly soluble drugs: Preparation and development by wet milling". In: *International Journal of Pharmaceutics* 411.12 (2011), pp. 215–222. DOI: http://dx.doi.org/10.1016/j.ijpharm.2011.03.050.

[76] Peng Liu et al. "Interaction Studies Between Indomethacin Nanocrystals and PEO/PPO Copolymer Stabilizers". In: *Pharmaceutical Research* 32.2 (2014), pp. 628–639. DOI: 10.1007/s11095-014-1491-3.

[77] Walid S Saad and Robert K Prudhomme. "Principles of nanoparticle formation by flash nanoprecipitation". In: *Nano Today* 11.2 (2016), pp. 212–227. ISSN: 1748-0132. DOI: http://dx.doi.org/10.1016/j.nantod.2016.04.006.

[78] Jing Han et al. "A simple confined impingement jets mixer for flash nanoprecipitation". In: *Journal of Pharmaceutical Sciences* 101.10 (2012), pp. 4018–4023. ISSN: 0022-3549. DOI: http://dx.doi.org/10.1002/jps.23259.

[79] Brian K. Johnson. "Flash NanoPrecipitation of organic actives via confined micromixing and block copolymer stabilization". PhD thesis. Princeton University, 2003, p. 337.

[80] Varun Kumar et al. "Formulation and stability of itraconazole and odanacatib nanoparticles: governing physical parameters." eng. In: *Molecular pharmaceutics* 6.4 (2009), pp. 1118–1124. ISSN: 1543-8384 (Print). DOI: 10.1021/mp900002t.

[81] Kevin M Pustulka et al. *Flash Nanoprecipitation: Particle Structure and Stability*. eng. Nov. 2013. DOI: 10.1021/mp400337f.

[82] N Di Pasquale, D L Marchisio, and A A Barresi. "Model validation for precipitation in solvent-displacement processes". In: *Chemical Engineering Science* 84 (2012), pp. 671–683. DOI: 10.1016/j.ces.2012.08.043.

[83] N Di Pasquale et al. "Identification of nucleation rate parameters with MD and validation of the CFD model for polymer particle precipitation". In: *Chemical Engineering Research and Design* 91.11 (2013), pp. 2275–2290. DOI: 10.1016/j.cherd.2013.05.027.

[84] Federica Lince, Daniele L Marchisio, and Antonello A Barresi. "Strategies to control the particle size distribution of poly-ϵ-caprolactone nanoparticles for pharmaceutical applications". In: *Journal of Colloid and Interface Science* 322.2 (2008), pp. 505–515. DOI: http://dx.doi.org/10.1016/j.jcis.2008.03.033.

[85] M Ramezanpour et al. "Computational and experimental approaches for investigating nanoparticle-based drug delivery systems". In: *Biochimica et Biophysica Acta (BBA) - Biomembranes* 1858.7, Part B (2016), pp. 1688–1709. ISSN: 0005-2736. DOI: http://dx.doi.org/10.1016/j.bbamem.2016.02.028.

[86] C Forrey et al. "Prediction and validation of diffusion coefficients in a model drug delivery system using microsecond atomistic molecular dynamics simulation and vapour sorption analysis". In: *Soft Matter* 10.38 (2014), pp. 7480–7494. DOI: 10.1039/c4sm01297f.

[87] J A McCammon, B R Gelin, and M Karplus. "Dynamics of folded proteins". English. In: *Nature* 267.5612 (1977), pp. 585–590. DOI: 10.1038/267585a0.

[88] Siewert J Marrink et al. "The MARTINI force field: Coarse grained model for biomolecular simulations". In: *Journal of Physical Chemistry B* 111.27 (2007), pp. 7812–7824. DOI: 10.1021/jp071097f.

[89] S Nawaz and P Carbone. "Coarse-Graining Poly(ethylene oxide)-Poly(propylene oxide)-Poly(ethylene oxide) (PEO-PPO-PEO) Block Copolymers Using the MARTINI Force Field". English. In: *Journal of Physical Chemistry B* 118.6 (2014), pp. 1648–1659. DOI: 10.1021/jp4092249.

[90] P Carbone and C Avendano. "Coarse-grained methods for polymeric materials: enthalpy- and entropy-driven models". English. In: *Wiley Interdisciplinary Reviews-Computational Molecular Science* 4.1 (2014), pp. 62–70. DOI: 10.1002/wcms.1149.

[91] Hwankyu Lee and Ronald G Larson. "Molecular Dynamics Study of the Structure and Interparticle Interactions of Polyethylene Glycol-Conjugated PAMAM Dendrimers". In: *Journal of Physical Chemistry B* 113.40 (2009), pp. 13202–13207. DOI: 10.1021/jp906497e.

[92] Mohammed Zakaria Slimani et al. "Dynamic Heterogeneity in Random and Gradient Copolymers: A Computational Investigation". In: *Macromolecules* 46.12 (2013), pp. 5066–5079. DOI: 10.1021/ma400577d.

[93] R Mackenzie et al. "Multiscale Modeling of DrugPolymer Nanoparticle Assembly Identifies Parameters Influencing Drug Encapsulation Efficiency". In: *Journal of Chemical Theory and Computation* 11.6 (2015), pp. 2705–2713. DOI: 10.1021/ct501152a.

[94] S Ahmad et al. "In silico modelling of drug-polymer interactions for pharmaceutical formulations". In: *Journal of the Royal Society Interface* 7.SUPPL. 4 (2010), S423–S433. DOI: 10.1098/rsif.2010.0190.focus.

[95] R Bhattacharya et al. "A new microscopic insight into membrane penetration and reorganization by PETIM dendrimers". In: *Soft Matter* 10.38 (2014), pp. 7577–7587. DOI: 10.1039/c4sm01112k.

[96] G Rossi and L Monticelli. "Modeling the effect of nano-sized polymer particles on the properties of lipid membranes". In: *Journal of Physics Condensed Matter* 26.50 (2014). DOI: 10.1088/0953-8984/26/50/503101.

[97] Alexander Mirzoev and Alexander P Lyubartsev. "MagiC: Software Package for Multiscale Modeling". In: *Journal of Chemical Theory and Computation* 9.3 (2013), pp. 1512–1520. DOI: 10.1021/ct301019v.

[98] Loan Huynh et al. "Predicting the Solubility of the Anti-Cancer Agent Docetaxel in Small Molecule Excipients using Computational Methods". In: *Pharmaceutical Research* 25.1 (2007), pp. 147–157. DOI: 10.1007/s11095-007-9412-3.

[99] A D Costache et al. "Modeling polymer-drug interactions in biodegradable Tyrosine-derived nanospheres using Molecular dynamics simulations and docking studies". In: vol. 2. 2009, pp. 76–78. ISBN: 9781439817834 (ISBN); 9781439817834 (ISBN).

[100] Sarthak K Patel, Afsaneh Lavasanifar, and Phillip Choi. "Molecular dynamics study of the encapsulation capability of a PCL-PEO based block copolymer for hydrophobic drugs with different spatial distributions of hydrogen bond donors and acceptors". In: *Biomaterials* 31.7 (2010), pp. 1780–1786. DOI: 10.1016/j.biomaterials.2009.11.060.

[101] A O Kasimova et al. "Validation of a novel molecular dynamics simulation approach for lipophilic drug incorporation into polymer micelles". In: *Journal of Physical Chemistry B* 116.14 (2012), pp. 4338–4345. DOI: 10.1021/jp2104819.

[102] S Samanta and D Roccatano. "Interaction of Curcumin with PEO-PPO-PEO Block Copolymers: A Molecular Dynamics Study". English. In: *Journal of Physical Chemistry B* 117.11 (2013), pp. 3250–3257. DOI: 10.1021/jp309476u.

[103] K Karatasos. "Self-association and complexation of the anti-cancer drug doxorubicin with PEGylated hyperbranched polyesters in an aqueous environment". In: *Journal of Physical Chemistry B* 117.8 (2013), pp. 2564–2575. DOI: 10.1021/jp312125c.

[104] M Kang and S M Loverde. "Molecular simulation of the concentration-dependent interaction of hydrophobic drugs with model cellular membranes". In: *Journal of Physical Chemistry B* 118.41 (2014), pp. 11965–11972. DOI: 10.1021/jp5047613.

[105] S Nawaz et al. "Interactions of PEO-PPO-PEO block copolymers with lipid membranes: a computational and experimental study linking membrane lysis with polymer structure". English. In: *Soft Matter* 8.25 (2012), pp. 6744–6754. DOI: 10.1039/c2sm25327e.

[106] N Di Pasquale et al. "Solvent structuring and its effect on the polymer structure and processability: The case of water-acetone poly-ϵ-caprolactone mixtures". In: *Journal of Physical Chemistry B* 118.46 (2014), pp. 13258–13267. DOI: 10.1021/jp505348t.

[107] Loan Huynh et al. "Systematic design of unimolecular star copolymer micelles using molecular dynamics simulations". In: *Soft Matter* 6.21 (2010), pp. 5491–5501. DOI: 10.1039/c001988g.

[108] V A Rigo, L S De Lara, and C R Miranda. "Energetics of formation and hydration of functionalized silica nanoparticles: An atomistic computational study". In: *Applied Surface Science* 292 (2014), pp. 742–749. DOI: 10.1016/j.apsusc.2013.12.042.

[109] K M Salerno et al. "Coating thickness and coverage effects on the forces between silica nanoparticles in water". English. In: *Journal of Chemical Physics* 140.19 (2014), p. 8. DOI: 10.1063/1.4874638.

[110] Vincenzo Taresco et al. "Self-Assembly of Catecholic Moiety-Containing Cationic Random Acrylic Copolymers". In: *The Journal of Physical Chemistry B* (2015). DOI: 10.1021/acs.jpcb.5b05022.

[111] M Subashini et al. "Molecular dynamics simulation of drug uptake by polymer". In: *Journal of Molecular Modeling* 17.5 (2011), pp. 1141–1147. DOI: 10.1007/s00894-010-0811-8.

[112] M Cui and X Yang. "Molecular simulation of gold nanoparticle dispersion and aggregation in supercritical CO2". In: *Journal of Materials Science* 48.2 (2013), pp. 891–899. DOI: 10.1007/s10853-012-6811-6.

[113] J Meena Devi. "Aggregation of thiol coated gold nanoparticles: A simulation study on the effect of polymer coverage density and solvent". In: *Computational Materials Science* 86 (2014), pp. 174–179. DOI: 10.1016/j.commatsci.2014.01.042.

[114] Z Yang et al. "Molecular dynamics simulations of hydrogen bond dynamics and far-infrared spectra of hydration water molecules around the mixed monolayer-protected Au nanoparticle". In: *Journal of Physical Chemistry C* 119.4 (2015), pp. 1768–1781. DOI: 10.1021/jp506875m.

[115] Ardeshir Goliaei et al. "Behavior of P85 and P188 Poloxamer Molecules: Computer Simulations Using United-Atom Force-Field". In: *The Journal of Physical Chemistry B* 120.33 (Aug. 2016), pp. 8631–8641. ISSN: 1520-6106. DOI: 10.1021/acs.jpcb.6b03030.

[116] Hwankyu Lee et al. "Molecular Dynamics Studies of Polyethylene Oxide and Polyethylene Glycol: Hydrodynamic Radius and Shape Anisotropy". In: *Biophysical Journal* 95.4 (2008), pp. 1590–1599. DOI: http://dx.doi.org/10.1529/biophysj.108.133025.

[117] A Bunker. "Poly(ethylene glycol) in drug delivery, why does it work, and can we do better? All atom molecular dynamics simulation provides some answers". English. In: *Proceedings of the 25th Workshop on Computer Simulation Studies in Condensed Matter Physics*. Ed. by D P Landau et al. Vol. 34. Amsterdam: Elsevier Science Bv, 2012, pp. 24–33. ISBN: 1875-3892. DOI: 10.1016/j.phpro.2012.05.004.

[118] N Martinho et al. "Molecular modeling to study dendrimers for biomedical applications". In: *Molecules* 19.12 (2014), pp. 20424–20467. DOI: 10.3390/molecules191220424.

[119] A D Costache et al. "Polymer-drug interactions in tyrosine-derived triblock copolymer nanospheres: A computational modeling approach". In: *Molecular Pharmaceutics* 6.5 (2009), pp. 1620–1627. DOI: 10.1021/mp900114w.

[120] Andrew R. Leach. *Molecular Modelling: Principles and Applications*. Second. Pearon Education Limited, 2001, p. 744. ISBN: 0-582-38210-6.

[121] Tom Darden, Darrin York, and Lee Pedersen. "Particle mesh Ewald: An Nlog(N) method for Ewald sums in large systems". In: *The Journal of Chemical Physics* 98.12 (1993).

[122] Ulrich Essmann et al. "A smooth particle mesh Ewald method". In: *The Journal of Chemical Physics* 103.19 (1995).

[123] *Periodic Boundary Conditions*.

[124] Alpeshkumar K Malde et al. "An Automated Force Field Topology Builder (ATB) and Repository: Version 1.0". In: *Journal of Chemical Theory and Computation* 7.12 (2011), pp. 4026–4037. DOI: 10.1021/ct200196m.

[125] Katarzyna B Koziara et al. "Testing and validation of the Automated Topology Builder (ATB) version 2.0: prediction of hydration free enthalpies". In: *Journal of Computer-Aided Molecular Design* 28.3 (2014), pp. 221–233. ISSN: 1573-4951. DOI: 10.1007/s10822-014-9713-7.

[126] Chris Oostenbrink et al. "A biomolecular force field based on the free enthalpy of hydration and solvation: The GROMOS force-field parameter sets 53A5 and 53A6". In: *Journal of Computational Chemistry* 25.13 (2004), pp. 1656–1676. DOI: 10.1002/jcc.20090.

[127] L Martinez et al. "PACKMOL: A Package for Building Initial Configurations for Molecular Dynamics Simulations". English. In: *Journal of Computational Chemistry* 30.13 (2009), pp. 2157–2164. DOI: 10.1002/jcc.21224.

[128] H J C Berendsen et al. "Interaction Models for Water in Relation to Protein Hydration". In: *Intermolecular Forces: Proceedings of the Fourteenth Jerusalem Symposium on Quantum Chemistry and Biochemistry Held in Jerusalem, Israel, April 13–16, 1981*. Ed. by Bernard Pullman. Dordrecht: Springer Netherlands, 1981, pp. 331–342. ISBN: 978-94-015-7658-1. DOI: 10.1007/978-94-015-7658-1{_}21.

[129] N Schmid et al. "Definition and testing of the GROMOS force-field versions 54A7 and 54B7". English. In: *European Biophysics Journal with Biophysics Letters* 40.7 (2011), pp. 843–856. DOI: 10.1007/s00249-011-0700-9.

[130] S Pronk et al. "GROMACS 4.5: a high-throughput and highly parallel open source molecular simulation toolkit". English. In: *Bioinformatics* 29.7 (2013), pp. 845–854. DOI: 10.1093/bioinformatics/btt055.

[131] UK National Supercomputing Service. *ARCHER*. DOI: http://www.archer.ac.uk/.

[132] William Humphrey, Andrew Dalke, and Klaus Schulten. "VMD: Visual molecular dynamics". In: *Journal of Molecular Graphics* 14.1 (Feb. 1996), pp. 33–38. DOI: 10.1016/0263-7855(96)00018-5.

[133] Paul J Flory. *Principles of Polymer Chemistry*. Cornell University Press, 1953. ISBN: 978-0-8014-0134-3.

[134] M S Kim et al. "Ring-opening polymerization of ϵ-caprolactone by poly(ethylene glycol) by an activated monomer mechanism". In: *Macromolecular Rapid Communications* 26.8 (2005), pp. 643–648.

[135] F Leroux et al. "Synthesis and polymerization of cyclobutenyl-functionalized polylactide and polycaprolactone: a consecutive ROP/ROMP route towards poly(1,4-butadiene)-g-polyesters". English. In: *Polymer Chemistry* 5.10 (2014), pp. 3476–3486. DOI: 10.1039/c3py01611k.

[136] A Olivier et al. "Semi-crystalline poly(epsilon-caprolactone) brushes on gold substrate via "grafting from" method New insights with AFM characterization". English. In: *European Polymer Journal* 47.1 (2011), pp. 31–39. DOI: 10.1016/j.eurpolymj.2010.04.022.

[137] Vincenzo Taresco et al. "Properties of acyl modified poly(glycerol-adipate) comb-like polymers and their self-assembly into nanoparticles". In: *Journal of Polymer Science Part A: Polymer Chemistry* (July 2016). ISSN: 0887624X. DOI: 10.1002/pola.28215.

[138] ACD/I-Lab. *Indomethacin*. 2014. DOI: https://ilab.acdlabs.com/iLab2/.

[139] Drugbank. *Indomethacin*. DOI: http://www.drugbank.ca/drugs/DB00328.

[140] Maria Malamatari et al. "Nanoparticle agglomerates of indomethacin: The role of poloxamers and matrix former on their dissolution and aerosolisation efficiency". In: *International Journal of Pharmaceutics* 495.1 (2015), pp. 516–526. DOI: http://dx.doi.org/10.1016/j.ijpharm.2015.09.013.

[141] Edward Mansfield. *Dynamic Light Scattering schematic*. DOI: http://www.slideshare.net/EdwardMansfield1/dynamic-light-scattering-48645581.

[142] B Derjaguin. "A theory of interaction of particles in presence of electric double layer and the stability of lyophobe colloids and disperse systems." In: *Acta Physicochim.* 10 (1939), p. 333.

[143] Malvern. *Malvern's introduction to zeta potential*. DOI: http://www.malvern.com/en/support/resource-center/technical-notes/TN101104ZetaPotentialIntroduction.aspx.

[144] *Uv-Vis*. 2016. DOI: https://upload.wikimedia.org/wikipedia/commons/9/95/Schematic{_}of{_}UV-{_}visible{_}spectrophotometer.png.

[145] Mauro Ferrario et al. "Molecular dynamics simulation of aqueous mixtures: Methanol, acetone, and ammonia". In: *The Journal of Chemical Physics* 93.7 (1990), pp. 5156–5166. DOI: doi:http://dx.doi.org/10.1063/1.458652.

[146] W L Jorgensen, J M Briggs, and M Leonor Contreras. "Relative partition coefficients for organic solutes from fluid simulations". In: *Journal of Physical Chemistry* 94.4 (1990), pp. 1683–1686.

[147] Samantha Weerasinghe and Paul E. Smith. "KirkwoodBuff derived force field for mixtures of acetone and water". In: *The Journal of Chemical Physics* 118.23 (2003), p. 10663. ISSN: 00219606. DOI: 10.1063/1.1574773.

[148] Daan P Geerke and Wilfred F van Gunsteren. "Force Field Evaluation for Biomolecular Simulation: Free Enthalpies of Solvation of Polar and Apolar Compounds in Various Solvents". In: *Chemphyschem* 7.3 (2006), pp. 671–678. DOI: 10.1002/cphc.200500510.

[149] Aurlien Perera and Franjo Sokoli. "Modeling nonionic aqueous solutions: The acetone-water mixture". In: *The Journal of Chemical Physics* 121.22 (2004), pp. 11272–11282. DOI: doi:http://dx.doi.org/10.1063/1.1817970.

[150] J M Stubbs, J J Potoff, and J I Siepmann. "Transferable potentials for phase equilibria. 6. United-atom description for ethers, glycols, ketones, and aldehydes". English. In: *Journal of Physical Chemistry B* 108.45 (2004), pp. 17596–17605. DOI: 10.1021/jp049459w.

[151] E R Hatcher, O Guvench, and A D MacKerell Jr. "CHARMM Additive All-Atom Force Field for Acyclic Polyalcohols, Acyclic Carbohydrates, and Inositol". English. In: *Journal of Chemical Theory and Computation* 5.5 (2009), pp. 1315–1327. DOI: 10.1021/ct9000608.

[152] Ganesh Kamath, Grigor Georgiev, and and Jeffrey J. Potoff*. "Molecular Modeling of Phase Behavior and Microstructure of AcetoneChloroformMethanol Binary Mixtures". In: *The Journal of Physical Chemistry B* 109.41 (2005), pp. 19463–19473. DOI: 10.1021/jp0535238.

[153] P Jedlovszky, A Idrissi, and G Jancsó. "Can existing models qualitatively describe the mixing behavior of acetone with water?" English. In: *Journal of Chemical Physics* 130.12 (2009). DOI: 10.1063/1.3086859.

[154] R G Pereyra, M L Asar, and M A Carignano. "The role of acetone dipole moment in acetone-water mixture". English. In: *Chemical Physics Letters* 507.4-6 (2011), pp. 240–243. DOI: 10.1016/j.cplett.2011.04.015.

[155] Steven W Rick. "A reoptimization of the five-site water potential (TIP5P) for use with Ewald sums". In: *The Journal of Chemical Physics* 120.13 (2004), pp. 6085–6093. DOI: doi:http://dx.doi.org/10.1063/1.1652434.

[156] M G Martin and M J Biddy. "Monte Carlo molecular simulation predictions for the heat of vaporization of acetone and butyramide". In: *Fluid Phase Equilibria* 236.1-2 (2005), pp. 53–57. DOI: http://dx.doi.org/10.1016/j.fluid.2005.06.003.

[157] Anita Pinke and Pál Jedlovszky. "Modeling of Mixing Acetone and Water: How Can Their Full Miscibility Be Reproduced in Computer Simulations?" In: *The Journal of Physical Chemistry B* 116.20 (2012), pp. 5977–5984. DOI: 10.1021/jp302629r.

[158] Myo T Tyn and Waclaw F Calus. "Temperature and concentration dependence of mutual diffusion coefficients of some binary liquid systems". In: *Journal of Chemical & Engineering Data* 20.3 (1975), pp. 310–316. DOI: 10.1021/je60066a009.

[159] F Bally et al. "Improved size-tunable preparation of polymeric nanoparticles by microfluidic nanoprecipitation". English. In: *Polymer (United Kingdom)* 53.22 (2012), pp. 5045–5051. DOI: 10.1016/j.polymer.2012.08.039.

[160] F Lince, D L Marchisio, and A A Barresi. "A comparative study for nanoparticle production with passive mixers via solvent-displacement: Use of CFD models for optimization and design". English. In: *Chemical Engineering and Processing: Process Intensification* 50.4 (2011), pp. 356–368. DOI: 10.1016/j.cep.2011.02.015.

[161] Yi-ping Huang et al. "Molecular weight dependence of the melting behavior of poly (ϵ-caprolactone)". In: 20.1 (2002), pp. 45–51.

[162] Suzanne M DAddio et al. "Novel Method for Concentrating and Drying Polymeric Nanoparticles: Hydrogen Bonding Coacervate Precipitation". In: *Molecular Pharmaceutics* 7.2 (2010), pp. 557–564. DOI: 10.1021/mp900260q.

[163] W Zhu et al. "Atomistic simulation study of surfactant and polymer interactions on the surface of a fenofibrate crystal". In: *European Journal of Pharmaceutical Sciences* 42.5 (2011), pp. 452–461. DOI: 10.1016/j.ejps.2011.01.009.

[164] Lee Moir. "The use of thermoresponsive nanoparticles for targeting cancer cells". PhD thesis. University of Nottingham, 2016.

[165] Jian Xiang Zhang et al. "Indomethacin-loaded polymeric nanocarriers based on amphiphilic polyphosphazenes with poly (N-isopropylacrylamide) and ethyl tryptophan as side groups: Preparation, in vitro and in vivo evaluation". In: *Journal of Controlled Release* 116.3 (2006), pp. 322–329. DOI: http://dx.doi.org/10.1016/j.jconrel.2006.09.013.

[166] Debamitra Dutta et al. "Adsorbed proteins influence the biological activity and molecular targeting of nanomaterials." eng. In: *Toxicological sciences : an official journal of the Society of Toxicology* 100.1 (Nov. 2007), pp. 303–315. ISSN: 1096-6080 (Print). DOI: 10.1093/toxsci/kfm217.

[167] Varun Kumar and Robert K. Prud'homme. "Thermodynamic limits on drug loading in nanoparticle cores". In: 97.11 (Nov. 2008), pp. 4904–4914. ISSN: 00223549. DOI: 10.1002/jps.21342.

[168] D Dupeyron et al. "Design of indomethacin-loaded nanoparticles: effect of polymer matrix and surfactant". eng. In: *Int J Nanomedicine* 8 (2013), pp. 3467–3477. DOI: 10.2147/ijn.s47621.

[169] Yancai Wang et al. “Stability of nanosuspensions in drug delivery”. In: *Journal of Controlled Release* 172.3 (2013), pp. 1126–1141. DOI: http://dx.doi.org/10.1016/j.jconrel.2013.08.006.

[170] Sofia Papadimitriou and Dimitrios Bikiaris. “Novel self-assembled coreshell nanoparticles based on crystalline amorphous moieties of aliphatic copolyesters for efficient controlled drug release”. In: *Journal of Controlled Release* 138.2 (2009), pp. 177–184. DOI: http://dx.doi.org/10.1016/j.jconrel.2009.05.013.

[171] Thirumala Govender et al. “PLGA nanoparticles prepared by nanoprecipitation: drug loading and release studies of a water soluble drug”. In: *Journal of Controlled Release* 57.2 (1999), pp. 171–185. DOI: http://dx.doi.org/10.1016/S0168-3659(98)00116-3.

[172] Michal E Matteucci et al. “Drug nanoparticles by antisolvent precipitation: Mixing energy versus surfactant stabilization”. In: *Langmuir* 22.21 (2006), pp. 8951–8959. DOI: 10.1021/1a061122t.

[173] Z Zhu. “Effects of amphiphilic diblock copolymer on drug nanoparticle formation and stability”. In: *Biomaterials* 34.38 (2013), pp. 10238–10248. DOI: 10.1016/j.biomaterials.2013.09.015.

APPENDIX A

Parameter files

A.1 Acetone Topology - UAC.itp

```
;----------------------------TITLE -------------------------------------------
;   acetone
;
; This file was generated at 01:26 on 2014-09-24 by
;
;                   Automatic Topology Builder
;
;                    REVISION 2014-09-22
;------------------------------------------------------------------------------
; Authors     : Alpeshkumar K. Malde, Le Zuo, Matthew Breeze, Martin Stroet,
; Alan E. Mark
;
; Institute   : Molecular Dynamics group,
;               School of Chemistry and Molecular Biosciences (SCMB),
;               The University of Queensland, QLD 4072, Australia
; URL         : http://compbio.biosci.uq.edu.au/atb
; Citation    : Malde AK, Zuo L, Breeze M, Stroet M, Poger D, Nair PC,
; Oostenbrink C, Mark AE.
;               An Automated force field Topology Builder (ATB) and
```

```
; repository: version 1.0.
;               Journal of Chemical Theory and Computation, 2011, 7(12), 4026-4037.
;               http://pubs.acs.org/doi/abs/10.1021/ct200196m
;
; Disclaimer  :
;      While every effort has been made to ensure the accuracy and validity of
; parameters provided below the assignment of parameters is being based
; on an automated procedure combining data provided by a given user as
;       well as calculations performed using third party software. They are
;       provided as a guide.The authors of the ATB cannot guarantee that the
;       parameters are complete or that the parameters provided are appropriate
;       for use in any specific application. Users are advised to treat these
;       parameters with discretion and to perform additional validation tests
;       for their specific application if required. Neither the authors of the
;       ATB or The University of Queensland except any responsibly for
; how the parameters may be used.
;
; Release notes and warnings:
;  (1) The topology is based on a set of atomic coordinates and other data provided
; by the user after quantum mechanical optimization of the structure using
;        different levels of theory depending on the nature of the molecule.
;  (2) In some cases the automatic bond, bond angle and dihedral type assignment
; is ambiguous. In these cases alternative type codes are provided at the
;        end of the line.
;  (3) While bonded parameters are taken where possible from the nominated force
; field non-standard bond, angle and dihedral type code may be incorporated
;        in cases where an exact match could not be found. These are marked as
;        "non-standard" or "uncertain" in comments.
;  (4) In some cases it is not possible to assign an appropriate parameter
; automatically. "%" is used as a place holder for those fields that could not
;        be determined automatically. The parameters in these fields must be
;        assigned manually before the file can be used.
;--------------------------------------------------------------------------
; Input Structure : UAC
```

```
; Output          : UNITED ATOM topology
; Use in conjunction with the corresponding united atom PDB file.
;------------------------------------------------------------------------
; Final Topology Generation was performed using:
; A B3LYP/6-31G* optimized geometry.
; Bonded and van der Waals parameters were taken from the GROMOS 53A6
; parameter set.
; Initial charges were estimated using the ESP method of Merz-Kollman.
; Final charges and charge groups were generated by method described
; in the ATB paper.
; If required, additional bonded parameters were generated from a
; Hessian matrix calculated at the B3LYP/6-31G* level of theory.
;
; Topology file generated at 01:09 on 24 Sep 2014 for molecule
; acetone (IUPAC: propan-2-one, database identifier: UAC)
; by Automatic Topology Builder(revision 2014-09-22).
;
[ moleculetype ]
; Name   nrexcl
UAC     3
[ atoms ]
;  nr  type  resnr  resid  atom  cgnr  charge    mass    total_charge
    1   CH3    1    UAC     C3    1   -0.083  15.0350
    2     C    1    UAC     C2    1    0.734  12.0110
    3     O    1    UAC     O1    1   -0.568  15.9994      ;  0.083
    4   CH3    1    UAC     C1    2   -0.083  15.0350      ; -0.083
; total charge of the molecule:   0.000
[ bonds ]
;  ai   aj  funct   c0         c1
    1    2    2   0.1520   5.4300e+06
    2    3    2   0.1230   1.6600e+07
    2    4    2   0.1520   5.4300e+06
[ pairs ]
;  ai   aj  funct  ;  all 1-4 pairs but the ones excluded in GROMOS itp
```

```
[ angles ]
;  ai   aj   ak  funct   angle     fc
    1    2    3    2    125.00   750.00
    1    2    4    2    120.00   560.00
    3    2    4    2    125.00   750.00
[ dihedrals ]
; GROMOS improper dihedrals
;  ai   aj   ak   al  funct   angle     fc
    2    1    3    4    2      0.00   167.36
[ dihedrals ]
;  ai   aj   ak   al  funct    ph0      cp     mult
[ exclusions ]
;  ai   aj  funct  ;  GROMOS 1-4 exclusions
```

A.2 mPEG-PCL topology - polymers.rtp

```
[ bondedtypes ]
; bonds  angles  dihedrals  impropers
    2       2          1          2

[ pgs ]
  [ atoms ]
; name type charge chargegroup
C1 CH3 0.260 1
OX OE -0.260 1
  [ bonds ]
; ai aj gromos type
C1 OX gb_18 ;0.1430  8.1800e+06
OX +C1 gb_18 ;0.1430  8.1800e+06
  [ angles ]
; ai aj ak gromos type
C1 OX +C1 118.00      1080.00 ;109.50      320.00
OX +C1 +C2 ga_15
```

```
  [ dihedrals ]
; ai aj ak al gromos type
C1 OX +C1 +C2 gd_23
OX +C1 +C2 +OX gd_23

;The following is the REPEAT PEG part
;consists of -[CH2-CH2-O]-
; the oxygen has been named OX but it is an ether so it is an OE oxygen
[ pgr ]
[ atoms ]
; name type charge chargegroup
C1 CH2 0.171 1
C2 CH2 0.118 1
OX OE -0.289 2
[ bonds ]
; ai aj gromos type
C1 C2 gb_27 ;0.1530  7.1500e+06
C2 OX gb_18
OX +C1 gb_18 ;for any of the next peg units
[ angles ]
; ai aj ak gromos type
C1 C2 OX ga_15 ;repeat unit
C2 OX +C1 118.00     1080.00 ;for the repeat and the 1st CL unit
OX +C1 +C2 ga_15 ; for the repeat
[ dihedrals ]
; ai aj ak al gromos type
C1 C2 OX +C1 gd_23 ;for the next PEG and the 1st PCL
C2 OX +C1 +C2 gd_23 ;for the next PEG
OX +C1 +C2 +OX gd_23 ;for the PEG repeat CHANGED IT FROM 37
OX +C1 +C2 +C3 gd_23 ;for the CL

[ pge ] ; we need this connecting site because the bonds and dihedrals
; in the connection oxygen carbons are different from those on mpeg
[ atoms ]
```

```
; name type charge chargegroup
C1 CH2 0.147 1
C2 CH2 0.143 1
OX OE -0.290 2
[ bonds ]
; ai aj gromos type
C1 C2 gb_27 ;0.1530  7.1500e+06
C2 OX gb_18
OX +C1 gb_5 ;for the CLs that is coming after
[ angles ]
; ai aj ak gromos type
C1 C2 OX ga_15 ; 111.00 530
C2 OX +C1 118.00     1080.00
OX +C1 +C2 ga_19
OX +C1 +OC ga_33
[ dihedrals ]
; ai aj ak al gromos type
C1 C2 OX +C1 gd_12
C2 OX +C1 +C2 gd_13
C2 OX +C1 +OC gd_12 ;for the CL carbonyl dihedral
OX +C1 +C2 +OC gd_12 ;
OX +C1 +C2 +C3 gd_12
[ impropers ]
OX +C1 +OC +C2 gi_1 ;0.00 167.36 ;for the connection with the CL unit

;Caprolactone connecting unit
[ pcs ]
[ atoms ]
;  name    type    charge  chargegroup
C1 C 0.350 1
OC O -0.385 1
C2 CH2 0.029 2
C3 CH2 0.006 2
C4 CH2 0.000 3
```

```
C5 CH2 0.057 3
C6 CH2 0.203 4
OX OA -0.260 4
[ bonds ]
; ai aj gromos type
C1 OC gb_5
C1 C2 gb_27
C2 C3 gb_27
C3 C4 gb_27
C4 C5 gb_27
C5 C6 gb_27
C6 OX gb_18
OX +C1 gb_18 ;for the repeat residue
[ angles ]
; ai aj ak gromos type
OC C1 C2 ga_30 ;121.00      685.00
C1 C2 C3 ga_15 ;111.00      530.00
C2 C3 C4 ga_15
C3 C4 C5 ga_15
C4 C5 C6 ga_15
C5 C6 OX ga_13 ;109.50      520.00
C6 OX +C1 118.00      1080.00
OX +C1 +C2 ga_30
OX +C1 +OC ga_33
[ dihedrals ]
; ai aj ak al gromos type
OC C1 C2 C3 gd_12 ;
C1 C2 C3 C4 gd_29 ;0.00     3.77    3
C2 C3 C4 C5 gd_29 ;0.00     3.77    3
C3 C4 C5 C6 gd_29 ;0.00     3.77    3
C4 C5 C6 OX gd_23 ;
C5 C6 OX +C1 gd_12  ;
C6 OX +C1 +C2 gd_13 ;for the repeat residue
C6 OX +C1 +OC gd_12 ;repeat residue
```

```
OX +C1 +C2 +C3 gd_12 ;repeat residue
[ impropers ]
OX +C1 +OC +C2 gi_1 ;0.00 167.36

; CAPROLACTONE  UNITED atom
; Constructed by Ioanna
;The following is the cl monomer residue
;consists of -[O=C-CH2-CH2-CH2-CH2-CH2-O]-this is an ester so the oxygen is OA
[ pcl ]
[ atoms ]
;  name    type    charge  chargegroup
C1 C 0.370 1
OC O -0.375 1
C2 CH2 0.173 2
C3 CH2 0.006 2
C4 CH2 0.011 3
C5 CH2 0.028 3
C6 CH2 0.047 4
OX OA -0.260 4
[ bonds ]
; ai aj gromos type
C1 OC gb_5
C1 C2 gb_27
C2 C3 gb_27
C3 C4 gb_27
C4 C5 gb_27
C5 C6 gb_27
C6 OX gb_18
OX +C1 gb_18 ;for the repeat residue
[ angles ]
; ai aj ak gromos type
OC C1 C2 ga_30 ;121.00      685.00
C1 C2 C3 ga_15 ;111.00      530.00
C2 C3 C4 ga_15
```

```
C3 C4 C5 ga_15
C4 C5 C6 ga_15
C5 C6 OX ga_13 ;109.50      520.00
C6 OX +C1 118.00      1080.00
OX +C1 +C2 ga_30
OX +C1 +OC ga_33
[ dihedrals ]
; ai aj ak al gromos type
OC C1 C2 C3 gd_12 ;
C1 C2 C3 C4 gd_29 ;0.00     3.77    3
C2 C3 C4 C5 gd_29 ;0.00     3.77    3
C3 C4 C5 C6 gd_29 ;0.00     3.77    3
C4 C5 C6 OX gd_23 ;
C5 C6 OX +C1 gd_12  ;
C6 OX +C1 +C2 gd_13 ;for the repeat residue
C6 OX +C1 +OC gd_12 ;repeat residue
OX +C1 +C2 +C3 gd_12 ;repeat residue
[ impropers ]
OX +C1 +OC +C2 gi_1 ;0.00 167.36

[ pce]
[ atoms ]
;  name    type    charge  chargegroup
C1 C 0.360 1
OC O -0.397 1
C2 CH2 0.037 2
C3 CH2 0.000 2
C4 CH2 0.017 3
C5 CH2 -0.017 3
C6 CH2 0.138 4
OX OA -0.366 4
HA H 0.228 4
[ bonds ]
; ai aj gromos type
```

```
C1 OC gb_5
C1 C2 gb_27
C2 C3 gb_27
C3 C4 gb_27
C4 C5 gb_27
C5 C6 gb_27
C6 OX gb_18
OX HA gb_1
[ angles ]
; ai aj ak gromos type
OC C1 C2 ga_30 ;121.00      685.00
C1 C2 C3 ga_15 ;111.00      530.00
C2 C3 C4 ga_15
C3 C4 C5 ga_15
C4 C5 C6 ga_15
C5 C6 OX ga_13 ;109.50      520.00
C6 OX HA 118.00      1080.00
[ dihedrals ]
; ai aj ak al gromos type
OC C1 C2 C3 gd_12 ;
C1 C2 C3 C4 gd_29 ;0.00     3.77    3
C2 C3 C4 C5 gd_29 ;0.00     3.77    3
C3 C4 C5 C6 gd_29 ;0.00     3.77    3
C4 C5 C6 OX gd_23 ;
C5 C6 OX HA gd_30  ;
```

A.3 Acetone models

		OPLS	μ=	2.35 D
	C	**O**	**CH3**	**CH3**
x	0	0	0.1286	-0.1286
y	0.0069	0.129	-0.0716	-0.0716
z	0	0	0	0
ε (KJ/mol)	0.4397	0.8795	0.6701	0.6701
σ (nm)	0.375	0.296	0.391	0.391
q (e)	0.3	-0.424	0.062	0.062

		FHMK		2.7 D
	C	**O**	**CH3**	**CH3**
x	0	0	0.1342	-0.1342
y	0.0086	0.131	-0.0732	-0.0732
z	0	0	0	0
ε (KJ/mol)	0.4395	0.879	0.797	-0.797
σ (nm)	0.375	0.296	0.388	0.388
q (e)	0.566	-0.502	-0.032	-0.032

		WS	μ=	3.31 D
	C	**O**	**CH3**	**CH3**
x	0	0	0.1286	-0.1286
y	0.0069	0.129	-0.0717	-0.0717
z	0	0	0	0
ε (KJ/mol)	0.3361	0.5602	0.8675	0.8675
σ (nm)	0.336	0.31	0.375	0.375
q (e)	0.565	-0.565	0	0

		TraPPE -UA	μ= 2.8024 D	
	C	O	CH3	CH3
x	0	0	0.129739721	-0.129739721
y	0	0.1229	0.079193464	-0.079193464
z	0	0	0	0
ε (KJ/mol)	0.3327	0.657	0.815	0.815
σ (nm)	0.382	0.305	0.375	0.375
q (e)	0.424	-0.424	0	0

		Kamath	μ= 2.9739 D	
	C	O	CH3	CH3
x	0	0	0.129739721	-0.129739721
y	0	0.1229	0.079193464	-0.079193464
z	0	0	0	0
ε (KJ/mol)	0.3327	0.657	0.815	0.815
σ (nm)	0.382	0.305	0.375	0.375
q (e)	0.662	0.564	-0.049	-0.049

		CHARMM	μ=	
	C	O	C(H3)	H
x	0	0	0.129910431	-0.129739721
y	0	0.123	0.079193464	-0.079193464
z	0	0	0	0
ε (KJ/mol)	0.292943916	0.502191947	0.334791859	0.092070464
σ (nm)	0.3564	0.3029	0.3671	0.2352
q (e)	0.55	-0.55	-0.27	0.09

A.4 Packmol Example Building code

Packmol site

http://www.ime.unicamp.br/ martinez/packmol/home.shtml/

```
# An empty water region containing an indomethacin amorphous of  5nm radiu
#/ initial structure that will be solvated in GROMACS with acetone -
#Control simulation of Indomethacin dissolving in water & Acetone
# All atoms from different molecules will be at least 2.0 Angstroms apart
# at the solution
tolerance 2.0
# The type of the files will be pdb
filetype pdb
# The name of the output file
output con350_indo.pdb
#residue test
resnumber 0
add_box_sides 1.0
#nloop 30
structure indo.pdb
number 145
inside sphere 249 138 138 25.
end structure
structure UAC.pdb
number 68766
inside box 0. 0. 0. 110. 276. 276.
end structure
structure UAC.pdb
number 5
```

```
inside box 110. 0. 0. 386 276 276
end structure
```

A.5 Example of topol.top file

```
#include "forcefield.itp"
#include "spc.itp"
#ifdef POSRES_water
#include "posres_water.itp"
#endif
#include "indo.itp"
#ifdef POSRES_indo
#include "posres_indo.itp"
#endif
#include "UAC.itp"
#ifdef POSRES_acetone
#include "posres_acetone.itp"
#endif
#include "polymer1.itp"
#ifdef POSRES_polymer
#include "posres_polymer1.itp"
#endif

[ system ]
Indo_350 54a7 new charges-Acetone removal 1

[ molecules ]
; Compound    #mols
```

```
INDO 145
POL1 31
UAC  55056
SOL     845592
```

A.6 grompp.mdp file

```
title =  Indo350 with new polymer charges and 54a7
; Run parameters
integrator = md ; leap-frog integrator
nsteps = 5000000
dt = 0.002
; Output control
nstxout = 0
nstvout = 0
nstfout = 0
nstxtcout = 5000
nstenergy = 0
nstlog = 1000
; Bond parameters
continuation = yes ; Restarting after NPT
; Neighborsearching
ns_type = grid ; search neighboring grid cells
nstlist = 10 ; 10 fs
rlist = 1 ; short-range neighborlist cutoff (in nm)
rcoulomb = 1 ; short-range electrostatic cutoff (in nm)
rvdw = 1 ; short-range van der Waals cutoff (in nm)
; Electrostatics
```

```
coulombtype = PME ; Particle Mesh Ewald for long-range electrostatics
pme_order = 8
fourierspacing = 0.1 ; grid spacing for FFT
; Temperature coupling is on
tcoupl = V-rescale ; modified Berendsen thermostat
tc-grps = system ; two coupling groups - more accurate
tau_t = 0.1 ; time constant, in ps
ref_t = 298 ; reference temperature, one for each group, in K
; Pressure coupling is on
pcoupl = Parrinello-Rahman ; Pressure coupling on in NPT
pcoupltype = isotropic ; uniform scaling of box vectors
tau_p = 2.0 ; time constant, in ps
ref_p = 1.0 ; reference pressure, in bar
compressibility = 4.5e-5 ; isothermal compressibility of water, bar^-1
; Periodic boundary conditions
pbc = xyz ; 3-D PBC
; Dispersion correction
DispCorr = EnerPres ; account for cut-off vdW scheme
; Velocity generation
gen_vel = no ; Velocity generation is off
constraints = hbonds
```

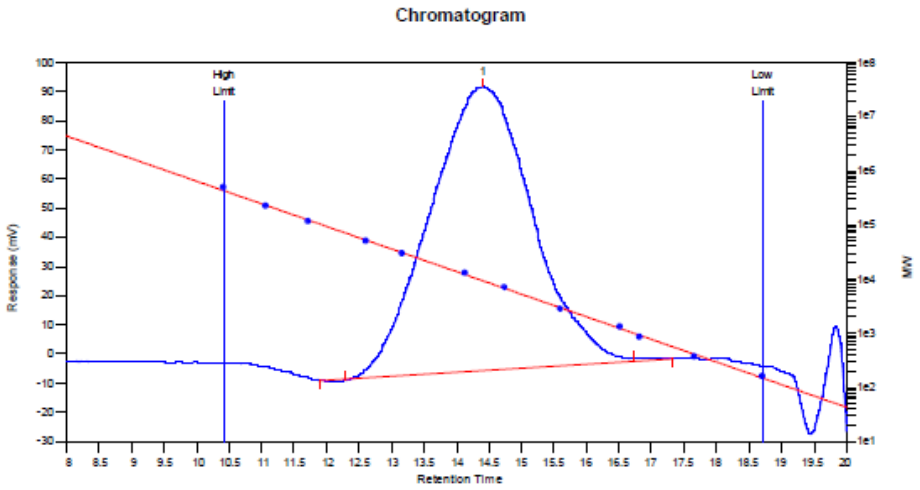
APPENDIX B

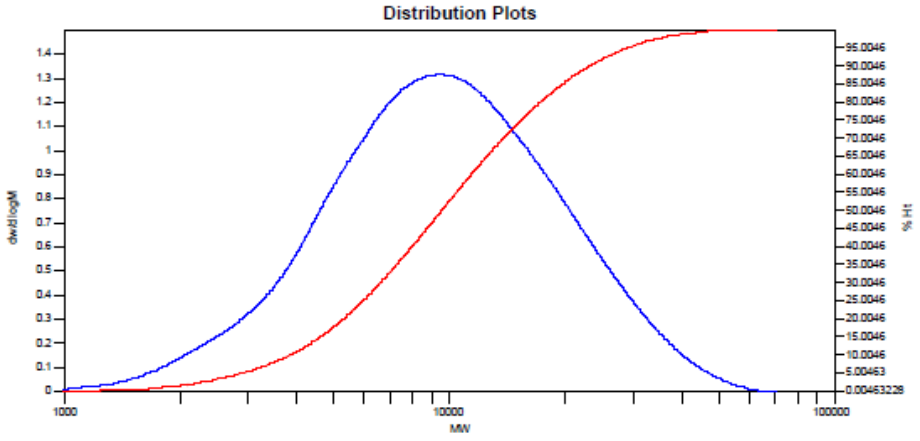
Experimental Appendix

B.1 GPC traces

Sample:IDSA09 **Date:24/04/2015 17:32:03**

Workbook: CHCl3_conv_150420.plw Inj File: 150424-0006.cgrm
Path: C:\Cirrus Workbooks\2015\CHCl3_conv_150420\CHCl3_conv_150420.plw
Res. File: 150424-0006.rst
Method: PSeasy_CHCl3_150420 Batch: 150424
Eluent: Chloroform





Peak No	Mp	Mn	Mw	Mz	Mz+1	Mv	PD
1	9447	7384	11839	17751	24269	11081	1.60333

Fig. B.1 GPC chromatograph of PEG350PCL.

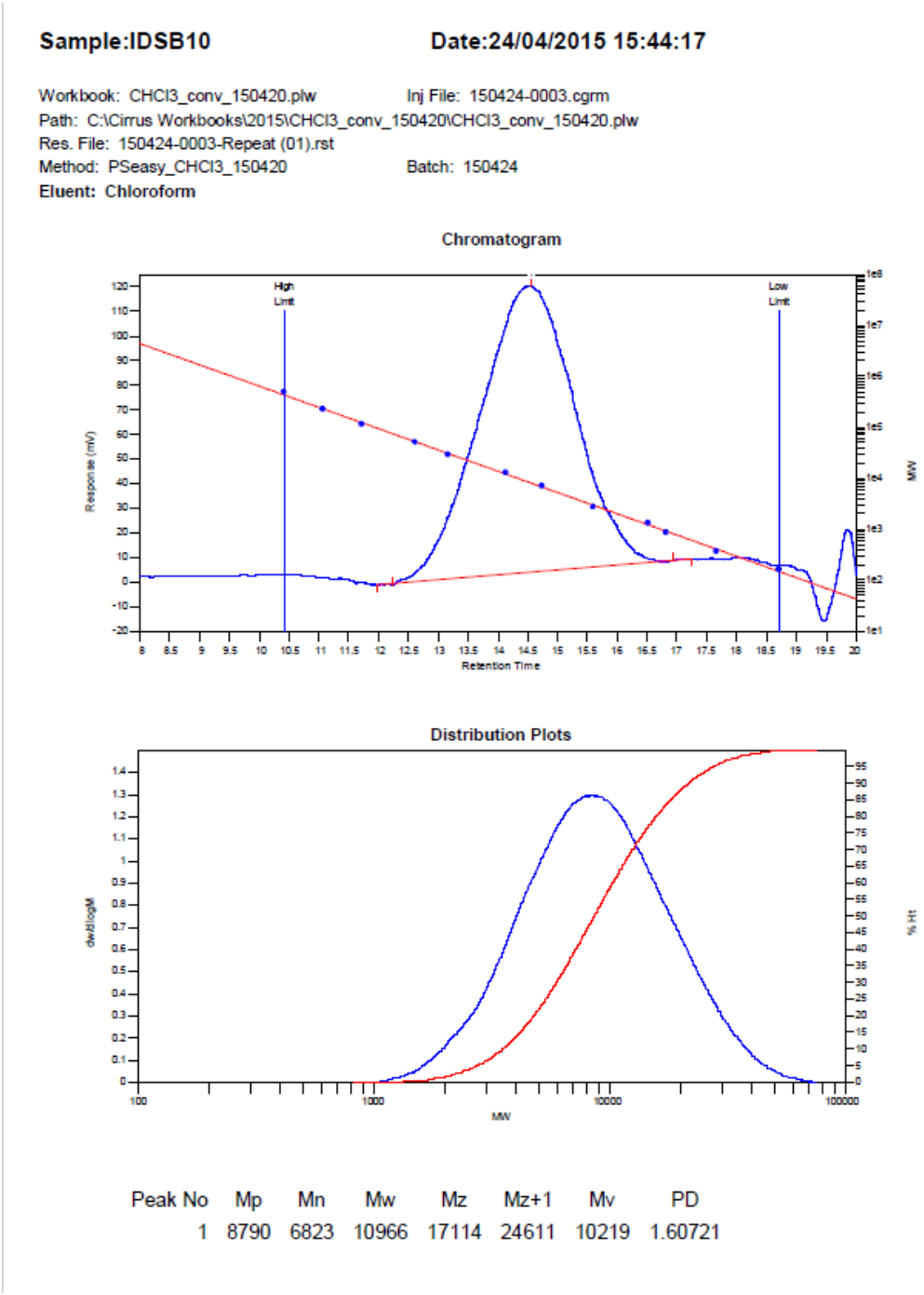
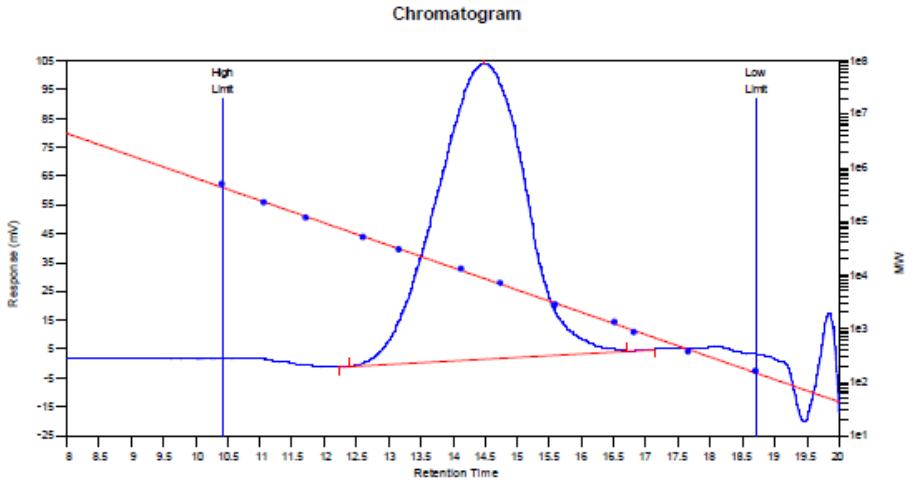
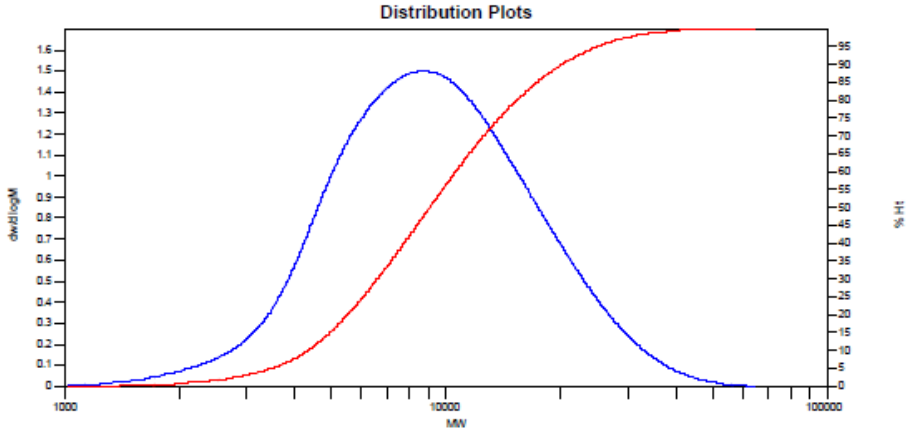


Fig. B.2 GPC chromatograph of PEG350PCL.

Sample:IDSC11 **Date:24/04/2015 16:56:13**

Workbook: CHCl3_conv_150420.plw Inj File: 150424-0005.cgrm
Path: C:\Cirrus Workbooks\2015\CHCl3_conv_150420\CHCl3_conv_150420.plw
Res. File: 150424-0005-Repeat (01).rst
Method: PSeasy_CHCl3_150420 Batch: 150424
Eluent: Chloroform



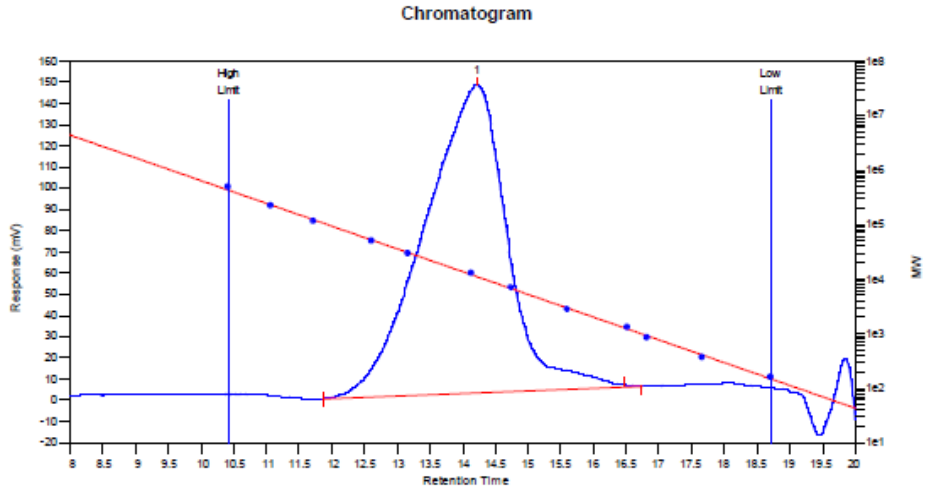


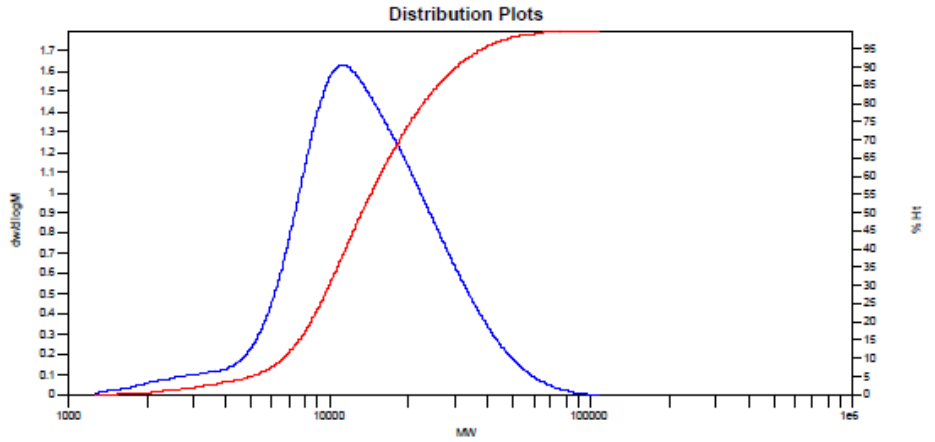
Peak No	Mp	Mn	Mw	Mz	Mz+1	Mv	PD
1	8678	7601	10911	15380	20763	10345	1.43547

Fig. B.3 GPC chromatograph of PEG750PCL.

Sample:IDSF16 **Date:24/04/2015 15:08:27**

Workbook: CHCl3_conv_150420.plw Inj File: 150424-0002.cgrm
Path: C:\Cirrus Workbooks\2015\CHCl3_conv_150420\CHCl3_conv_150420.plw
Res. File: 150424-0002-Repeat (01).rst
Method: PSeasy_CHCl3_150420 Batch: 150424
Eluent: Chloroform





Peak No	Mp	Mn	Mw	Mz	Mz+1	Mv	PD
1	11268	10957	16353	23604	32805	15456	1.49247

Fig. B.4 GPC chromatograph of PEG2000PCL.

B.2 DSC and equation for the calculation of PCL % crystallinity.

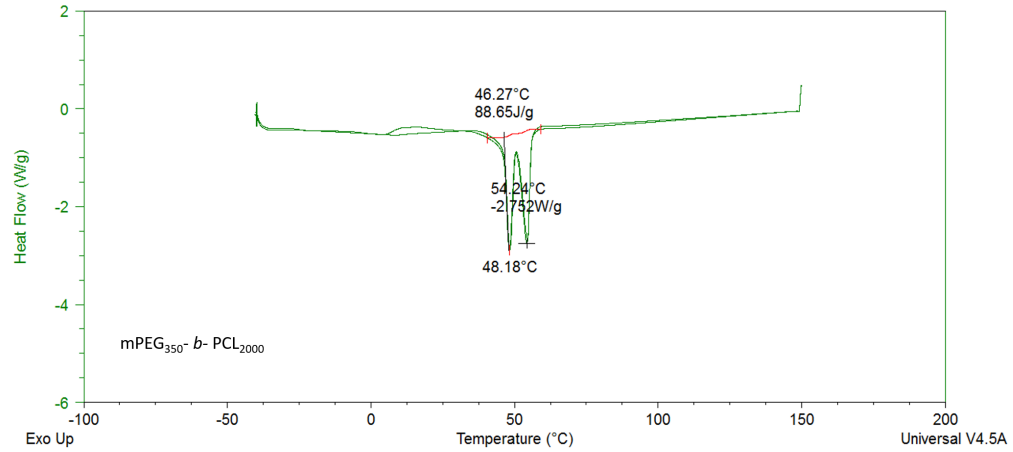


Fig. B.5 DSC of PEG350PCL.

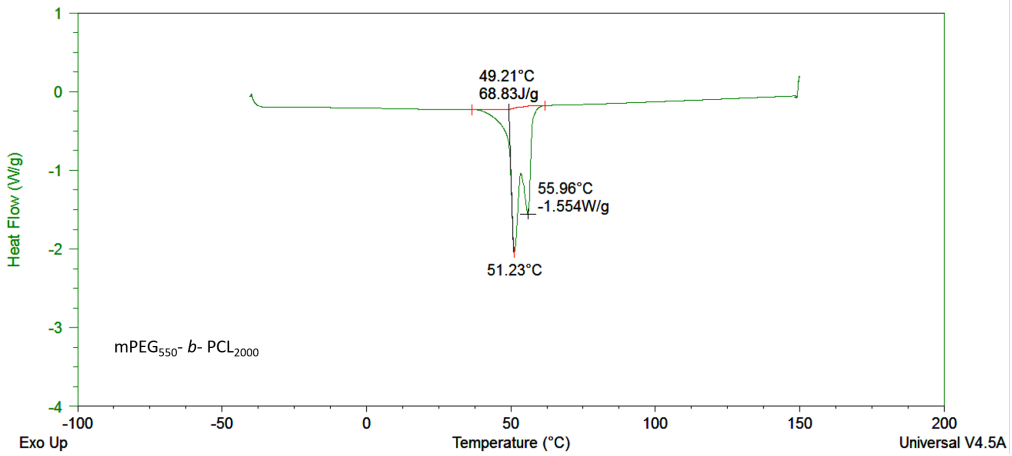


Fig. B.6 DSC of PEG550PCL.

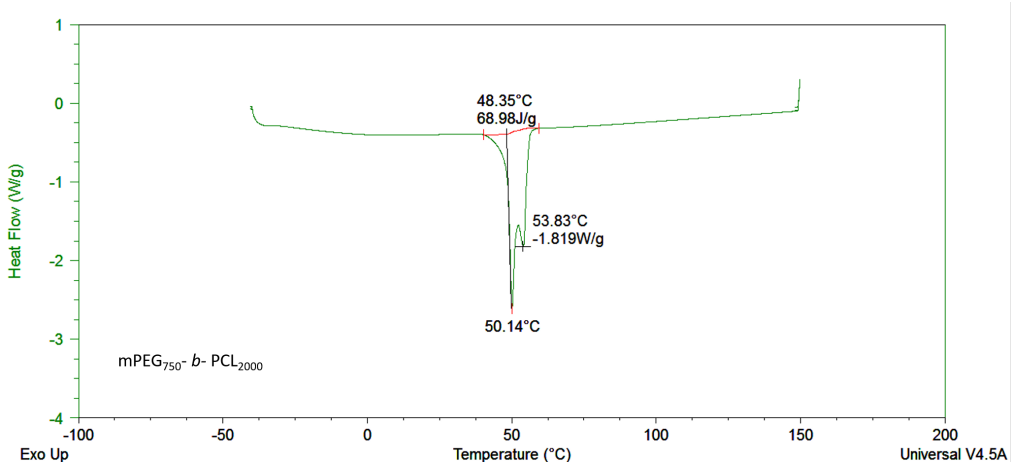


Fig. B.7 DSC of PEG750PCL.

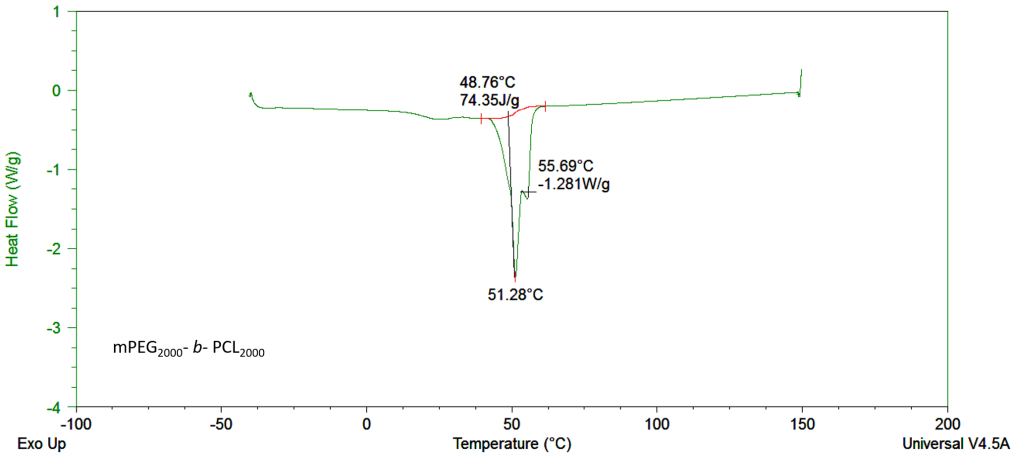


Fig. B.8 DSC of PEG2000PCL.

The contribution of the mPEG in the ΔH of the copolymers that can be calculated via:

$$\begin{aligned} \Delta H_{mPEG} &= \Delta H * (w/w\%(mPEG)) \\ &= \Delta H * \frac{M_{wmPEG}}{114.14 * DP_{PCL} + M_{wmPEG}} \end{aligned} \tag{B.2.1}$$

where DP_{PCL} is the number of CL units in the PCL blocks, as calculated via ^{1}H NMR. With the use of equation B.2.1, the percentage of PCL's

crystallinity can be calculated via: ΔH_{PCL}=ΔH- ΔH_{mPEG} and results of these calculations are graphically illustrated in figure 4.3.

B.3 Wet ball milled indomethacin



Fig. B.9 Indomethacin after the wet-bead milling in the absence of a surfactant. A white foam has been created in the pot resulting in great drug losses.

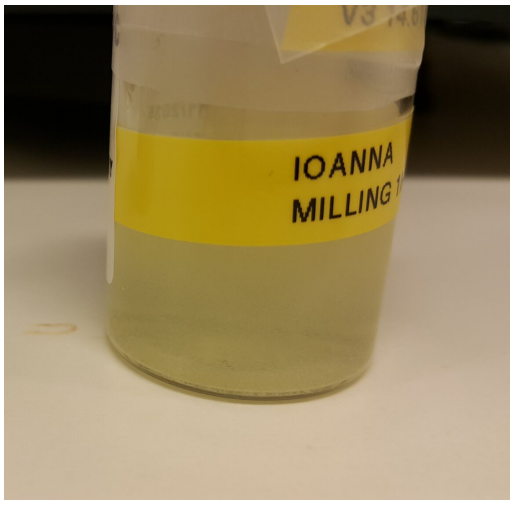


Fig. B.10 Indomethacin suspension created by wet-bead milling in the absence of a surfactant. The suspension was very unstable and was sedimenting quickly.

B.4 Cryomilled indomethacin characteristics

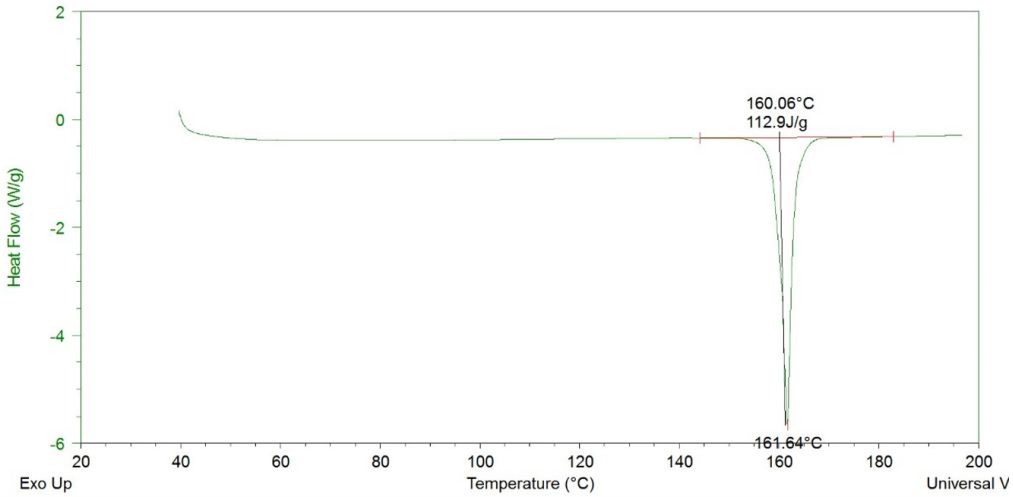


Fig. B.11 DSC of indomethacin as received.

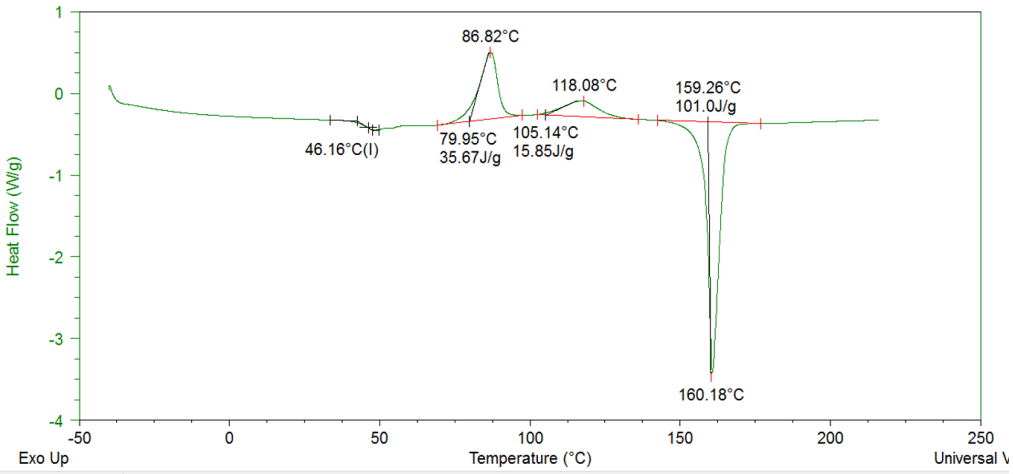


Fig. B.12 DSC of freshly cryomilled indomethacin.

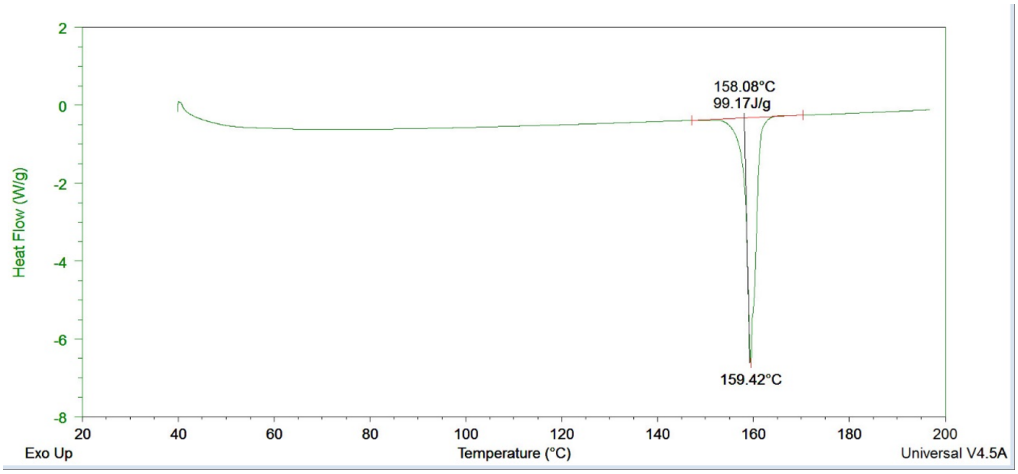


Fig. B.13 DSC of indomethacin as used for the interfacial deposition method, 3 weeks after it was cryomilled.

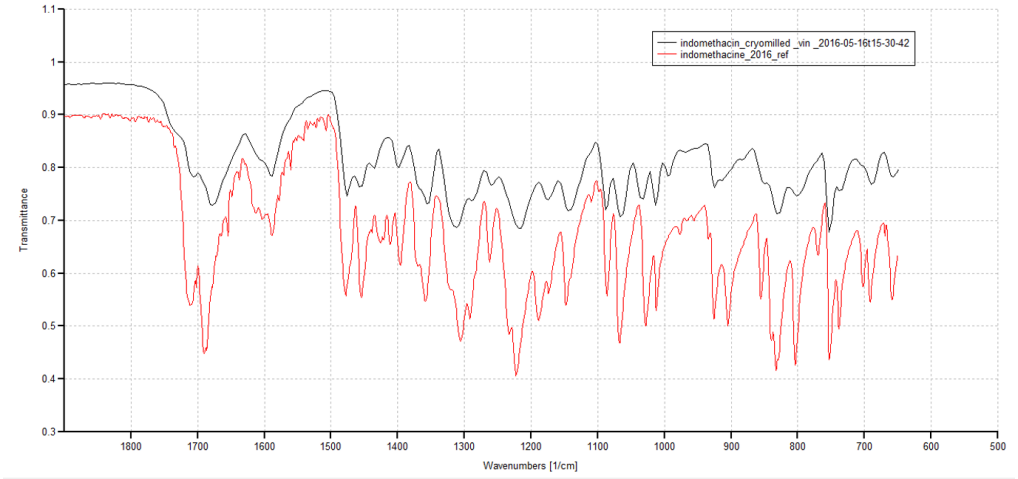


Fig. B.14 ATR-IR spectra of freshly cryomilled indomethacin (black line) and as received (red line). The absence of the sharps peaks in the cryomilled sample indicate a lack of crystallinity in comparison with the original state of the drug.

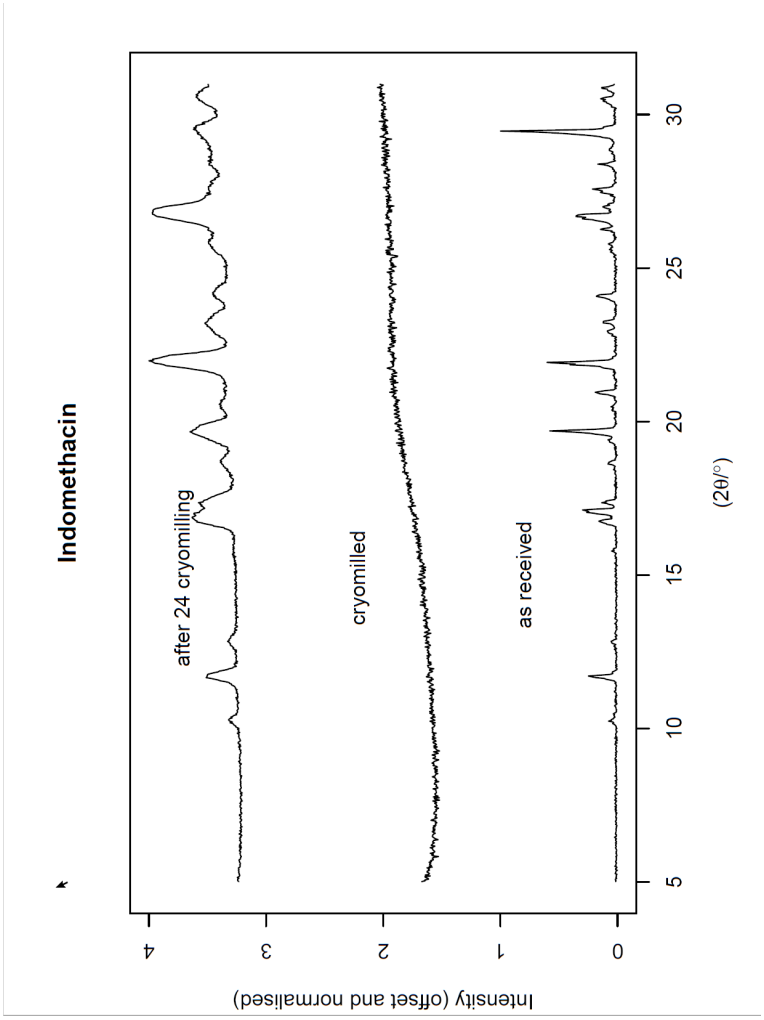


Fig. B.15 X-Ray Powder Diffraction spectra of indomethacin as received, after the cryomilling and after 24h. The drug is no longer amorphous during the interfacial deposition. Data from Ghaidaa Hameed.

B.5 DLS intensity distributions

B.5.1 Reproducibility of the method

		Size (d.nm):	% Intensity:	St Dev (d.nm):
Z-Average (d.nm): 89.41	Peak 1:	98.81	94.0	44.12
PdI: 0.234	Peak 2:	3489	6.0	1228
Intercept: 0.923	Peak 3:	0.000	0.0	0.000
Result quality : Good				

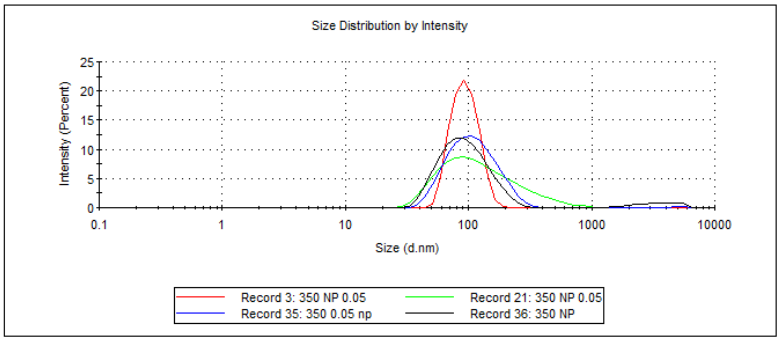


Fig. B.16 Reproducibility of interfacial deposition method; Overlay of size measurements (DLS) of 4 batches of polymer NPs formed with PEG350PCL at a 0.05 mg/ml polymer concentration.

		Size (d.nm):	% Intensity:	St Dev (d.nm):
Z-Average (d.nm): 305.6	Peak 1:	344.2	99.1	140.7
PdI: 0.190	Peak 2:	5136	0.9	550.0
Intercept: 0.907	Peak 3:	0.000	0.0	0.000
Result quality : Good				

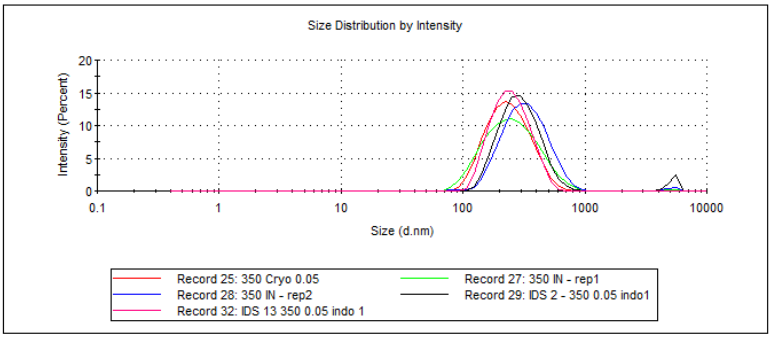


Fig. B.17 Reproducibility of interfacial deposition method; Overlay of size measurements (DLS) of 5 batches of the PEG350PCL-coated indomethacin NPs, (0.05 mg/ml polymer concentration in acetone, 1 mg/ml indomethacin concentration in water.)

B.5.2 Polymer Concentration effect

		Size (d.nm):	% Intensity:	St Dev (d.nm):
Z-Average (d.nm): 129.2	Peak 1:	153.0	100.0	66.72
PdI: 0.164	Peak 2:	0.000	0.0	0.000
Intercept: 0.953	Peak 3:	0.000	0.0	0.000
Result quality : Good				

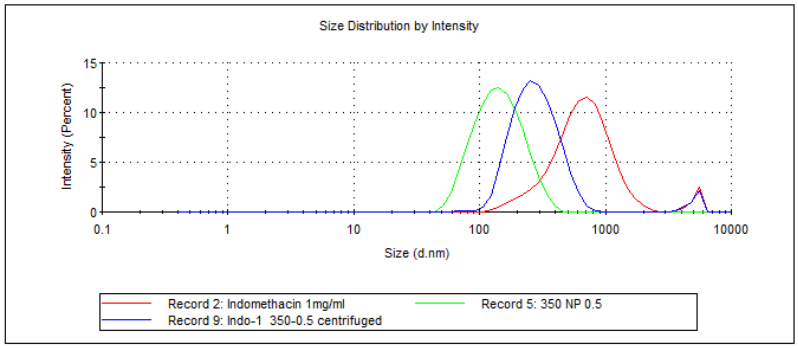


Fig. B.18 Overlay of 3 DLS samples to show 3 different NP populations: PEG350PCL polymer NPs (green 0.5 mg/ml), indomethacin sonnicated as used in the aqueous suspension (red 1mg/ml) and polymer-coated indomethacin NP (blue). Each peak corresponds to the average intensity distribution of three measurements.

		Size (d.nm):	% Intensity:	St Dev (d.nm):
Z-Average (d.nm): 171.5	Peak 1:	191.4	100.0	68.28
PdI: 0.127	Peak 2:	0.000	0.0	0.000
Intercept: 0.933	Peak 3:	0.000	0.0	0.000
Result quality : Good				

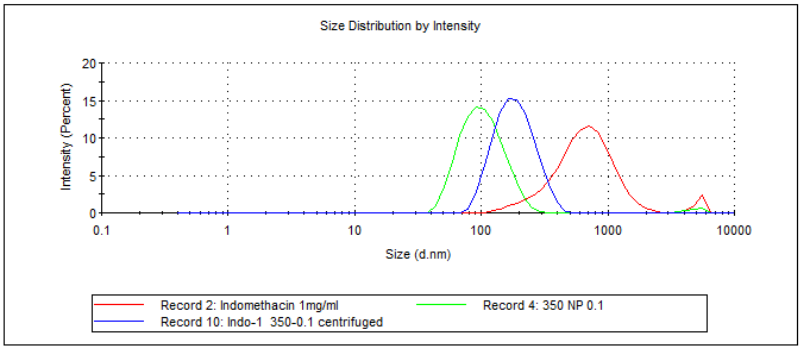


Fig. B.19 Overlay of 3 DLS samples to show 3 different NP populations: PEG350PCL polymer NPs (green 0.1 mg/ml), indomethacin sonnicated as used in the aqueous suspension (red 1mg/ml) and polymer-coated indomethacin NP (blue). Each peak corresponds to the average intensity distribution of three measurements.

B.5.3 Temperature stability

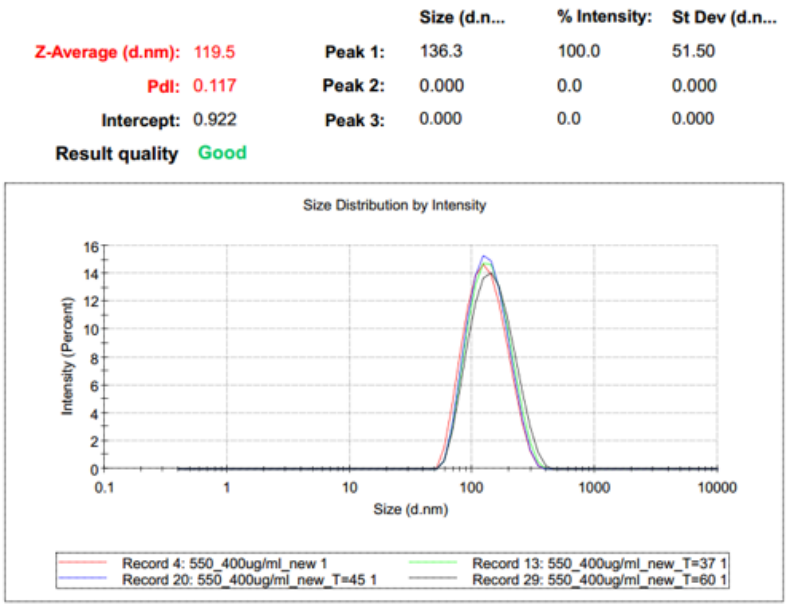


Fig. B.20 Stability of the PEG550PCL polymer NPs in 4 different temperatures, (25, 37, 45 60 ^{o}C)

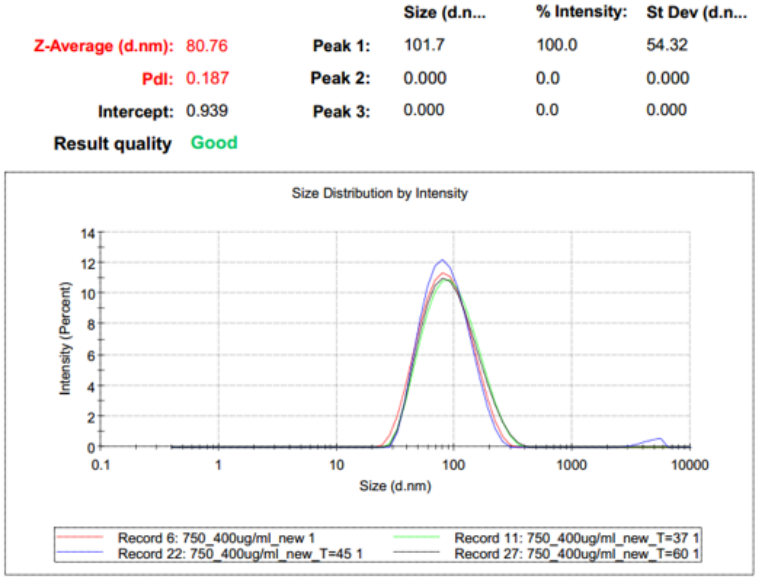


Fig. B.21 Stability of the PEG750PCL polymer NPs in 4 different temperatures, (25, 37, 45 60 ^{o}C)

B.5.4 Physical Stability

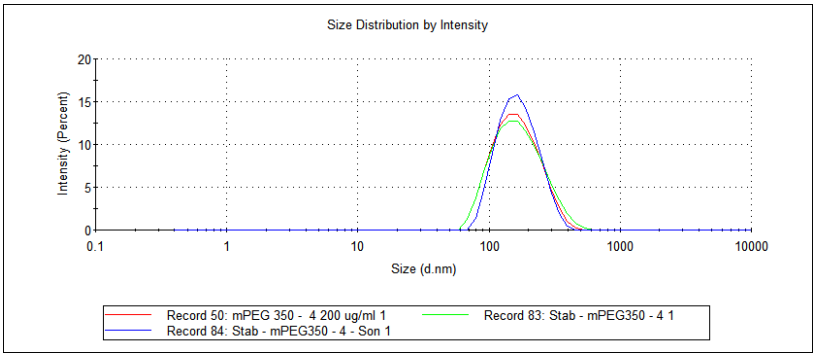


Fig. B.22 Stability of the PEG350PCL polymer NPs (final polymer concentration in water 0.2 mg/ml): The original measurement in red, the same sample after 1 month in green and the latter after 5 minutes of sonnication. The size distribution is the same in all 3 cases.

B.5.5 Miscellaneous

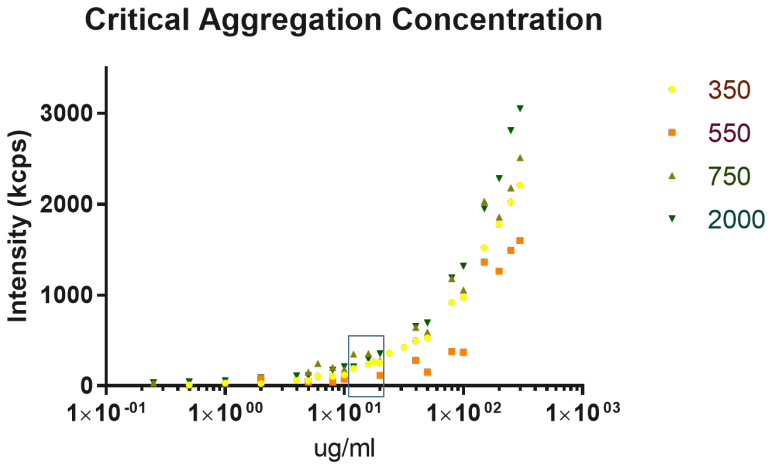


Fig. B.23 Critical Aggregation concentration (CAC) as measured by DLS.

B.6 UV-Vis calibration

$$Absorbance = 7.81007 * [drugconcentration] - 0.00702 R^2 = 0.98816 \tag{B.6.1}$$